Universidad de Málaga

Escuela Técnica Superior de Ingeniería de Telecomunicación

TESIS DOCTORAL

Performance analysis of MIMO-OFDM systems using complex Gaussian quadratic forms

Autor:

FCO. JAVIER LÓPEZ MARTÍNEZ

Directores:

EDUARDO MARTOS NAYA

JOSÉ TOMÁS ENTRAMBASAGUAS MUÑOZ

UNIVERSIDAD DE MÁLAGA
ESCUELA TÉCNICA SUPERIOR DE INGENIERÍA DE TELECOMUNICACIÓN

Reunido el tribunal examinador en el día de la fecha, constituido por:

Presidente: Dr. D. _____

Secretario: Dr. D. _____

Vocales: Dr. D. _____

Dr. D. _____

Dr. D. _____

para juzgar la Tesis Doctoral titulada *Performance analysis of MIMO-OFDM systems using complex Gaussian quadratic forms* realizada por D. Fco. Javier López Martínez y dirigida por los Profesores Dr. D. Eduardo Martos Naya y Dr. D. José Tomás Entrambasaguas Muñoz, acordó por

_____ otorgar la calificación de

_____ y para que conste,

se extiende firmada por los componentes del tribunal la presente diligencia.

Málaga a ____ de _____ del ____

El Presidente: El Secretario:

Fdo.: _____   Fdo.: _____

El Vocal: El Vocal: El Vocal:

Fdo.: _____   Fdo.: _____   Fdo.: _____

Table of Contents

List of Figures

List of Tables

x

Abstract

In this thesis, the performance analysis of wireless communication systems affected by different impairments is addressed. The BER calculation is accomplished by means of modelling the decision variable at the receiver as a particular case of quadratic form D in complex Gaussian random variables. Relevant results are obtained when circularly-symmetric RVs are considered, providing exact as well as approximate closed-form expressions for $\Pr\{D < 0\}$. The general case of non circularly-symmetric RV is also considered, which had not been previously analyzed in the literature, obtaining novel exact (and approximate) closed-form expressions for $\Pr\{D < 0\}$.

Additionally, a general framework for the probability calculation in QAM system is presented, which allows to express the BER as a weighted sum of *components of error probability*. Closed-form expressions for these weights are given for QAM constellations with arbitrary independent bit-mapping, which include previous results in the literature as particular cases.

With these tools, the BER of a number of MIMO-OFDM systems in non ideal conditions has been obtained in exact closed form. Particularly, the following system model have been analyzed:

- A $1 \times N_R$ QAM system with MRC reception, affected by Ricean fading, Ricean-faded interferences and ICSI.

- A $2 \times N_R$ QAM system with Alamouti transmission and MRC reception, affected by Ricean fading and ICSI.

- A $1 \times N_R$ OFDM system with MRC reception, affected by Rayleigh fading, CFO, ICSI and DC offset.

- An OFDM system affected by Rayleigh fading, ICSI and I/Q imbalances.

- A $N_T \times N_R$ OFDM system with transmit beamforming and MRC reception, affected by Rayleigh fading and ICSI.

Resumen

En esta tesis se aborda el problema del análisis de prestaciones en sistemas de comunicaciones inalámbricas afectados por diferentes no idealidades. El cálculo de la BER se lleva a cabo modelando la variable de decisión en el receptor como una forma cuadrática D de variables aleatorias Gaussianas complejas. Se han obtenido resultados relevantes para el caso de variables aleatorias circularmente simétricas, proporcionando expresiones cerradas (tanto exactas como aproximadas) para el cálculo de $\Pr\{D < 0\}$. También ha sido considerado el caso general de variables aleatorias no circularmente simétricas, que no había sido analizado con anterioridad en la bibliografía, obteniendo expresiones expresiones cerradas (tanto exactas como aproximadas) para $\Pr\{D < 0\}$

Además, se presenta un marco analítico para el cálculo de probabilidades en sistemas basados en QAM, que permite expresar la BER como una suma ponderada de componentes de probabilidad de error. Se deriva una expresión cerrada para los coeficientes de esta suma ponderada, que son válidos para constelaciones QAM arbitrarias con mapeo independiente de los bits, y que incluye resultados previos como casos particulares.

Con estas herramientas, se han obtenido expresiones exactas y cerradas para la BER de diferentes sistemas MIMO-OFDM no ideales. En particular, se han analizado los siguientes modelos de sistema:

- Un sistema $1 \times N_R$ QAM con recepción MRC, afectado por desvanecimientos tipo Rice, interferencias tipo Rice y estimación de canal imperfecta (ICSI)

- Un sistema $2 \times N_R$ QAM con transmisión de Alamouti y recepción MRC, afectado por desvanecimientos tipo Rice e ICSI.

- Un sistema $1 \times N_R$ OFDM con recepción MRC, canal Rayleigh, offset de frecuencia de portadora (CFO), ICSI y offset de continua (DC).

- Un sistema OFDM afectado por desvanecimientos tipo Rayleigh, ICSI y desbalanceos I/Q.

- Un sistema $N_T \times N_R$ OFDM con *beamforming* en transmisión y recepción MRC, canal Rayleigh e ICSI.

Chapter 1

Introduction

THIS chapter introduces the reader into the main motivations of this thesis. The state of the art in performance analysis is reviewed, and some open problems of interest are identified. Then, the aims and organization of this thesis are presented, and the publications obtained within this work are summarized.

1.1 Motivation

The measurement of the performance in communication systems has always been a matter of extreme interest since their very origin [1–3]. Besides the channel capacity, which basically provides information about the limiting error-free information rate that can be achieved, this performance is usually quantified in terms of the Symbol Error Rate (SER) or the Bit Error Rate (BER). Depending on the characteristics of the channel fading and the modulation scheme, the performance analysis can be conducted following different approaches.

One of the milestone reference works in this area was published by Simon and Alouini [4], where the performance of a number of digital communication systems under different fading conditions was analyzed following a common strategy. Most of the results provided in this paper allowed to obtain the SER in exact closed-form, whereas in other cases a numerical integration was necessary.

The appearance of new digital communication systems that employ new modulation or transmission schemes leads to the necessity of evaluating their performance in order to enable a fair comparison with the existing techniques. Some examples are the use of multiple

antennas, usually referred to as multiple-input multiple-output (MIMO) systems, or the orthogonal frequency division multiplexing (OFDM) technique. Both MIMO and OFDM have been incorporated in many commercial and under-development wireless communication technologies.

The analytical performance of most of wireless communication systems under different fading conditions has already been accomplished when perfect channel state information (CSI) is assumed to be known at the receiver side (or even at the transmitter side, if required) [5, 6]. These results hence are useful to determine the maximum achievable performance of these systems under ideal conditions. However, in practice there exist many factors which may limit their performance: the appearance of *interfering signals*, the consideration of *imperfect CSI*, or non-idealities due to physical implementation such as *carrier frequency offset* (CFO), *in-phase/quadrature* (I/Q) *imbalance* and *direct-current* (DC) *offsets* are valid examples.

In these situations, the system model becomes more complicated than the originally considered in [4] due to the different natures of the random variables (RVs) involved in the process. This implies not only that the analytical performance evaluation may result more difficult, but that the simulation of these scenarios becomes unfeasible. Thus, the derivation of exact closed-form expressions for the performance analysis of these systems is of utmost necessity, in order to be able to efficiently determine how these impairments affect the system performance.

There exist different approaches for the BER calculation in these scenarios: the derivation of the *probability density function* (PDF) or the *cumulative distribution function* (CDF) of the decision variable, the *moment generating function* (MGF) method [7] and the *characteristic function* method are the most extended strategies. However, many of these systems allow to express the decision variable as a particular case of a general quadratic form; hence, the performance analysis can be conducted by following a common procedure.

In this line, the probability calculation in quadratic form receivers when complex Gaussian circularly-symmetric RVs are considered was studied in [6, 8]. These results have enabled the analysis of different scenarios [9, 10] where the involved RVs have non-zero mean, in which

the BER calculation following other approaches was not feasible. Therefore, the possibility of expressing the decision variable as a quadratic form provides an efficient way to evaluate the BER in exact closed-form in a number of scenarios.

Recently, Di Renzo [11] generalized the results given by Proakis, providing a means to obtain the characteristic function of a general quadratic form for a number of fading conditions (i.e., different natures of RVs). However, all the analyses in the literature assume that the RVs have circular symmetry, which means that their real and imaginary parts are not correlated and have the same variance. Since the condition of circular symmetry [12, 13] may not be always fulfilled, it seems interesting to analyze general quadratic forms where the RVs lack from circular symmetry.

Another matter that arises when evaluating the performance of a communication system is related with the error probability calculation for a family of constellations. The calculation of the BER must take into account that different symbols may have different error probabilities. This may be due to some factors, e.g. the decision regions vary for the symbols located in the outer zone of the constellation, or the equivalent noise affects differently to the I and Q components.

Many analyses in the literature, tough of unquestionable interest, usually are performed for particular constellations such as Binary Phase-Shift Keying (BPSK), 4-Quadrature Amplitude Modulation (4-QAM) or 16-QAM [9, 14, 15]. As the constellation size is increased, the calculation is often carried out by explicitly deriving the different probabilities of the received symbol to be above or below a number of decision boundaries, and then these individual probabilities are combined accordingly. It seems hence desirable the use of a systematic method which allows for a generic BER calculation, independently of the constellation size.

There exist some previous works in the literature devoted to this task, that allow for the BER calculation in particular scenarios, such as additive white Gaussian noise (AWGN) channels [16] and fading channels [17]. These results are based on the empirical observation of regular patterns in the constellation mapping, and hence lack from a mathematical background. Besides, some assumptions are taken both in the constellation mapping (Gray mapping) and in the RVs (circular symmetry). Thus, there are some scenarios which cannot

be analyzed using these approaches.

The motivation of this thesis is twofold: On the one hand, to provide a general method for the BER calculation in QAM based systems with arbitrary constellation size; on the other hand, to obtain exact-closed form expressions for the BER of MIMO and OFDM systems in non-ideal conditions, by means of a general analysis of Gaussian quadratic forms in complex RVs.

1.2 Aims and organization

According to the motivation of this thesis, the following aims have been defined

a. The provision of a general framework for the BER calculation in M-QAM systems. Independent bit mapping for the I and Q components will be assumed, which includes the common case of Gray mapping.

b. The derivation of exact closed-form expressions for the BER of MIMO and OFDM systems in some scenarios of interest. The analyzed scenarios will include one or several of the following effects:

   - Imperfect CSI (ICSI).

   - Rayleigh and Ricean fading.

   - Rayleigh and Ricean faded interferences.

   - Transmit beamforming.

   - Alamouti transmit diversity technique.

   - Multibranch reception with maximal ratio combining (MRC).

   - DC offset.

   - I/Q Imbalance.

c. The derivation of approximate closed-form expressions for the BER of MIMO and OFDM systems in some scenarios of interest, which allow the provision of a better insight into the system performance.

The analyzed scenarios must allow that the decision metric may be expressed in terms of a general quadratic form in complex Gaussian RVs. Hence, a common procedure can be used for the analysis of the different scenarios which are to be considered in this thesis.

With these aims, the contents of this thesis are structured as follows. The first two chapters are devoted to introduce the mathematical tools which have been used and developed in this work. Particularly,

- Chapter 2 presents the general framework for the BER calculation of M-QAM systems.

- Chapter 3 illustrates some key aspects related with the problem of probability calculation, and provides analytical results when general quadratic forms in complex Gaussian RVs with and without circular symmetry are considered.

Chapters 4 to 6 use these tools to analyze different MIMO and OFDM systems, which had not been previously analyzed in exact closed-form in the literature. Additional approximate expressions are provided for particular scenarios of interest.

- In Chapter 4, two scenarios considering MIMO configurations in Ricean fading channels and ICSI are considered: (1) MRC reception in the presence of Ricean-faded Interferences, and (2) Alamouti transmission with MRC reception.

- In Chapter 5, the effects of two major impairments associated with OFDM systems with direct conversion are analyzed: (1) DC-offset and (2) I/Q imbalance. Rayleigh fading and ICSI are considered in both scenarios.

- Chapter 6 analyzes a MIMO-OFDM system under Rayleigh fading with ICSI at both the transmitter and receiver sides, where transmit beamforming and MRC reception are used.

Finally, the main conclusions and the future work are outlined in Chapter 7.

1.3 Publications

The following publications have been derived from the work developed in this thesis

- [18] Lopez-Martinez, F.J.; Martos-Naya, E.; Paris, J.F.; Goldsmith, A.J.; ,"BER Analysis for MIMO-OFDM Beamforming with MRC under Channel Prediction and Interpolation Errors," Global Telecommunications Conference, 2009. GLOBECOM 2009. IEEE , vol., no., pp.1-7, Nov. 30 2009-Dec. 4 2009.

- [19] Lopez-Martinez, F. J.; Martos-Naya, E.; Paris, J. F.; Fernandez-Plazaola, U.; , "Generalized BER Analysis of QAM and its Application to MRC under Imperfect CSI and Interference in Ricean Fading Channels," IEEE Transactions on Vehicular Technology, vol.59, no.5, pp. 2598-2604, June 2010.

- [20] Lopez-Martinez, F.J.; Martos-Naya, E.; Paris, J.F.; Entrambasaguas, J.T.; , "BER analysis of direct conversion OFDM systems with MRC under channel estimation errors," IEEE Communications Letters, vol.14, no.5, pp.423-425, May 2010.

- [21] Lopez-Martinez, F.J.; Martos-Naya, E.; Wong, K.K.; Entrambasaguas, J.T.; , "Closed-Form BER Analysis of Alamouti-MRC Systems with ICSI in Ricean Fading Channels," IEEE Communications Letters, accepted for publication.

- [22] Lopez-Martinez, F.J.; Martos-Naya, E.; Paris, J.F.; Entrambasaguas, J.T.; , "Exact Closed-Form BER Analysis of OFDM Systems with ICSI in the presence of IQ imbalance," IEEE Transactions on Wireless Communications, 2nd round of reviews.

Chapter 2

Generalized BER analysis of QAM systems

THIS chapter presents a general framework for the performance analysis of M-QAM systems. This methodology is valid for any QAM system with independent bit mapping for the in-phase (I) and quadrature (Q) components, and includes previous analyses in the literature as particular cases.

This framework allows for the separation of the analysis in two main tasks, which can be performed independently: the calculation of *elementary coefficients*, which values depend only on the constellation mapping, and the calculation of *components of error probability*, which values depend on the probability distribution of the random variables.

Firstly, the related work in the literature is briefly outlined in Section 2.1. Then, the proposed framework is introduced in Section 2.2, providing expressions for a general case (where no assumptions about the statistical distributions of the RVs are made) as well as for some simplified scenarios of interest in communications. Finally, the calculation of the elementary coefficients is accomplished in Section 2.3, for an arbitrary constellation mapping. Compact expressions for the elementary coefficients are also provided for the usual case of Gray mapping.

2.1 Related Work

QAM is today the most extended modulation scheme in modern communication systems [23], either in monocarrier transmission or in combination with other schemes: adaptive modulation [24], multicarrier transmission [15] or MIMO systems [10]. BER analysis in QAM systems has been widely studied by many authors.

For AWGN channels, closed-form expressions for arbitrary QAM with Gray mapping are obtained in [16], based on the empirical observation of regular patterns in the constellation mapping. In [25], an exact expression for the BER in QAM systems with arbitrary bit-mapping is proposed, based on the Hamming distance between symbols. This technique requires to calculate the probability of a received symbol to be within a square region in the two-dimensional Euclidean space formed by the I and Q components.

In the case of fading channels, different results have been obtained. In [14], approximated expressions for the BER in Rayleigh fading channels with imperfect CSI (ICSI) are obtained when 16/64-QAM modulation is used. Closed-form expressions for different scenarios are obtained in [9, 15, 26], and [27], but their results are calculated separately for particular QAM constellations. Finally, Najafizadeh and Tellambura [17] present a general expression for the BER of an arbitrary QAM constellation with Gray mapping. Similarly to [16], the analysis is based on the observation of a regular pattern in the constellation mapping. This result is used to analyze the BER in systems with MRC diversity with ICSI in generalized Ricean fading channels.

Previous results allow for the exact BER computation in QAM systems for many scenarios, but under some restrictions. Particularly, the analysis presented in [16] is valid in scenarios with Gray mapping, perfect channel state information (PCSI) and noise with circularly symmetric PDF. On the other hand, the analysis in [17] assumes Gray mapping and equivalent noise with circularly symmetric PDF.

Here, we propose a new framework which allows to unify the BER calculation in QAM based systems. This methodology is valid for any QAM-based system, independently of the

constellation mapping or the distribution of the channel gain and the noise. The only restriction in our analysis is that in-phase and quadrature components can be detected separately, that is, independent bit mapping. The BER expression obtained in our analysis is expressed as a weighted sum of components of error probability (CEPs) which depend on the probability distribution of the random variables in the scenario under analysis. The calculation of these weights (namely *elementary coefficients*) depends on the particular constellation mapping, so it can be tackled separately.

In contrast to [16] and [17], where the final expressions are derived attending to the observation of regular patterns in the bit mapping, our method provides a mathematical background to the analysis. Unlike [25], our method only needs to calculate the probability of a received symbol to be within a half-plane in the I-Q plane, which is generally easier to derive.

2.2 Generalized BER Analysis

2.2.1 Analytical Framework

Let us consider the general problem of the BER calculation when the symbol y to be detected can be expressed in the following canonical form

$$y = az + \zeta, \tag{2.2.1}$$

where a (gain mismatch) and ζ (equivalent noise) are complex random variables in the most general case. In this model, the gain mismatch a accounts for the effect of imperfect channel compensation, whereas the equivalent noise ζ includes the effect of additive noise, interferences and other receiver impairments.

Let z be the transmitted symbol, belonging to a rectangular QAM constellation which consists on the composition of two L_1-PAM and L_2-PAM constellations associated with the in-phase and quadrature signal components, respectively. Since different bits are mapped onto I and Q components for this family of constellations, both the I and Q components can be detected separately. Thus, the only restriction in the forthcoming analysis relies in the consideration of independent bit mapping for I and Q components.

Fig. 2.1 shows an example of a 64-QAM constellation, useful to present the adopted notation. The set of complex symbols is $\{s_{u,v} = (2u - L_1 - 1)d + j(2v - L_2 - 1)d\}_{u=1,\ldots,L_1;v=1,\ldots,L_2}$, where $2d$ is the minimum distance between symbols. Every $s_{u,v}$ symbol has associated a set of bits of the I component $\{b_i^{\mathcal{I}}(u)\}_{i=1,\ldots,\log_2(L_1)}$ and a set of the Q component $\{b_i^{\mathcal{Q}}(v)\}_{i=1,\ldots,\log_2(L_2)}$. The set of decision boundaries for the I and Q components are $\{\mathcal{B}_{\mathcal{I}}(k) = (2k - L_1)d\}_{k=1,\ldots,L_1-1}$ and $\{\mathcal{B}_{\mathcal{Q}}(k) = j(2k - L_2)d\}_{k=1,\ldots,L_2-1}$ respectively.
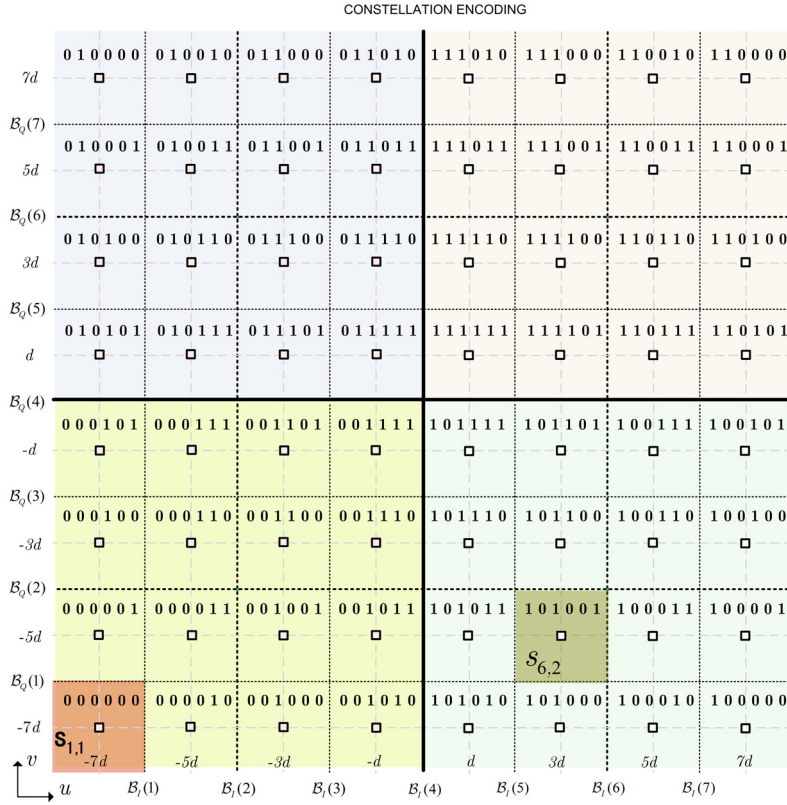
Figure 2.1: 64-QAM constellation with independent mapping of I and Q component. The bits for I and Q components are mapped as $\{b_3^{\mathcal{I}}(u); b_3^{\mathcal{Q}}(v); b_2^{\mathcal{I}}(u); b_2^{\mathcal{Q}}(v); b_1^{\mathcal{I}}(1); b_1^{\mathcal{Q}}(v)\}$, e.g. $s_{6,2} = 101001$.

The BER of the considered rectangular QAM constellations can be expressed as the average, over all the bits and transmitted symbols, of the error probability of a given bit

conditioned on a given transmitted symbol

$$BER_{\text{QAM}} = \frac{1}{L_1 L_2} \sum_{u=1}^{L_1} \sum_{v=1}^{L_2} \frac{1}{\log_2(L_1 L_2)} \left\{ \sum_{i=1}^{\log_2(L_1)} P_{\mathcal{I}}(i, u, v) + \sum_{i=1}^{\log_2(L_2)} P_{\mathcal{Q}}(i, u, v) \right\}, \quad (2.2.2)$$

where $P_{\mathcal{I}}(i, u, v) = \Pr\{\text{error in } b_i^{\mathcal{I}}(u)|\ z = s_{u,v}\}$ and $P_{\mathcal{Q}}(i, u, v) = \Pr\{\text{error in } b_i^{\mathcal{Q}}(v)|\ z = s_{u,v}\}$, respectively. Each term $P_{\mathcal{I}}(i, u, v)$ can be calculated as a linear combination of probabilities of the real part of the received symbol y to be above or below of a variable number of decision boundaries. This assert is also valid for the Q component terms, when considering the imaginary part of y. For example, the error probability of bit $\{b_2^{\mathcal{I}}(1)\}$ of the symbol y conditioned on transmitted symbol $z = s_{1,1}$ is (considering the bit mapping used in Fig. 2.1) expressed as

$$P_{\mathcal{I}}(2, 1, 1) = \Pr\{\Re\{y - \mathcal{B}_{\mathcal{I}}(2)\} > 0|\ z = s_{1,1}\} - \Pr\{\Re\{y - \mathcal{B}_{\mathcal{I}}(6)\} > 0|\ z = s_{1,1}\}. \quad (2.2.3)$$

The idea underlying the example in (2.2.3) can be formalized in order to write the BER expression (2.2.2) as

$$BER_{\text{QAM}} = \frac{1}{L_1 L_2} \sum_{u=1}^{L_1} \sum_{v=1}^{L_2} \frac{1}{\log_2(L_1 L_2)} \left[\sum_{i=1}^{\log_2(L_1)} \left\{ \sum_{k=1}^{u-1} \alpha_u^-(i, k) \cdot \mathcal{I}_{u,v}^-(k) + \sum_{k=u}^{L_1-1} \alpha_u^+(i, k) \cdot \mathcal{I}_{u,v}^+(k) \right\} \right.$$
$$\left. + \sum_{i=1}^{\log_2(L_2)} \left\{ \sum_{k=1}^{v-1} \beta_v^-(i, k) \cdot \mathcal{Q}_{u,v}^-(k) + \sum_{k=v}^{L_2-1} \beta_v^+(i, k) \cdot \mathcal{Q}_{u,v}^+(k) \right\} \right],$$
$$(2.2.4)$$

where the *components of error probability* (CEP) are defined as

$$\mathcal{I}_{u,v}^-(k) = \Pr\{\Re\{y - \mathcal{B}_{\mathcal{I}}(k)\} < 0|\ z = s_{u,v}\}, \quad \mathcal{I}_{u,v}^+(k) = \Pr\{\Re\{y - \mathcal{B}_{\mathcal{I}}(k)\} > 0|\ z = s_{u,v}\},$$
$$\mathcal{Q}_{u,v}^-(k) = \Pr\{\Im\{y - \mathcal{B}_{\mathcal{Q}}(k)\} < 0|\ z = s_{u,v}\}, \quad \mathcal{Q}_{u,v}^+(k) = \Pr\{\Im\{y - \mathcal{B}_{\mathcal{Q}}(k)\} > 0|\ z = s_{u,v}\}.$$
$$(2.2.5)$$

The values of the *elementary coefficients* $\alpha_u^\pm(i, k)$ and $\beta_v^\pm(i, k)$ belong to the set $\{-1, 0, 1\}$ and represent changes in the corresponding value of bit i across the k-th decision boundary for the $s_{u,v}$ symbol: 0 indicates no bit value change, 1 indicates a bit change from the correct value to a wrong one, and -1 from the wrong value to the correct one. For the example presented in (2.2.3), the values for the elementary coefficients are $\alpha_1^+(2, 2) = 1$,

$\alpha_1^+(2,6) = -1$ and $\alpha_1^+(2,m) = 0$, for $m \in \{1,3,4,5,7\}$. Note that α and $\mathcal{I}$ are associated with the I component, whereas β and $\mathcal{Q}$ are associated with the Q component. The sign on the super index of α, β, $\mathcal{I}$ and $\mathcal{Q}$ indicates if the k-th decision boundary is below or above (respectively - or +) either the real part (for α and $\mathcal{I}$) or imaginary part (for β and $\mathcal{Q}$) of the symbol $s_{u,v}$. The calculation of these elementary coefficients is tackled in Section 2.3.

Since $\alpha_u^\pm(i,k)$ and $\beta_u^\pm(i,k)$ are the only constants that depend on the bit i, they can be grouped in the following way

$$\alpha_u^\pm(k) = \sum_{i=1}^{\log_2(L)} \alpha_u^\pm(i,k), \quad \beta_v^\pm(k) = \sum_{i=1}^{\log_2(L)} \beta_v^\pm(i,k). \tag{2.2.6}$$

This leads to the final BER expression

$$BER_{\text{QAM}} = \frac{1}{L_1 L_2} \sum_{u=1}^{L_1} \sum_{v=1}^{L_2} \frac{1}{\log_2(L_1 L_2)} \left[\sum_{k=1}^{u-1} \alpha_u^-(k) \cdot \mathcal{I}_{u,v}^-(k) + \sum_{k=u}^{L_1-1} \alpha_u^+(k) \cdot \mathcal{I}_{u,v}^+(k) \right.$$
$$\left. + \sum_{k=1}^{v-1} \beta_v^-(k) \cdot \mathcal{Q}_{u,v}^-(k) + \sum_{k=v}^{L_2-1} \beta_v^+(k) \cdot \mathcal{Q}_{u,v}^+(k) \right]. \tag{2.2.7}$$

Hence, expression (2.2.7) allows for the exact BER calculation in any scenario which can be reduced to the canonical form $y = az + \zeta$, independently of the distribution of the random variables a and ζ. Thus, the derivation of the BER expression is reduced to two main calculations: the *elementary coefficients*, whose value only depends on the constellation mapping, and the CEPs, whose expression is determined only by the distribution of the random variables a and ζ.

Although expression (2.2.7) is general, some simplifications can be done for particular scenarios of interest in order to obtain more compact expressions. For the sake of clarity and without loss of generality, square M-QAM is considered ($M = L^2$) in the forthcoming analysis. However, equivalent expressions for rectangular QAM or PAM can be obtained by following the same procedure.

2.2.2 Arbitrarily distributed gain mismatch and circularly symmetric noise

Preliminary definitions

Definition 1. *A random variable z is said to be circularly symmetric with respect to μ if $z - \mu$ and $z' \triangleq (z - \mu)\, e^{j\theta}$ have the same distribution $\forall \theta$. In case $\mu = 0$, it is usual to omit the center of symmetry in the definition of circular symmetry [13].*

Corollary 1. *Let $z \triangleq x + jy$ be a complex continuous circularly symmetric RV. Then x and y are identically distributed RVs, and the PDFs of x and y are even functions.*

Proof. Let the PDF of z be denoted as $f_Z(z) = f_{X,Y}(x,y)$. According to Definition (1), we have $z' = ze^{j\theta} = x' + jy'$. Therefore,

$$x \triangleq g_1(x',y') = x'\cos\theta + y'\sin\theta, \tag{2.2.8}$$

$$y \triangleq g_2(x',y') = -x'\sin\theta + y'\cos\theta. \tag{2.2.9}$$

Then, the function $f_{X',Y'}(x',y')$ can be calculated as

$$f_{X',Y'}(x',y') = f_{X,Y}(x,y)\,\big|_{x=g_1(x',y'),y=g_2(x',y')}\,|\mathcal{J}|, \tag{2.2.10}$$

where $|\mathcal{J}|$ is the Jacobian of the transformation of random variables defined as

$$|\mathcal{J}| \triangleq \begin{vmatrix} \frac{\partial g_1}{\partial x'} & \frac{\partial g_1}{\partial y'} \\ \frac{\partial g_2}{\partial x'} & \frac{\partial g_2}{\partial y'} \end{vmatrix}. \tag{2.2.11}$$

Due to the circular symmetry of z, we have $f_{X',Y'}(x',y') \equiv f_{X,Y}(x',y')$. Hence,

$$f_{X,Y}(x'\cos\theta + y'\sin\theta, -x'\sin\theta + y'\cos\theta) = f_{X,Y}(x',y'). \tag{2.2.12}$$

For different values of θ, we have

$$\theta = \frac{\pi}{2}, \qquad \implies \quad f_{X,Y}(y',-x') = f_{X,Y}(x',y'); \tag{2.2.13}$$

$$\theta = \pi, \qquad \implies f_{X,Y}(-x',-y') = f_{X,Y}(x',y'); \tag{2.2.14}$$

$$\theta = \frac{3\pi}{2}, \qquad \implies \quad f_{X,Y}(-y',x') = f_{X,Y}(x',y'). \tag{2.2.15}$$

Using these symmetries, it is easy to see that

$$f_X(x) = \int_{-\infty}^{\infty} f_{X,Y}(x,y)dy = \int_{-\infty}^{\infty} f_{X,Y}(-x,-y)dy = f_X(-x); \tag{2.2.16}$$

$$f_X(x) = \int_{-\infty}^{\infty} f_{X,Y}(x,y)dy = \int_{-\infty}^{\infty} f_{X,Y}(y,-x)dy = f_Y(-x) = f_Y(x). \tag{2.2.17}$$

$\square$

Simplified BER expression

Let us consider a scenario where the equivalent noise ζ is a circularly symmetric RVs with respect to zero.

Due to the circular symmetry, the real and imaginary parts of ζ are identically distributed, and hence the quadrature CEPs are equivalent to the in-phase CEPs, i.e $\mathcal{I}_{u,v}^{\pm}(k) = \mathcal{Q}_{L-v+1,u}^{\pm}(k)$. Besides, as the PDF of the real and imaginary parts of ζ are assumed to be even functions, the CEPs also present the following symmetry $\mathcal{I}_{u,v}^{+}(k) = \mathcal{I}_{L-u+1,L-v+1}^{-}(L - k)$. Summarizing, we can write

$$BER_{\text{QAM}} = \sum_{u=1}^{L} \sum_{v=1}^{L} \sum_{k=u}^{L-1} \omega_u(k) \cdot \mathcal{I}_{u,v}^{+}(k), \qquad (2.2.18)$$

where

$$\omega_u(k) = \frac{1}{M} \frac{1}{\log_2(M)} \left[\alpha_u^{+}(k) + \alpha_{L-u+1}^{-}(L - k) + \beta_u^{+}(k) + \beta_{L-u+1}^{-}(L - k) \right]. \qquad (2.2.19)$$

Therefore, the derivation of a closed-form expression for the BER is reduced to the calculation of the CEP $\mathcal{I}_{u,v}^{+}(k)$. For the particular case of Gray mapping, the resultant expression (2.2.18) is formally equivalent to that given in [17].

2.2.3 No gain mismatch and circularly symmetric noise

Another typical scenario in communications is presented when ideal channel compensation is assumed at the receiver (i.e. $a = 1$). This consideration allows for the application of additional simplifications. Thus, assuming that there is no gain mismatch, consequently there is no cross-quadrature interference. Hence, the Q component of the transmitted symbol z has no influence on the in-phase CEP, and vice versa. Thereby, equivalent CEPs can be defined

$$\mathcal{I}_u^{\pm}(k) \triangleq \mathcal{I}_{u,v}^{\pm}(k), \quad \mathcal{Q}_v^{\pm}(k) \triangleq \mathcal{Q}_{u,v}^{\pm}(k). \qquad (2.2.20)$$

Moreover, the CEPs depend both on the distance between the transmitted symbol z and the decision boundary and on the fact that z is above or below a certain boundary.

Therefore, e.g. $\mathcal{I}_u^+(k)$ can be expressed as

$$
\begin{aligned}
\mathcal{I}_u^+(k) &= \Pr\left\{\Re\left\{y - \mathcal{B}_\mathcal{I}(k)\right\} > 0 \middle| z = s_{u,v}\right\} = \Pr\left\{\Re\left\{y - s_{u,v}\right\} > \Re\left\{\mathcal{B}_\mathcal{I}(k) - s_{u,v}\right\}\right\} \\
&= \Pr\left\{\Re\left\{\zeta\right\} > (2(k-u)+1)d\right\}.
\end{aligned}
\tag{2.2.21}
$$

Thus, we can exploit these symmetries to define

$$
\begin{aligned}
\mathcal{I}^+(m) &\triangleq \mathcal{I}_u^+(u+m-1), & 1 \le m \le L - u, \\
\mathcal{Q}^+(m) &\triangleq \mathcal{Q}_v^+(v+m-1), & 1 \le m \le L - v, \\
\mathcal{I}^-(m) &\triangleq \mathcal{I}_u^-(u-m), & 1 \le m \le u - 1, \\
\mathcal{Q}^-(m) &\triangleq \mathcal{Q}_v^-(v-m), & 1 \le m \le v - 1.
\end{aligned}
\tag{2.2.22}
$$

Considering that PDF of ζ is circularly symmetric, we can write:

$$
\mathcal{I}^+(m) = \mathcal{I}^-(m) = \mathcal{Q}^+(m) = \mathcal{Q}^-(m) = \Pr\left\{\Re\left\{\zeta\right\} > (2m-1)d\right\}.
\tag{2.2.23}
$$

Under these assumptions, the previous definitions allow us to obtain the following compact BER expression

$$
BER_{\text{QAM}} = \sum_{m=1}^{L-1} \omega(m)\mathcal{I}^+(m),
\tag{2.2.24}
$$

where

$$
\omega(m) = \frac{1}{M\log_2(M)}\left[\sum_{u=1}^{L-m} \alpha_u^+(u+m-1) + \alpha_{u+m}^-(u) + \beta_u^+(u+m-1) + \beta_{u+m}^-(u)\right].
\tag{2.2.25}
$$

An equivalent expression can be derived for a L-PAM

$$
BER_{\text{PAM}} = \sum_{m=1}^{L-1} \omega(m)\mathcal{I}^+(m),
\tag{2.2.26}
$$

where

$$
\omega(m) = \frac{1}{L\log_2(L)}\left[\sum_{u=1}^{L-m} \alpha_u^+(u+m-1) + \alpha_{u+m}^-(u)\right].
\tag{2.2.27}
$$

In the particular case of Gray mapping, expressions (2.2.24) and (2.2.26) are formally equivalent to the expression obtained in [16]. In the special case of BPSK, it is easy to show that (2.2.24) reduces to

$$
BER_{\text{BPSK}} = \mathcal{I}^+(1).
\tag{2.2.28}
$$
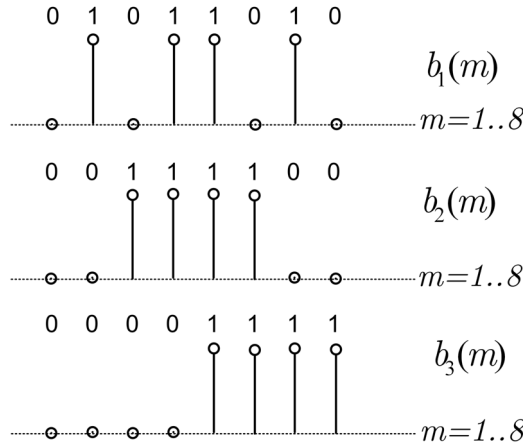
Figure 2.2: Definition of the mapping sequence of Fig. 2.1 as a set of discrete time signals.

2.3 Calculation of Elementary Coefficients

The closed-form expressions for the BER calculated in the previous Section are reduced to a weighted sum of CEPs. The weights or *elementary coefficients*, namely α and β in (2.2.7), are constants which value only depends on the constellation mapping. In this Section, we tackle the calculation of these constants from a novel point of view, based on the definition of the constellation mapping as a set of discrete time signals. Firstly, we illustrate the calculation procedure for a generic constellation mapping, and then we particularize for the relevant case of Gray mapping.

2.3.1 General Case

Let the bit sequence to be mapped in the QAM constellation (either in I or Q components) be expressed, for instance, as depicted in Fig. 2.2, where the index $i = 1 \ldots \log_2 L$ addresses the bits within each symbol whereas $m = 1 \ldots L$ points the symbol along the I or Q components. Note that the bit sequence in Fig. 2.2 is coincident with the constellation in Fig. 2.1, and corresponds to a 64-QAM with independent bit mapping (although not Gray mapping).

Let us consider the bit sequence as a set of i discrete time signals denoted as $b_i(m)$, in order to mathematically represent the binary values in the i-th bit of the m-th symbol. From

this definition, the discrete derivative of the bit sequence in the k-th boundary is given by

$$b_i'(k) = b_i(k+1) - b_i(k), \quad 1 \leq k \leq L-1. \tag{2.3.1}$$

Note that $b_i(m)$ may represent either $b_i^{\mathcal{I}}(u)$ or $b_i^{\mathcal{Q}}(v)$ according to the notation in Fig. 2.1. Expression (2.3.1) provides us the information about the bit error occurrence after boundary crossing. In this case, according to the constellation mapping in the example, the expression for the bit $i = 2$ is $b_2'(k) = [0, 1, 0, 0, 0, -1, 0]$. The interpretation of $b_i'(k)$ values is done as follows: 0 indicates no bit value change, 1 indicates a bit change from 0 to 1, and -1 indicates a change from 1 to 0.

Since the elementary coefficients $\alpha_u^\pm(i,k)$ and $\beta_v^\pm(i,k)$ represent changes in the detected value of bit i across the k-th decision boundary, we can directly express the elementary coefficients (e.g. α^+) as:

$$\alpha_u^+(i,k) = (1 - 2b_i(u))b_i'(k), \tag{2.3.2}$$

where $(1 - 2b_u(i))$ operation is performed to translate the values of $b_i(u)$ from the set $\{0, 1\}$ to $\{1, -1\}$. The calculation of $\alpha_u^-(i,k)$ and $\beta_v^\pm(i,k)$ is performed in a similar way

$$\begin{aligned}
\alpha_u^-(i,k) &= -(1 - 2b_i(u))b_i'(k), \\
\beta_v^+(i,k) &= (1 - 2b_i(v))b_i'(k), \\
\beta_v^-(i,k) &= -(1 - 2b_i(v))b_i'(k).
\end{aligned} \tag{2.3.3}$$

2.3.2 Gray Mapping

For the relevant case of Gray mapping, an explicit expression for the calculation of elementary coefficients can be derived. First, we will focus on the case of the coefficients $\alpha_u^+(i,k)$ associated with the I component. The remainder coefficients $\alpha_u^-(i,k)$, $\beta_v^+(i,k)$ and $\beta_v^-(i,k)$ are deduced in a similar way.

Let us observe the sequence $b_i(u)$ of the bits with Gray mapping for square M-QAM along the I component, for the case of $M = 256$, as depicted in figure 2.3. The index $i = 1 \ldots \log_2 L$ addresses the bits within each symbol whereas $u = 1 \ldots L$ points the symbol along the I component. If the bit sequence is considered as a set of i discrete time signals,
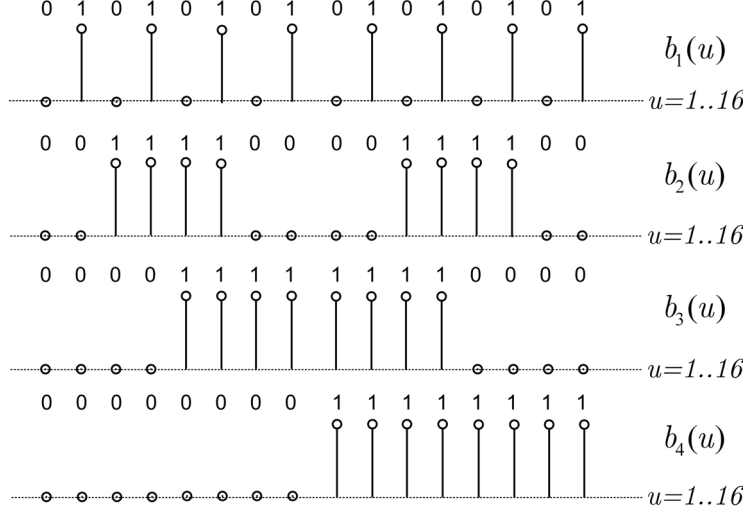
Figure 2.3: Definition of a 256-QAM Gray mapping sequence as a set of discrete time signals.

we can easily deduce the following mathematical representation for the binary value in the i-th bit of the u-th symbol

$$b_i(u) = \frac{1}{2}\left(1 - \Omega\left(i, u\right)\right), \tag{2.3.4}$$

where $\Omega(i, x)$ is defined in (2.3.5) as

$$\Omega\left(i, x\right) \triangleq \text{sign}\left\{\cos\left(\omega_i(x - 1/2)\right)\right\}, \tag{2.3.5}$$

and the frequency $\omega_i = \frac{2\pi}{2^{i+1}}$ accounts for the periodicity of the discrete signal $b_i(u)$.

Otherwise, the discrete derivative of the bits sequence in the k-th boundary is given by

$$b_i'(k) = b_i(k+1) - b_i(k) = \frac{1}{2}\left(\Omega\left(i, k\right) - \Omega\left(i, k+1\right)\right) = \frac{1}{2}\left(\Omega\left(i, k\right) - \Omega\left(i, -k\right)\right), \tag{2.3.6}$$

where $k = 1 \ldots L - 1$. Hence, combining (2.3.4) and (2.3.6) we obtain the following expression

$$\alpha_u^+(i, k) = (1 - 2b_i(u))b_i'(k) = \frac{1}{2}\Omega\left(i, m\right)\left[\Omega\left(i, k\right) - \Omega\left(i, -k\right)\right]. \tag{2.3.7}$$

The remainder coefficients $\alpha_u^-(i, k)$, $\beta_v^+(i, k)$ and $\beta_v^-(i, k)$ can be deduced following the same procedure, yielding

$$\alpha_m^\pm(i, k) = \beta_m^\pm(i, k) = \pm\frac{1}{2}\Omega\left(i, m\right)\left[\Omega\left(i, k\right) - \Omega\left(i, -k\right)\right], \tag{2.3.8}$$

18

where $m = u$ or $m = v$ for $\alpha^{\pm}$ or $\beta^{\pm}$ coefficients, respectively.

As previously stated, $\alpha_u^{\pm}(i, k)$ and $\beta_v^{\pm}(i, k)$ are the only constants in (2.2.4) that depend on the bit i. Therefore, they can be grouped as

$$\alpha_m^{\pm}(k) = \sum_{i=1}^{\log_2(L)} \pm \frac{1}{2} \Omega(i, m) \left[\Omega(i, k) - \Omega(i, -k) \right] = \beta_m^{\pm}(k). \tag{2.3.9}$$

2.4 Discussion

In this chapter, a general framework for the BER analysis of QAM systems with independent bit-mapping has been presented. Using the proposed methodology, the BER is expressed as a weighted sum of components of error probability, where the values of the weights or *elementary coefficients* only depends on the constellation mapping.

A closed-form expression is given for a general scenario (2.2.7), and additional simplified expressions are provided for two particular scenarios of interest in communications: (1) circularly symmetric equivalent noise (2.2.18), and (2) perfect channel estimation with circularly symmetric equivalent noise (2.2.24).

Additionally, a systematic procedure for the calculation of the elementary coefficients is presented, which enables an easy computation for any constellation mapping (2.3.3). Compact results are also given for the relevant case of Gray mapping (2.3.8).

The proposed framework is to be used in Chapters 4 to 6 to obtain closed-form expressions for the BER in a number of scenarios. The main contributions of this section have been published in [19].

Chapter 3

BER analysis using quadratic forms in complex Gaussian RVs

IN this chapter, we tackle the problem of the error probability calculation in systems where the decision variable at the receiver side can be expressed in terms of a general quadratic form in complex Gaussian RVs.

The contents of this chapter can be summarized as follows: Firstly, the most usual strategies for probability calculation in the literature are presented. Then, we focus on the probability calculation using complex Gaussian quadratic forms, which is the approach to be used in this thesis. Separate analyses are provided depending whether the involved RVs are circularly symmetric or not. In both cases, exact expressions for the calculated probabilities are obtained, as well as approximate expressions for some particular scenarios of interest.

In the following, we use * to denote the *complex conjugate* operation, $|\cdot|$ to indicate the modulus of a complex number, and $\mathrm{E}\{\cdot\}$ to represent the expectation operation. The superindex ^{T} is used to indicate the *transpose* operation, and $^{\mathcal{H}}$ denotes *conjugate transpose* operation.

3.1   Formulation

In most scenarios, the major difficulty in carrying out performance analysis of communication systems is to calculate the probability that a random variable X is greater (or smaller,

equivalently) than a certain value X_0, i.e., $\Pr\{X < X_0\}$. Hence, depending on the statistical distribution of X, the calculation of $\Pr\{X < X_0\}$ may be conducted under different approaches.

The more direct strategy is the calculation of the cumulative distribution function (CDF) $F_X(x)$, which represents the probability that the random variable X takes on a value less than or equal to X_0, i.e., $F_X(X_0) = \Pr\{X \leq X_0\}$. Unfortunately, the CDF calculation may result unfeasible for many practical statistical distributions of X, and therefore alternative approaches must be taken in order to calculate analytical expressions for these probabilities.

3.1.1 Probability Density Function

The probability density function (PDF) of a random variable X, namely $f_X(x)$, describes the probability of a random variable to take a certain value within the observation space. The probability of a X to fall within a given range of values is given by the integral of its PDF over this range, as

$$\Pr\{a < x \leq b\} = \int_a^b f_X(x)dx. \tag{3.1.1}$$

Hence, the relationship between the PDF and CDF is clearly established as

$$F_X(X_0) = \int_{-\infty}^{X_0} f_X(x)dx. \tag{3.1.2}$$

3.1.2 Moment Generating Function

The moment generating function (MGF) of a random variable X is defined as

$$M_X(t) \triangleq \mathrm{E}\{e^{tX}\} = \int_{-\infty}^{\infty} e^{tx}dF_X(x). \tag{3.1.3}$$

The MGF is often used as a calculation tool, since its mth derivative evaluated at $t = 0$ provides the mth moment of X. Besides, it allows to compute the PDF (in case this PDF is a continuous function) by taking the inverse two-sided Laplace transform of $M_X(t)$. However, the calculation of the PDF when the MGF is known is usually performed through identification, since there exist a uniqueness relationship between $M_X(t)$ and $f_X(x)$.

3.1.3 Characteristic Function

The characteristic function $\Phi_X(\omega)$ of a random variable X is defined as

$$\Phi_X(\omega) \triangleq \mathrm{E}\{e^{j\omega X}\} = \int_{-\infty}^{\infty} e^{j\omega x} dF_X(x). \tag{3.1.4}$$

In case the PDF exists, the characteristic function is related with the PDF via the Fourier transform. In some scenarios, either the moments or the MGF may not exist, since the involved integrals are not convergent. On the contrary the characteristic function always exists, and hence it is used instead.

3.1.4 Conditional Probability

In some cases the probability $\Pr\{X < X_0\}$ cannot be calculated in closed-form, specially when the RV X is composed by a combination of individual RVs with different statistical distributions, i.e., $X = g(X_1, \ldots, X_m)$. In this situation, it may result more appropriated to generate an auxiliary RV, namely Y, conditioned to a particular value of a set of X_i, i.e., $\{Y(X_i) \triangleq X \,|X_i\}$. Hence, $\Pr\{Y(X_i) < X_0\}$ is referred to as the conditional probability.

Thus, the probability $\Pr\{X < X_0\}$ can be calculated as

$$\Pr\{X < X_0\} = \int_{-\infty}^{\infty} f_Y(X_0, X_i) p(X_i) dX_i, \tag{3.1.5}$$

where $p(X_i)$ is the PDF of the RV set X_i.

3.1.5 General Quadratic Forms

In many communication systems, it is very usual that the decision variable can be expressed as a special case of the general quadratic form D, as

$$D \triangleq \sum_{k=1}^{L} A|X_k|^2 + B|Y_k|^2 + CX_kY_k^* + C^*X_k^*Y_k, \tag{3.1.6}$$

where $A, B \in \mathbb{R}$ and $C \in \mathbb{C}$ are constant values, and X_k and Y_k are in general pairs of arbitrarily distributed complex RVs. In this thesis, we will focus on the special case of general quadratic forms in complex Gaussian RVs, which naturally appear in many scenarios when evaluating the performance analysis in terms of the BER.

3.2 Quadratic forms in circularly symmetric complex Gaussian RVs

3.2.1 Exact analysis

Let us consider a general quadratic form (3.1.6), in complex valued Gaussian RVs. In the following, we will use the compact notation for quadratic forms introduced in [10], as

$$D = \sum_{k=1}^{L} \mathbf{x}_k^T \mathbf{Q} \mathbf{x}_k, \tag{3.2.1}$$

where the RV vector $\mathbf{x}_k$ and the quadratic form matrix $\mathbf{Q}$ are given by

$$\mathbf{x}_k = \begin{bmatrix} X_k \\ Y_k \end{bmatrix}; \mathbf{Q} = \begin{bmatrix} A & C \\ C^* & B \end{bmatrix}. \tag{3.2.2}$$

In [6] it is presented a general exact closed-form expression for $\Pr\{D < 0\}$, under some restrictions:

- The X_k and Y_k are a pair of correlated complex-valued Gaussian RVs.

- The $\{X_k, Y_k\}$ L pairs are mutually statistically independent and identically distributed.

- The RVs $\{X_k - \mathrm{E}\{X_k\}\}$ and $\{Y_k - \mathrm{E}\{Y_k\}\}$ are circularly symmetric, i.e., their real and imaginary parts are independent and have the same variance [13].

In this scenario, the probability $\Pr\{D < 0\}$ can be calculated as

$$P_b \triangleq \Pr\{D < 0\} = \frac{1}{2\pi} \int_{-\infty}^{0} dD \int_{-\infty}^{\infty} \Phi(\omega) e^{-j\omega D} d\omega, \tag{3.2.3}$$

where $\Phi(\omega)$ is the characteristic function of D.

In [28], the characteristic function of a quadratic form in complex Gaussian RVs in the form $\mathbf{x}_k^T \mathbf{Q} \mathbf{x}_k$ is expressed as

$$\Phi(\omega) = \frac{\exp\left(\mathbf{m}_k^{\mathcal{H}} \mathbf{R}^{-1} \left[\mathbf{I} - (\mathbf{I} - j\omega \mathbf{R} \mathbf{Q})^{-1}\right] \mathbf{m}_k\right)}{|\mathbf{I} - j\omega \mathbf{R} \mathbf{Q}|}, \tag{3.2.4}$$

where $\mathbf{I}$ is the identity matrix, $\mathbf{m}_k \triangleq \mathrm{E}\{\mathbf{x}_k\}$ and $\mathbf{R} \triangleq \mathrm{E}\left\{(\mathbf{x}_k - \mathbf{m}_k)(\mathbf{x}_k^{\mathcal{H}} - \mathbf{m}_k^{\mathcal{H}})\right\}$ are the mean vector and the covariance matrix of $\mathbf{x}_k$, respectively.

After some algebra, the terms in (3.2.4) can be rearranged, leading the characteristic function to be expressed as

$$\Phi(\omega) = \frac{1}{(1 - j\omega\lambda_1)(1 - j\omega\lambda_2)} \exp\left(\frac{j\omega\mathbf{m}_k^{\mathcal{H}}\mathbf{Q}\mathbf{m}_k + \omega^2\lambda_1\lambda_2\mathbf{m}_k^{\mathcal{H}}\mathbf{R}^{-1}\mathbf{m}_k}{(1 - j\omega\lambda_1)(1 - j\omega\lambda_2)}\right), \qquad (3.2.5)$$

where λ_i are the eigenvalues of $\mathbf{RQ}$ matrix.

By means of changing the order of integration in (3.2.3), we can express

$$P_b = -\frac{1}{2\pi j}\int_{-\infty+j\varepsilon}^{\infty+j\varepsilon}\frac{\Phi(\omega)}{\omega}d\omega, \qquad (3.2.6)$$

where $\varepsilon > 0$ is a small number inserted to avoid the singularity at $\omega = 0$ in the integration path [6].

The final expression for P_b is given in exact closed-form [10] by

$$P_b = Q_1(a, b) + \sum_{m=0}^{L-1} C_m(a, b, \eta)I_m(ab) \times \exp\left\{-\frac{(a^2 + b^2)}{2}\right\}, \qquad (3.2.7)$$

where $Q_1(a, b)$ is the Marcum Q-function, $I_m(x)$ is the mth order Bessel function of the first kind, and a, b, η and $C_m(\cdot)$ parameters are calculated using the expressions in Table 3.1.

3.2.2 Approximate expression

Expression (3.2.7) allows for the exact calculation of $\Pr\{D < 0\}$ probability in closed-form. However, it may result useful to find an approximate expression which enables the provision of a better insight into the system performance. Here, we will use some asymptotical relationships between the special functions in (3.2.7) and the well-known Gaussian Q function, in order to derive approximate expressions for $\Pr\{D < 0\}$.

Particularly, we can use the asymptotic relations [5]

$$\begin{aligned} Q_1(a, b) &\sim \sqrt{\frac{b}{a}}Q(b - a), &&\text{when } b \to \infty, \\ I_m(ab) &\sim \frac{\exp(ab)}{\sqrt{2\pi ab}}, &&\text{when } a \cdot b \to \infty, \end{aligned} \qquad (3.2.8)$$

to express, after some algebra

$$\Pr\{D < 0\} \approx \sqrt{\frac{b}{a}}Q(b - a) + \frac{b - a}{\sqrt{ab}}\frac{\exp(-\frac{1}{2}(b - a)^2)}{\sqrt{2\pi}(b - a)}\sum_{m=0}^{N_R-1} C_m(a, b, \eta). \qquad (3.2.9)$$

Table 3.1: Probability computation of Gaussian quadratic form.

FUNCTIONS AND PARAMETERS	DEFINITIONS
$\{\lambda_i\}_{i=1,2}$	$\frac{1}{2}\operatorname{tr}(\mathbf{R}\mathbf{Q}) + (-1)^{i-1}\sqrt{\left(\frac{1}{2}\operatorname{tr}(\mathbf{R}\mathbf{Q})\right)^2 - \det(\mathbf{R}\mathbf{Q})}$
η	$\left\lvert\dfrac{\lambda_1}{\lambda_2}\right\rvert$
a	$\sqrt{\dfrac{2\lambda_2\left(\Sigma_{k=1}^{L}\mathbf{m}_k^{\mathcal{H}}\left[\mathbf{Q} - \lambda_1\mathbf{R}^{-1}\right]\mathbf{m}_k\right)}{(\lambda_1 - \lambda_2)^2}}$
b	$\sqrt{\dfrac{2\lambda_1\left(\Sigma_{k=1}^{L}\mathbf{m}_k^{\mathcal{H}}\left[\mathbf{Q} - \lambda_2\mathbf{R}^{-1}\right]\mathbf{m}_k\right)}{(\lambda_1 - \lambda_2)^2}}$
$C_m(a,b,\eta)$	$\begin{cases} -1 + \dfrac{1}{(1+\eta)^{2L-1}}\displaystyle\sum_{n=0}^{L-1}\binom{2L-1}{n}\eta^n, & m = 0 \\[2mm] \dfrac{1}{(1+\eta)^{2L-1}}\displaystyle\sum_{n=0}^{L-1-m}\binom{2L-1}{n}\left[\left(\dfrac{b}{a}\right)^m\eta^n - \left(\dfrac{a}{b}\right)^m\eta^{2L-1-n}\right], & m \neq 0 \end{cases}$

Finally, using the asymptotic relation for the Gaussian Q function, $Q(x) \sim \frac{\exp(-\frac{x^2}{2})}{\sqrt{2\pi x}}$, when $(b-a) \to \infty$, we obtain the final approximate expression

$$\Pr\{D < 0\} \approx T \cdot Q(b-a), \tag{3.2.10}$$

where T is a constant value defined as

$$T \triangleq \sqrt{\frac{b}{a}} + \frac{b-a}{\sqrt{ab}}\sum_{m=0}^{N_R-1} C_m(a,b,\eta). \tag{3.2.11}$$

3.3 Quadratic forms in non-circularly symmetric complex Gaussian RVs

3.3.1 Notation and preliminary concepts

Let $\mathbf{x} \in \mathbb{C}^{\mathbf{n}}$ and $\mathbf{A} \in \mathbb{C}^{\mathbf{m} \times \mathbf{P}}$. Then, we use the mappings $\mathbf{x} \to \breve{\mathbf{x}}$ and $\mathbf{A} \to \breve{\mathbf{A}}$ defined in [29], where

$$\breve{\mathbf{x}} \triangleq \left[\begin{array}{c} \Re(\mathbf{x}) \\ \Im(\mathbf{x}) \end{array} \right] = \left[\begin{array}{c} \mathbf{x_r} \\ \mathbf{x_i} \end{array} \right] \in \mathbb{R}^{2n}, \qquad \breve{\mathbf{A}} \triangleq \left[\begin{array}{cc} \Re(\mathbf{A}) & -\Im(\mathbf{A}) \\ \Im(\mathbf{A}) & \Re(\mathbf{A}) \end{array} \right] \in \mathbb{R}^{2m \times 2p}. \qquad (3.3.1)$$

Let $y \in \mathbb{C}$ be a complex RV. The real covariance matrix [13] of the composite real RV $\breve{\mathbf{y}}$ is denoted by

$$\Sigma_{\breve{\mathbf{y}}} \triangleq \mathrm{E}\{\breve{\mathbf{y}}\breve{\mathbf{y}}^T\} = \left[\begin{array}{cc} \sigma_{y_r}^2 & \sigma_{y_r y_i} \\ \sigma_{y_r y_i} & \sigma_{y_i}^2 \end{array} \right], \qquad (3.3.2)$$

and the variance of y is given by $\sigma_y^2 = \sigma_{y_r}^2 + \sigma_{y_i}^2$. According to (3.3.2), the RV y is said to be circularly symmetric if $\sigma_{y_r}^2 = \sigma_{y_i}^2$ and $\sigma_{y_r y_i} = 0$.

3.3.2 Exact analysis

In Section 3.2.1, a detailed analysis of general quadratic forms in complex-valued Gaussian RVs was presented, providing expressions for the calculation of $\Pr\{D < 0\}$ in terms of Marcum-Q and modified Bessel functions of the first kind. Nevertheless, these expressions are not valid when non-circularly symmetric RVs are considered. Here, we introduce the analysis of general quadratic forms in complex-valued non circularly-symmetric Gaussian RVs, for the particular case of zero-mean.

Let $D \triangleq A|X|^2 + B|Y|^2 + CXY^* + C^*X^*Y$ be a general quadratic form, which can be compactly expressed as

$$D = \mathbf{x}_k^T \mathbf{Q} \mathbf{x}_k, \qquad (3.3.3)$$

where

$$\mathbf{x}_k = \left[\begin{array}{c} X \\ Y \end{array} \right]; \mathbf{Q} = \left[\begin{array}{cc} A & C \\ C^* & B \end{array} \right]. \qquad (3.3.4)$$

Let us consider that the involved RVs are complex-valued non-circularly symmetric Gaussian RVs which real and imaginary parts are treated separately. Hence, adopting the notation

and the mappings presented in (3.3.1), we can express

$$D = \breve{\mathbf{x}}_k^T \breve{\mathbf{Q}} \breve{\mathbf{x}}_k. \tag{3.3.5}$$

In this scenario, the probability $\Pr\{D < 0\}$ can be calculated as

$$\Pr\{D < 0\} = \frac{1}{2\pi} \int_{-\infty}^{0} dD \int_{-\infty}^{\infty} \Phi(\omega) e^{-j\omega D} d\omega, \tag{3.3.6}$$

where $\Phi(\omega)$ is the characteristic function of D. By means of changing the order of integration, we can express

$$\Pr\{D < 0\} = -\frac{1}{2\pi j} \int_{-\infty+j\varepsilon}^{\infty+j\varepsilon} \frac{\Phi(\omega)}{\omega} d\omega, \tag{3.3.7}$$

where $\varepsilon > 0$ is a small number inserted to avoid the singularity at $\omega = 0$ in the integration path [6]. The characteristic function of D is given by

$$\Phi(\omega) = \frac{1}{\prod\limits_{i=1}^{4} \sqrt{1 - 2j\lambda_i \omega}}, \tag{3.3.8}$$

where λ_i are the eigenvalues of $\mathbf{R}\breve{\mathbf{Q}}$ matrix [30].

Since $\mathbf{Q}$ is an indefinite matrix, its two eigenvalues hold that ${}_{\mathbf{Q}}\lambda_1 > 0$ and ${}_{\mathbf{Q}}\lambda_2 < 0$. Using the properties of mapping $\mathbf{Q} \to \breve{\mathbf{Q}}$ given in [29], $\breve{\mathbf{Q}}$ matrix is also indefinite and its eigenvalues are double, such as ${}_{\breve{\mathbf{Q}}}\lambda_{1,2} = {}_{\mathbf{Q}}\lambda_1$ and ${}_{\breve{\mathbf{Q}}}\lambda_{3,4} = {}_{\mathbf{Q}}\lambda_2$. Therefore, as $\mathbf{R}$ is a positive-definite matrix, the resultant eigenvalues of $\mathbf{R}\breve{\mathbf{Q}}$ matrix hold that $\{\lambda_2 \geq \lambda_1 > 0\}$ and $\{\lambda_3 \leq \lambda_4 < 0\}$ under Sylvester's law of inertia [31]. Note that $\lambda_1 = \lambda_2$ and $\lambda_3 = \lambda_4$ only in the limit case of circular symmetry[1].

Combining (3.3.7) and (3.3.8), we obtain

$$\Pr\{D < 0\} = \frac{-1}{2\pi j} \int_{-\infty+j\varepsilon}^{\infty+j\varepsilon} \frac{d\omega}{\omega \prod\limits_{i=1}^{4} \sqrt{1 + j\frac{\omega}{\omega_i}}} \triangleq \int_{-\infty+j\varepsilon}^{\infty+j\varepsilon} \Upsilon(\omega) d\omega, \tag{3.3.9}$$

where $\omega_i \triangleq \frac{-1}{2\lambda_i}$. This integral can be calculated by contour integration as depicted in Fig. 3.1, where (3.3.9) is denoted as the integral along C_∞.

---

[1] For the particular case of circular symmetry, a 2×2 covariance matrix can be calculated as $\mathbf{R}_{\mathbb{C}} \triangleq \mathrm{E}\{\mathbf{x}_k \mathbf{x}_k^{\mathcal{H}}\}$. The eigenvalues of $\mathbf{R}_{\mathbb{C}}$ are $\lambda_a \equiv \lambda_1 = \lambda_2$ and $\lambda_b \equiv \lambda_3 = \lambda_4$, respectively.
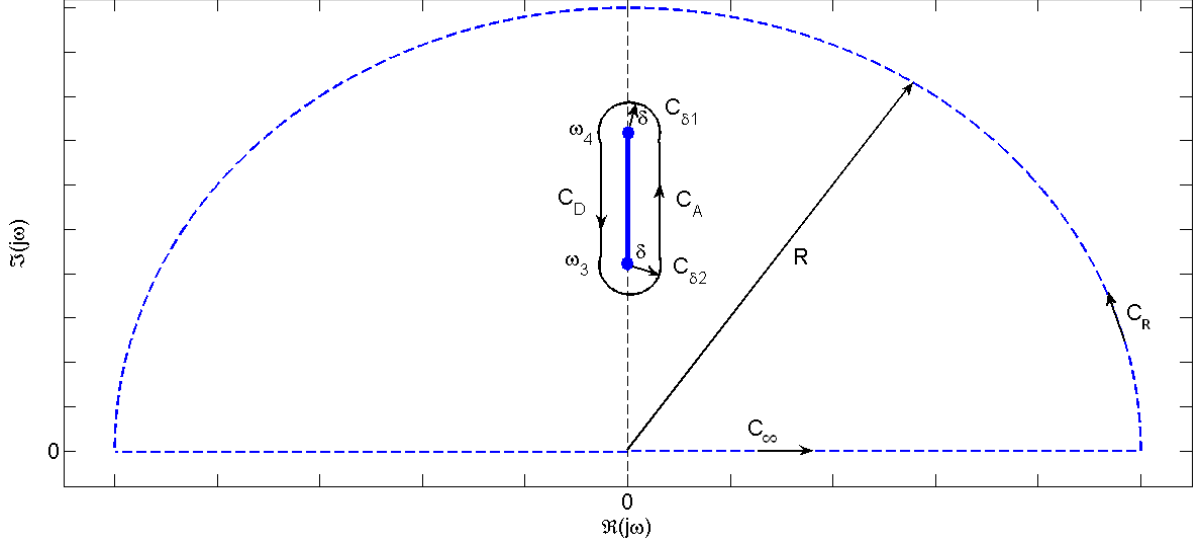
Figure 3.1: Contour integration for $\Pr\{\mathcal{D} < 0\}$ calculation around the branch cuts.

Since $\int_{C_R} \Upsilon(\omega)d\omega \to 0$ as $R \to \infty$, the integral in (3.3.9) is equivalent to the calculation of four integrals around the branch cuts of ω_3 and ω_4, as follows

$$\Pr\{D < 0\} = \int_{C_{\delta 1}} \Upsilon(\omega)d\omega + \int_{C_{\delta 2}} \Upsilon(\omega)d\omega + \int_{C_A} \Upsilon(\omega)d\omega + \int_{C_D} \Upsilon(\omega)d\omega. \qquad (3.3.10)$$

The integration paths can be parameterized as

$$C_{\delta 1} = \left\{ j\omega_4 + \delta e^{jt}; t \in [0, \pi) \right\}; \qquad (3.3.11)$$

$$C_{\delta 2} = \left\{ j\omega_3 - \delta e^{jt}; t \in [\pi, 2\pi) \right\}; \qquad (3.3.12)$$

$$C_A = \left\{ j\omega_3 - td_{3,4} + \delta; t \in [0, 1] \right\}; \qquad (3.3.13)$$

$$C_D = \left\{ j\omega_4 - td_{4,3} - \delta; t \in [0, 1] \right\}. \qquad (3.3.14)$$

When $\delta \to 0$, the integrals around C_{δ_1} and C_{δ_2} also tend to zero. The integral along the ascending path C_A can be expressed as

$$\int_{C_A} \Upsilon(\omega)d\omega = \frac{1}{2\pi j} \int_0^1 \frac{jd_{3,4}dt}{j(\omega_3 - td_{3,4})\prod_{i=1}^4 \sqrt{1 + j\frac{j(\omega_3 - td_{3,4})}{\omega_i}}}. \qquad (3.3.15)$$

After some algebra, we have

$$\int_{C_A} \Upsilon(\omega)d\omega = \frac{1}{2\pi}\sqrt{\frac{\omega_1\omega_2\omega_4}{\omega_3 d_{1,3}d_{2,3}}}\int_0^1 t^{-\frac{1}{2}}(1-t)^{-\frac{1}{2}}\left(1-t\frac{d_{3,4}}{\omega_3}\right)^{-1}\left(1+t\frac{d_{3,4}}{d_{1,3}}\right)^{-\frac{1}{2}}\left(1+t\frac{d_{3,4}}{d_{2,3}}\right)^{-\frac{1}{2}}dt.$$

(3.3.16)

This equation can be re-expressed in terms of the Lauricella F_D function, using its integral form [32] as

$$F_D\left(\frac{1}{2},1,\frac{1}{2},\frac{1}{2};1;a,b,c\right) = \frac{1}{\pi}\int_0^1 t^{-1/2}(1-t)^{-1/2}(1-at)^{-1}\left(1-bt\right)^{-1/2}\left(1-ct\right)^{-1/2}dt.$$

(3.3.17)

Hence, the final expression for the integral along C_A yields

$$\int_{C_A}\Upsilon(\omega)d\omega = \frac{1}{2}\sqrt{\frac{\omega_1\omega_2\omega_4}{d_{1,3}d_{2,3}\omega_3}}F_D\left(\frac{1}{2},1,\frac{1}{2},\frac{1}{2};1;\frac{d_{3,4}}{\omega_3},-\frac{d_{3,4}}{d_{1,3}},-\frac{d_{3,4}}{d_{2,3}}\right).$$

(3.3.18)

It can be shown that the integral along the descending path C_D is equal to (3.3.18). Therefore, the final expression for $\Pr\{D < 0\}$ is given by

$$\Pr\{D < 0\} = \sqrt{\frac{\omega_1\omega_2\omega_4}{d_{1,3}d_{2,3}\omega_3}}F_D\left(\frac{1}{2},1,\frac{1}{2},\frac{1}{2};1;\frac{d_{3,4}}{\omega_3},-\frac{d_{3,4}}{d_{1,3}},-\frac{d_{3,4}}{d_{2,3}}\right).$$

(3.3.19)

3.3.3   Approximate expressions

Approximation 1

Let the Lauricella function be expressed in integral form of Euler type [32] as

$$F_D(a,\{b_i\}_{i=1}^3;c;\{x_i\}_{i=1}^3) = \frac{\Gamma(c)}{\Gamma(a)\Gamma(c-a)}\int_0^1 t^{a-1}(1-t)^{c-a-1}\prod_{i=1}^3(1-x_it)^{-b_i}dt, \quad (3.3.20)$$

where $\Gamma(\cdot)$ is the Gamma function. According to the definitions in subsection 3.3.2, the ω_i can be grouped into pairs $\Omega_{1,2} \triangleq \{\omega_1,\omega_2\}$ and $\Omega_{3,4} \triangleq \{\omega_3,\omega_4\}$. Hence, it holds that

$$\{d_{i,j}/\omega_i,\omega_j \in \Omega_{i,j}\} \qquad\qquad \Rightarrow |d_{i,j}| << |\omega_k|,\ k \in \{1,\ldots,4\}, \qquad (3.3.21)$$

$$\{d_{i,j},d_{l,m}/\omega_i\cdot\omega_j > 0,\ \omega_l\cdot\omega_m < 0\} \qquad \Rightarrow |d_{l,m}| >> |d_{i,j}|. \qquad (3.3.22)$$

With these considerations, we have $d_{1,3} \approx d_{2,3}$ and hence $x_2 \approx x_3 = x$. Thus, the following relationship between Lauricella function and Appell hypergeometric function can

be found from (3.3.20), as

$$F_D(\frac{1}{2}, 1, \frac{1}{2}, \frac{1}{2}; 1; x_1, x, x) \equiv F_1(\frac{1}{2}, 1, 1; 1; x_1, x). \tag{3.3.23}$$

Hence, the probability $\Pr\{D < 0\}$ can be approximated by the following closed-form expression

$$\Pr\{D < 0\} \approx \sqrt{\frac{\omega_1 \omega_2 \omega_4}{d_{1,3} d_{2,3} \omega_3}} F_1\left(\frac{1}{2}, 1, 1; 1; \frac{d_{3,4}}{\omega_3}, \frac{d_{3,4}}{\bar{d}}\right), \tag{3.3.24}$$

where $F_1(\cdot)$ is the Appell hypergeometric function, and $\bar{d} \triangleq \frac{d_{1,3}+d_{2,3}}{2}$.

Approximation 2

From (3.3.21) and (3.3.22), it is easy to see that $|\omega_3| << |d_{1,3}|$ and $|d_{3,4}| <<< |d_{1,3}|$, respectively. Hence, it can be expected that $x \to 0$ in (3.3.24). Using some of the relationships given in [33, eq. 9.121], it yields

$$F_1(\frac{1}{2}, 1, 1; 1; x_1, x \to 0) \approx \frac{1}{\sqrt{1 - x_1}}. \tag{3.3.25}$$

Finally, after some algebra it is easy to obtain the following approximate expression

$$\Pr\{D < 0\} \approx \frac{\sqrt{\omega_1 \omega_2}}{\omega_3 - \frac{\omega_1 + \omega_2}{2}}. \tag{3.3.26}$$

3.4 Discussion

In this chapter, relevant expressions for the calculation of the probability of a general quadratic form D in complex Gaussian random variables to be less than zero are presented. Of special interest is the analysis of quadratic forms in non-circularly symmetric complex RVs, which had not been previously accomplished in the literature.

For the particular case of circularly symmetric RVs with arbitrary mean, an exact closed-form expression for this probability (3.2.7) is given in [6, 10], and an approximate closed-form expression (3.2.10) is proposed in this thesis. When non circularly symmetric RVs with zero mean are considered, exact (3.3.19) and approximate (3.3.24, 3.3.26) expressions are calculated here.

These results, in conjunction with the general framework presented in chapter 2, will be used in this thesis for the BER calculation in different scenarios using a common procedure. The main contributions in this chapter have been published in [19, 21] and [22].

Chapter 4

Analysis of MIMO systems in Ricean Fading

I N this chapter, we use the general framework presented in chapter 2 and the mathematical results introduced in chapter 3 to perform a BER analysis of QAM systems with multiple antennas affected by Ricean fading, in the presence of different impairments: first, a QAM system with MRC reception is analyzed, when Ricean-faded interferences and ICSI are considered. Then, a MIMO system employing Alamouti transmit diversity in conjunction with MRC reception and ICSI is investigated.

4.1 MRC reception with Ricean Interferences

4.1.1 Related Work

In the previous sections, we have presented a general framework which enables the analysis of QAM based systems as well as a method for calculating probabilities in scenarios where the decision variable may be expressed in terms of a general quadratic form in complex Gaussian RVs. Here, we illustrate the applicability of these tools to derive an exact closed-form expression for the BER of a QAM system when MRC diversity is used in Ricean fading channels with Ricean interference, under channel estimation errors. In this scenario, the PDF of the equivalent noise is not circularly symmetric with respect to zero, since its mean is different to zero due to the line-of-sight (LOS) component of the interfering signal.

Some authors have dealt with the analysis of QAM-based systems in the presence of interferences: In [34], the outage probability is calculated for some antenna reception strategies in the presence of interfering signals with arbitrary average powers, under different fading scenarios. For BPSK constellation, closed-form expressions for the BER are obtained in the case of Rayleigh [35, 36] and Ricean faded co-channel interference [37]. Particularly, the results in [37] were not exact since a saddlepoint approximation was considered. Therefore, a general BER analysis for QAM systems in the presence of Ricean-faded interferences has not been accomplished in the literature in exact closed-form, to the best of our knowledge.

In the investigated scenario, the signal of interest (SOI) is a generic QAM signal with independent bit-mapping, whereas the interferences may belong to any bidimensional constellation. Ricean fading is considered both for the SOI and interfering signals, with arbitrary average power, arbitrary Rice K parameter and equal scattering power, and MRC reception with ICSI is assumed. We obtain an exact closed-form expression for the BER in this general scenario. Additionally, we calculate a closed-form expression for a simplified scenario of interest, like PCSI in the presence of Rayleigh faded interferences, which provides a better insight into the problem.

4.1.2 System Model

Let us denote the received signal on the k-*th* branch as

$$r_k = g_k z + h_k \rho_i + w_k, \tag{4.1.1}$$

where z is the transmitted symbol belonging to a M-QAM constellation, g_k and h_k are complex Gaussian random variables with means m_{g_k}, m_{h_k} and variances σ_g^2, σ_h^2 respectively, ρ_i is the interfering symbol belonging to a set $\mathcal{S}$ and w_k is AWGN with zero mean and variance σ_w^2. For the sake of simplicity, yet without loss of generality, we consider one interfering signal per branch. However, the same analysis can be performed for an arbitrary number of interfering signals per branch.

When MRC is performed at the receiver, the decision metric y can be expressed as

$$y = \sum_{k=1}^{N_R} \frac{\hat{g}_k^* r_k}{|\hat{\mathbf{g}}|^2} = \sum_{k=1}^{N_R} \frac{\hat{g}_k^* g_k}{|\hat{\mathbf{g}}|^2} z + \sum_{k=1}^{N_R} \frac{\hat{g}_k^* (h_k \rho_i + w_k)}{|\hat{\mathbf{g}}|^2}, \tag{4.1.2}$$

where N_R is the number of diversity branches at the receiver side and $\hat{\mathbf{g}}$ is the channel estimation vector. We denote the components of $\hat{\mathbf{g}}$ as $\hat{g}_k = g_k + \psi_k$, where ψ_k is the Gaussian error in channel estimation with zero-mean and variance σ_ψ^2 [38]. Thus, according to the canonical form $y = az + \zeta$ given in 2.2.1, we can use the general expression (2.2.7) for the BER.

4.1.3 BER analysis

Exact analysis

BER calculation in this scenario is performed as follows: first, we calculate the CEPs conditioned to a certain interfering symbol ρ_i, and then we average this conditional probability for all the possible interfering symbols. Finally, we compute the elementary coefficients $\alpha_u^\pm(k)$ and $\beta_u^\pm(k)$ in order to obtain the final BER expression.

In this scenario the PDF of the equivalent noise is not circularly symmetric with respect to zero. Therefore, we have to calculate separately the probabilities for the I and Q components. The conditioned CEPs to be calculated are $\mathcal{I}_{u,v}^\pm(m|\rho_i)$ and $\mathcal{Q}_{u,v}^\pm(m|\rho_i)$. Then, the final CEPs are obtained averaging the conditional CEPs over the entire set $\mathcal{S}$ of interfering symbols

$$\mathcal{I}_{u,v}^\pm(m) = \sum_{\forall \rho \in \mathbf{S}} \mathcal{I}_{u,v}^\pm(m|\rho_i), \quad \mathcal{Q}_{u,v}^\pm(m) = \sum_{\forall \rho \in \mathbf{S}} \mathcal{Q}_{u,v}^\pm(m|\rho_i). \tag{4.1.3}$$

Let us define a random variable D as a quadratic form as follows

$$D(\mathbf{Q}_l) \triangleq D_l = \sum_{k=1}^{N_R} \mathbf{x}_k^{\mathcal{H}} \mathbf{Q}_l \mathbf{x}_k. \tag{4.1.4}$$

The quadratic form matrix $\mathbf{Q}_l$ and the random variable vector $\mathbf{x}_k$ are defined as

$$\mathbf{x}_k \triangleq \begin{bmatrix} r_k \\ \hat{g}_k \end{bmatrix} \quad \mathbf{Q}_l \triangleq \begin{bmatrix} 0 & \frac{1}{2}e^{j\frac{\pi}{2}l} \\ \frac{1}{2}e^{-j\frac{\pi}{2}l} & \mathcal{B}(m) \end{bmatrix}, \tag{4.1.5}$$

where $l \triangleq \{0, 1, 2, 3\}$ is used to index the CEPs $\{\mathcal{I}_{u,v}^-(m|\rho_i), \mathcal{Q}_{u,v}^-(m|\rho_i), \mathcal{I}_{u,v}^+(m|\rho_i), \mathcal{Q}_{u,v}^+(m|\rho_i)\}$ to be calculated, respectively, and $\mathcal{B}(m)$ are the decision boundaries defined in Section 2.2, whose sign is coincident with the sign of the considered CEP.

The calculation of $P_l \triangleq \Pr\{D_l < 0\}$ can be tackled through Proakis' analysis of complex Gaussian quadratic forms [6, eq. B-21], or using the alternative expression given in (3.2.7)

and Table 3.1. Thus, if we expand (4.1.4) and (4.1.5), we have

$$P_l = \Pr\left\{\sum_{k=1}^{N_R}\left[\frac{1}{2}r_k\hat{g}_k^* e^{-j\frac{\pi}{2}l} + \frac{1}{2}r_k^*\hat{g}_k e^{j\frac{\pi}{2}l} + |\hat{g}_k|^2\, \mathcal{B}(m)\right] < 0\right\}. \qquad (4.1.6)$$

For the different values of l index, we identify the relationship between (4.1.6) and the CEPs

as

$$P_0 = \Pr\{D_0 < 0\} = \mathcal{I}_{u,v}^-(m|\rho_i), \quad P_1 = \Pr\{D_1 < 0\} = \mathcal{Q}_{u,v}^-(m|\rho_i),$$
$$P_2 = \Pr\{D_2 < 0\} = \mathcal{I}_{u,v}^+(m|\rho_i), \quad P_3 = \Pr\{D_3 < 0\} = \mathcal{Q}_{u,v}^+(m|\rho_i). \qquad (4.1.7)$$

The mean vector $\mathbf{m}_k \triangleq \mathrm{E}\{\mathbf{x}_k\}$ and the covariance matrix $\mathbf{R} \triangleq \mathrm{E}\left\{(\mathbf{x}_k - \mathbf{m}_k)(\mathbf{x}_k^{\mathcal{H}} - \mathbf{m}_k^{\mathcal{H}})\right\}$ are expressed, after some calculations, as

$$\mathbf{m}_k = \begin{bmatrix} m_{g_k} s_{u,v} + m_{h_k}\rho_i \\ m_{g_k} \end{bmatrix},$$

$$\mathbf{R} = \begin{bmatrix} \sigma_g^2\, |s_{u,v}|^2 + \sigma_h^2\, |\rho_i|^2 + \sigma_w^2 & (\sigma_g^2 - \sigma_\psi^2)s_{u,v} \\ (\sigma_g^2 - \sigma_\psi^2)s_{u,v}^* & \sigma_g^2 - \sigma_\psi^2 \end{bmatrix}. \qquad (4.1.8)$$

Once $\mathbf{m}_k$ and $\mathbf{R}$ are known, the parameters η_l, a_l and b_l are calculated using the expressions in Table 3.1, for a certain $\mathbf{Q}_l$. Finally, the value of P_l is given by

$$P_l = \sum_{m=0}^{N_R-1} C_m(a_l, b_l, \eta_l) I_m(a_l b_l) \exp\left\{-\frac{1}{2}(a_l^2 + b_l^2)\right\} + Q_1(a_l, b_l), \qquad (4.1.9)$$

where $Q_1(a, b)$ is the first order Marcum Q function, $I_m(x)$ is the m-th order modified Bessel function of first kind, and $C_m(a, b, c)$ is defined in Table 3.1. We calculate the final expression by substituting in (2.2.7), thus obtaining the exact closed-form BER expression as

$$BER_{\mathrm{QAM}} = \frac{1}{M\log_2(M)}\sum_{u=1}^{L}\sum_{v=1}^{L}\sum_{\forall\rho\in\mathbf{S}}\left\{\vphantom{\sum}\right.$$
$$\sum_{n=1}^{u-1}\alpha_u^-(n)\left[Q_1(a_0, b_0) + \sum_{m=0}^{N_R-1}C_m(a_0, b_0, \eta_0)I_m(a_0 b_0)\exp\left\{-\tfrac{1}{2}(a_0^2 + b_0^2)\right\}\right] +$$
$$\sum_{n=u}^{L-1}\alpha_u^+(n)\left[Q_1(a_2, b_2) + \sum_{m=0}^{N_R-1}C_m(a_2, b_2, \eta_2)I_m(a_2 b_2)\exp\left\{-\tfrac{1}{2}(a_2^2 + b_2^2)\right\}\right] + \qquad (4.1.10)$$
$$\sum_{n=1}^{v-1}\beta_v^-(n)\left[Q_1(a_1, b_1) + \sum_{m=0}^{N_R-1}C_m(a_1, b_1, \eta_1)I_m(a_1 b_1)\exp\left\{-\tfrac{1}{2}(a_1^2 + b_1^2)\right\}\right] +$$
$$\left.\sum_{n=v}^{L-1}\beta_v^+(n)\left[Q_1(a_3, b_3) + \sum_{m=0}^{N_R-1}C_m(a_3, b_3, \eta_3)I_m(a_3 b_3)\exp\left\{-\tfrac{1}{2}(a_3^2 + b_3^2)\right\}\right]\right\}.$$

Note that a_l, b_l and η_l coefficients also depend on u and v, although this dependence has been omitted for notational simplicity. In the case of considering Gray mapping, the elementary coefficients $\alpha_u^{\pm}(n)$ and $\beta_v^{\pm}(n)$ are calculated from (2.2.6) and (2.3.8). Otherwise, they may be calculated following the procedure described in Section 2.3.1.

Although the exact BER expression in (4.1.10) is easily computed with Matlab or other mathematical tools, the provision of a good insight into the system performance is not obvious. However, it is possible to simplify this expression by means of asymptotic analysis as in [39].

Approximate analysis: Strong LOS, PCSI and Rayleigh-faded interferences.

Let us consider PCSI (i.e. $\hat{\mathbf{g}} = \mathbf{g}$) at the receiver side, and let us assume a line of sight (LOS) component only for the SOI. Therefore, a Rayleigh fading channel (i.e. $m_{h_k} = 0$) is considered for the interfering signals. In this scenario, we observe no gain mismatch and an equivalent noise with circularly symmetric PDF. Hence, this situation is coincident with the particular scenario considered in Section 2.2.3, and only the calculation of $\mathcal{I}^+(n|\rho_i)$ CEP is required. If we define

$$c_n = \frac{\sigma_g^2}{\sigma_w^2 + \sigma_h^2 |\rho_i|^2} \cdot \frac{3E_S(2n-1)}{2(M-1)}, \tag{4.1.11}$$

where E_S is the transmitted constellation energy, we can express after some algebra

$$\begin{aligned} a_n &= \left(\frac{1}{2} - \frac{1}{2}\sqrt{\frac{c_n}{c_n+1}} \right) \sqrt{2N_R K_{SOI}}; \\ b_n &= \left(\frac{1}{2} + \frac{1}{2}\sqrt{\frac{c_n}{c_n+1}} \right) \sqrt{2N_R K_{SOI}}, \end{aligned} \tag{4.1.12}$$

where $K_{SOI} = 10\log(|m_{gk}|^2/\sigma_g^2)$ is the Ricean K factor for the SOI. From (4.1.12), it is clear that $a_n, b_n \to \infty$ when $K_{SOI} \to \infty$, and $b_n > a_n$. Hence, it is shown in (3.2.10) that

$$\mathcal{I}^+(n|\rho_i) \approx T_n \cdot Q\left(\sqrt{\frac{c_n}{c_n+1} 2N_R K_{SOI}} \right), \tag{4.1.13}$$

where

$$T_n = \sqrt{\eta_n} + \sqrt{4c_n} \sum_{m=0}^{N_R-1} C_m(\eta_n), \tag{4.1.14}$$

and $\eta_n = b_n/a_n = 1 + 2c_n + 2\sqrt{c_n(c_n+1)}$.

Taking into account that the $\alpha_u^\pm, \beta_v^\pm$ coefficients can be grouped attending to expression (2.2.25), the closed-form expression for the BER is given by

$$P_e = \sum_{\forall \rho \in \mathbf{S}} \sum_{n=1}^{L-1} T_n \cdot \omega(n) \cdot Q\left(\sqrt{\frac{c_n}{c_n+1} 2 N_R K_{SOI}}\right). \tag{4.1.15}$$

4.1.4 Numerical Results

We use the closed-form expressions obtained in Section 4.1.3 to evaluate the BER in different scenarios. Gray mapping is considered for QAM constellations. As in [40], we consider the interfering signal ρ_i belonging to a square M-QAM constellation, with the same M value that the SOI and $E[|\rho_i|^2] = 1$. For the sake of simplicity, we assume equal mean for the Ricean channel and interferences for all the reception branches, i.e. $m_{g_k} = m_g$, $m_{h_k} = m_h$; $\forall k$.

We denote the signal-to-interference ratio (SIR) as $\gamma_I = E_S/E_I$, where $E_I = \sigma_h^2 + |m_h|^2$ is the energy of the interfering signal. Similarly, we denote the signal-to-channel estimation error ratio (SCER) as $\gamma_{CE} = E_S/\sigma_\psi^2$ and the signal to noise ratio (SNR) as $\gamma_N = E_S/\sigma_w^2$. We define the Ricean K factor for the interference as $K_I = 10 \log(|m_h|^2/\sigma_h^2)$.

Evaluation of exact expression

Fig. 4.1 illustrates the BER performance according to expression (4.1.10) as a function of γ_I, for different constellations (16/64-QAM) and different number of reception branches N_R. The SOI and the interference are affected by Ricean fading with K_{SOI}=10 dB and K_I=0 dB, respectively. The remainder parameters are γ_N=20 dB and γ_{CE}=20 dB.

It is seen that the Monte Carlo simulations and the analytical results are in excellent agreement. As expected, BER performance is improved as the number of reception branches N_R is increased, and when the constellation size M is reduced. It is interesting to highlight the appearance of an irreducible floor in the BER, for high SIR values. This floor is due to the noise as well as to ICSI, when either SCER or SNR values become comparable to the current SIR.

For convenience of discussion, we will particularize the following results for the case of an interference-limited system, which corresponds to a typical case of wireless cellular systems
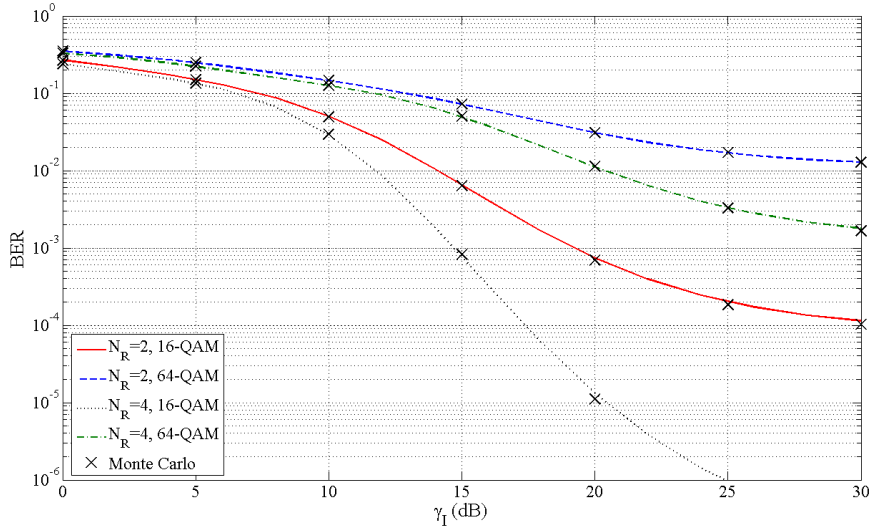
Figure 4.1: BER vs SIR, for different number of reception branches N_R, 16/64-QAM constellations, $\gamma_N=\gamma_{CE}=20$ dB, $K_{SOI}=10$ dB, $K_I=0$ dB.

(i.e $\gamma_N \rightarrow \infty$). Besides, we will consider PCSI (i.e. $\gamma_{CE} \rightarrow \infty$) in order to avoid the appearance of an error floor due to ICSI.

In Figures 4.2 to 4.5, the influence of every single parameter of the system in the BER is studied, when the rest of the parameters remain unchanged. Fig. 4.2 shows the BER results for different values of K_I factor.

It is interesting to observe that for low SIR values, the LOS component of the interference provokes the received symbol to be shifted beyond the correct decision boundaries. Since the magnitude of this shift grows with K_I, we appreciate that the BER grows with K_I value. On the opposite, when the SIR is very low the received symbol is likely to be shifted beyond more than just one boundary. Hence, we can have more than one erroneous bit per symbol. In this case, we appreciate that the BER decays with K_I value due to the effect of the NLOS component of the interference. Finally, for high SIR values it is observed that the BER is increased when K_I decreases.

Fig. 4.3 shows the BER performance for different values of K_{SOI} factor, when $K_I=0$ dB, 16-QAM constellation and $N_R = 2$ reception branches are considered. The same assumptions
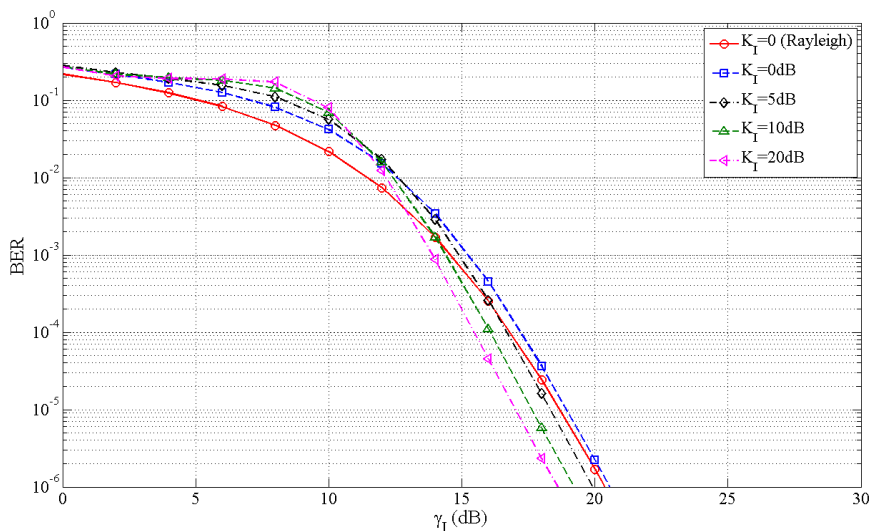
Figure 4.2: BER vs SIR, for different values of interference Ricean K_I factor, N_R=2, 16-QAM constellation, PCSI, $\gamma_N \to \infty$, K_{SOI}=10 dB.

about channel estimation error and noise that in Fig. 4.2 are taken. As expected, better values of BER correspond with greater values of K_{SOI} factor, i.e. a stronger LOS component.

The effect of SNR is studied in Fig. 4.4. Simulation parameters in this case are 16-QAM constellation, $N_R = 2$ reception branches, PCSI, K_{SOI} =10 dB and K_I =0 dB. We observe the appearance of an error floor in the BER for those ranges of γ_I comparable to the fixed γ_N values. In this case, the noise dominates the interference so that the assumption of interference-limited system becomes invalid. When the SIR is much lower than the SNR (e.g. γ_N=30 dB), the BER is very close to the $\gamma_N \to \infty$ scenario.

Now, the influence of an imperfect channel estimation is showed in Fig. 4.5, when 16-QAM constellation, $N_R = 2$ reception branches, K_{SOI}=10 dB and K_I=0 dB are assumed. Similarly to Fig. 4.4, an error floor in the BER is appreciated when the SCER and SIR are of similar magnitudes.
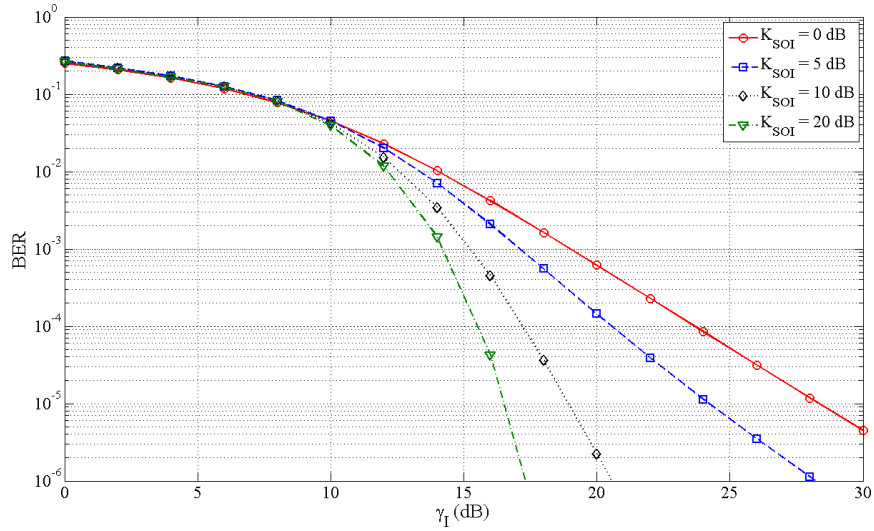
Figure 4.3: BER vs SIR, for different values of SOI Ricean K_{SOI} factor, N_R=2, 16-QAM constellation, PCSI, $\gamma_N \to \infty$, K_I=0 dB.
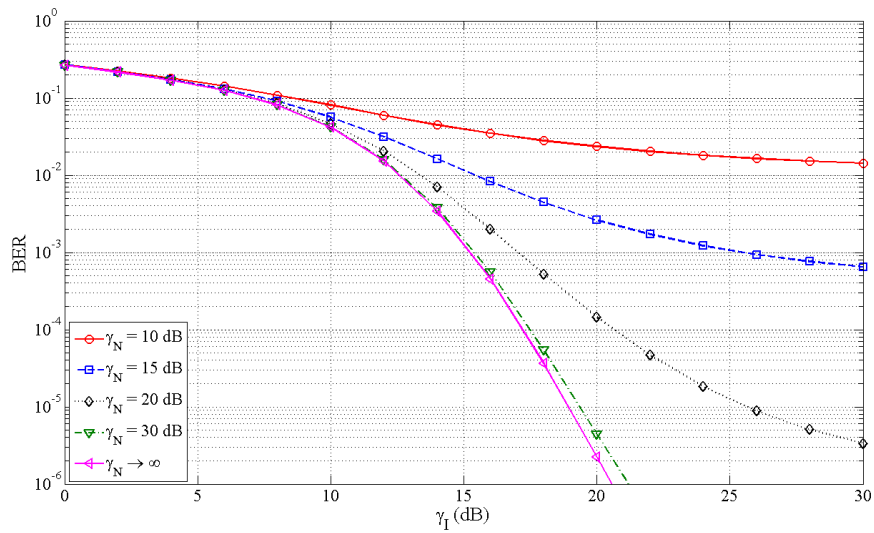
Figure 4.4: BER vs SIR, for different values of SNR, N_R=2, 16-QAM constellation, PCSI, K_I= 0 dB, K_{SOI}= 10 dB.
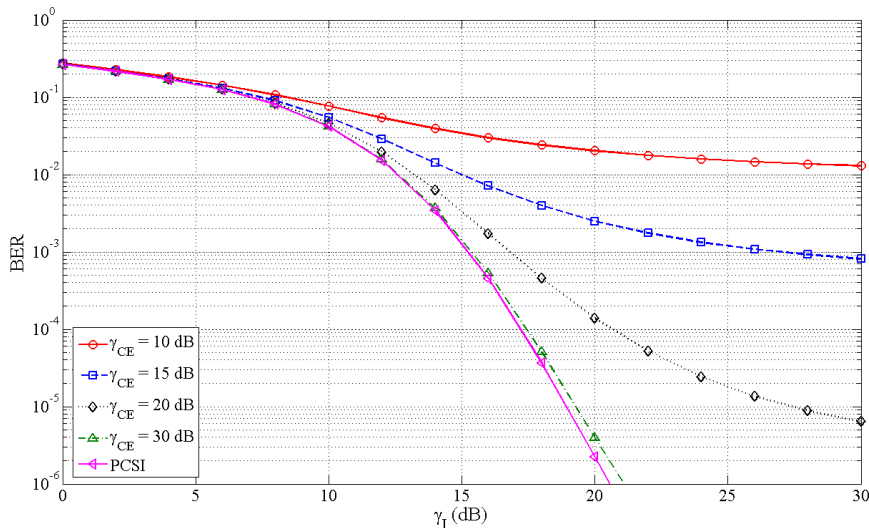
Figure 4.5: BER vs SIR, for different values of SCER, N_R=2, 16-QAM constellation, $\gamma_N \to \infty$, K_I=0 dB, K_{SOI}=10 dB.

Evaluation of approximate expression

Once the BER results for the general scenario of Ricean fading channel in the presence of Ricean-faded interferences with ICSI and MRC reception have been presented (according to expression (4.1.10)), we will focus on the particular case of Rayleigh-faded interferences, when PCSI is considered. In this scenario, we provide a simplified closed-form expression in (4.1.15), with the only assumption of a strong LOS component for the SOI.

Fig. 4.6 shows the exact and approximate BER given by (4.1.15), for different values of K_{SOI} and constellation sizes. We observe an excellent match between the approximate and exact curves, either for 16 and 64-QAM constellations, for values of K_{SOI} in the range of 10 dB. It is observed that as the relative power of the LOS component is increased, the accuracy of the approximation is also improved.

Finally, Fig. 4.7 shows the BER performance in the Rayleigh-faded interference scenario, for different number of reception branches N_R and constellation sizes, when no noise influence and K_{SOI} =10 dB are considered. The approximate expression provides an accurate BER value for the different configurations of constellation sizes and number of receive antennas.
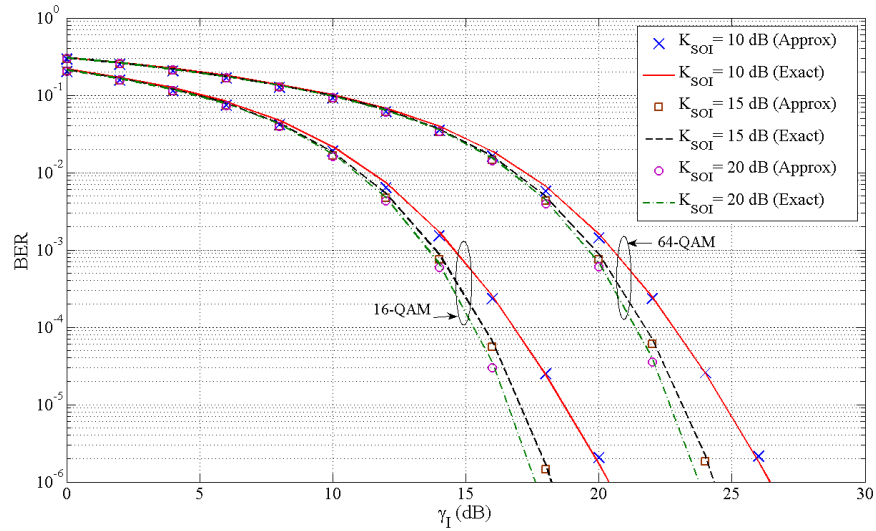
Figure 4.6: BER vs SIR (exact and approximate) for different values of SOI Ricean K_{SOI}-factor, N_R=2, 16/64-QAM constellations, $\gamma_N = \to \infty$, PCSI and Rayleigh-faded interference.
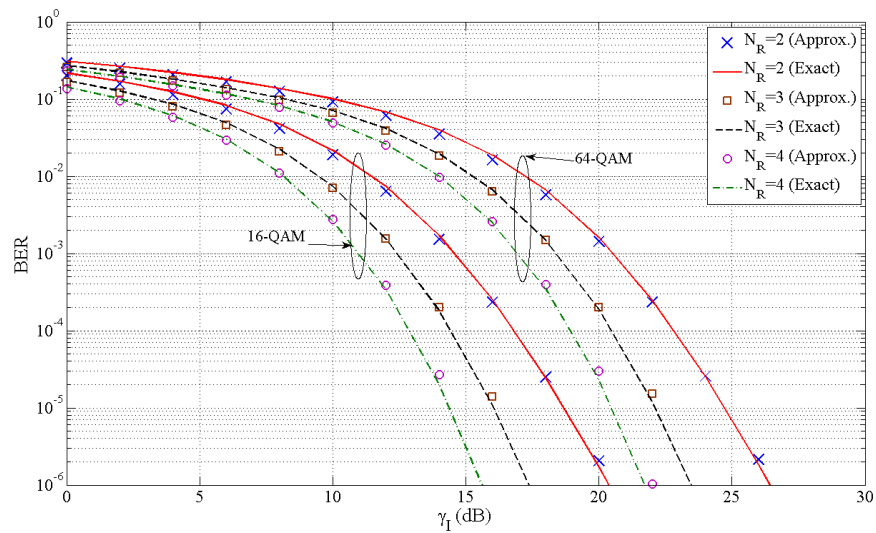
Figure 4.7: BER vs SIR (exact and approximate) for different reception branches N_R, K_{SOI}= 10 dB, 16/64-QAM constellations, $\gamma_N = \to \infty$, PCSI and Rayleigh-faded interference.

4.1.5 Discussion

We have illustrated the applicability of the proposed analysis method for the exact closed-form BER calculation in a M-QAM system with MRC reception in Ricean fading channel and Ricean-faded interferences, when imperfect channel estimation is considered. Besides, we also propose an approximate closed-form expression for the particular case of Rayleigh-faded interferences and perfect channel estimation, in terms of a weighted sum of elementary Gaussian Q functions. This approximate expression is valid for strong LOS scenarios in our particular case, although may be used in other scenarios involving Gaussian quadratic forms.

Numerical results show how imperfect channel estimation leads to an irreducible BER floor. This error floor is also to appear when SNR and SIR have similar values. It is appreciated that the effect of K_I value on the BER varies depending of the magnitude of the SIR. We can also observe a very good match between the exact closed-form and the approximate expression when a strong LOS component is considered.

The main contributions in this section have been published in [19].

4.2 Alamouti transmission with MRC reception

4.2.1 Related Work

The use of multiple antennas for transmission or reception, usually referred to as multiple-input multiple-output (MIMO), is nowadays an extended strategy for improving the capacity and coverage in wireless communication systems. One of the simpler MIMO configurations relies on the use of space time block codes (STBCs), since they do not require the knowledge of channel state information (CSI) at the transmitter side.

Alamouti [41] proposed a coding scheme for two transmit antennas, which was demonstrated to provide full diversity order when perfect CSI is available at the receiver side. This technique has been incorporated in many wireless communication standards such as IEEE 802.11, 802.16 and 3GPP-LTE, and it also has recently been considered for cooperative transmission [42, 43]. The performance of Alamouti's like schemes has widely been analyzed by many authors, in different scenarios and configuration. Most analyses in the literature

however assume perfect CSI at the receiver side [42–47].

It is known that the effect of imperfect CSI (ICSI) at the receiver side results in a performance degradation of Alamouti's scheme [48]. The effect of ICSI has also been analyzed in [49–52], when Rayleigh fading is considered. However, to the best of author's knowledge, analytical results for Alamouti's transmission schemes impaired by ICSI in Ricean fading channels are largely unknown.

In this section, we present an exact closed-form BER analysis of a MIMO system that employs Alamouti transmission in conjunction with MRC reception with N_R receive antennas in a Ricean fading channel, when ICSI is considered, for a generic M-ary quadrature amplitude modulation (QAM) constellation. An approximate expression is also obtained for the case of a strong line of sight (LOS) path, in terms of the Gaussian Q function. We demonstrate that the investigated scenario can be reduced to an equivalent $1 \times 2N_R$ MRC reception scheme, where the equivalent noise term is affected by the loss of orthogonality of Alamouti's code due to ICSI. The final expressions are used to study how the different parameters (e.g., number of receive antennas, constellation size, channel estimation error, Ricean K factor) affect the BER performance, and to evaluate the degradation compared to a conventional $1 \times 2N_R$ MRC reception [9].

The remainder of this section is organized as follows: In (4.2.2), it is presented the system model considered in our analysis: M-QAM modulation, Alamouti transmission, MRC reception with ICSI and Ricean fading channel. Then (4.2.3), the exact and approximate closed-form expressions for the BER in this scenario are calculated. Numerical results are given in (4.2.4) in order to determine how the different parameters affect the BER performance. Finally, main conclusions are presented in (4.2.5).

4.2.2 System Model

We consider a MIMO $2 \times N_R$ system, where Alamouti scheme is applied at the transmitter, and MRC with N_R antennas is performed at the receiver. During two consecutive symbol intervals, the symbols z_1 and z_2 belonging to a square M-QAM constellation are transmitted according to the block code described in [41]. The set of complex symbols is $\mathcal{S}_M \triangleq \{s_{u,v} =$

$(2u - \sqrt{M} - 1)d + j(2v - \sqrt{M} - 1)d\}_{u=1...\sqrt{M};v=1...\sqrt{M}}$, where $2d$ is the minimum distance between symbols, and independent bit mapping is assumed for in-phase (I) and quadrature (Q) components.

The received signals in the i-th reception branch, during two consecutive symbol intervals, can be expressed as

$$r_{1,i} = g_{1,i}z_1 + g_{2,i}z_2 + w_{1,i}, \tag{4.2.1}$$

$$r_{2,i} = -g_{1,i}z_2^* + g_{2,i}z_1^* + w_{2,i}, \tag{4.2.2}$$

where * denotes complex conjugation, $\{g_{j,i}\}_{j=1,2;i=1...N_R}$ is the complex channel gain between the j-th transmit antenna and the i-th receive antenna, and $\{w_{j,i}\}_{j=1,2;i=1...N_R}$ denote the additive white Gaussian noise (AWGN) terms. We assume that $\{g_{j,i}\}$ are independent complex random variables (RVs) with $m_{g_{j,i}}$ mean and σ_g^2 variance, i.e., $g_{j,i} \sim \mathcal{CN}(m_{g_{j,i}}, \sigma_g^2)$, where $\sim$ means *"statistically distributed as"*, and $w_{j,i} \sim \mathcal{CN}(0, \sigma_w^2)$. After using the combination method given in [41], the decision metrics along the block code interval in the i-th reception branch can be expressed as:

$$y_{1,i} = \hat{g}_{1,i}^* r_{1,i} + \hat{g}_{2,i} r_{2,i}^*, \tag{4.2.3}$$

$$y_{2,i} = \hat{g}_{2,i}^* r_{1,i} - \hat{g}_{1,i} r_{2,i}^*, \tag{4.2.4}$$

where $\hat{g}_{j,i} = g_{j,i} + \psi_{j,i}$ denotes the estimate of the channel gain, and $\psi_{j,i} \sim \mathcal{CN}(0, \sigma_\psi^2)$ represents the channel estimation error according to the channel model proposed in [38] (i.e., $E[\hat{g}_{j,i}\psi_{j,i}^*] = 0$). Finally, the decision metrics per receive branch are combined using MRC, providing the final j-th decision metrics as

$$y_j = \frac{\sum_{i=1}^{N_R} y_{j,i}}{\sum_{i=1}^{N_R} \left(|\hat{g}_{1,i}|^2 + |\hat{g}_{2,i}|^2\right)}. \tag{4.2.5}$$

4.2.3 BER analysis

Exact analysis

Due to the existing symmetry in the decision metrics in (4.2.5), it is equivalent to calculate the BER for z_1 and z_2 symbols. Hence, in the following we focus our analysis on z_1 symbol.

Let us express the BER as the average, over all the transmitted z_1 and z_2 symbols, of a weighted sum of components of error probability

$$BER = \frac{1}{M} \sum_{\forall s_{u,v}, s_{u',v'} \in \mathcal{S}_M} \sum_{n=u}^{\sqrt{M}-1} \omega_u(n) \mathcal{I}_{u,v,u',v'}(n),$$ (4.2.6)

where the coefficients $\omega_u(n)$ are given in (2.2.19), and $\mathcal{I}_{u,v,u',v'}(n)$ is defined as the component of error probability conditioned on a particular value of z_1 and z_2, i.e.,

$$\mathcal{I}_{u,v,u',v'}(n) = \Pr \left\{ \Re \left\{ y_1 - \mathcal{B}(n) \right\} > 0 \big|_{z_1 = s_{u,v}, z_2 = s_{u',v'}} \right\}$$ (4.2.7)

where $\mathcal{B}(n) = (2n - \sqrt{M})d$ are the decision boundaries for the M-QAM constellation.

Expanding (4.2.5), and after some algebra, $\mathcal{I}_{u,v,u',v'}(n)$ can be expressed as

$$\mathcal{I}_{u,v,u',v'}(n) = \Pr \Bigg\{ \sum_{i=1}^{N_R} \left\{ \left(|\hat{g}_{1,i}|^2 + |\hat{g}_{2,i}|^2 \right) \Re \left(s_{u,v} - B(n) \right) \right.$$
$$\left. + \Re \left\{ \hat{g}_{1,i}^* \eta_{1,i} \right\} + \Re \left\{ \hat{g}_{2,i} \eta_{2,i}^* \right\} \right\} > 0 \Bigg\},$$ (4.2.8)

where $\{\eta_{j,i}\}$ are the equivalent noise terms defined as

$$\eta_{1,i} = \left(w_{1,i} - \Psi_{1,i} s_{u,v} - \Psi_{2,i} s_{u',v'} \right),$$ (4.2.9)

$$\eta_{2,i} = \left(w_{2,i} + \Psi_{1,i} s_{u',v'}^* - \Psi_{2,i} s_{u,v}^* \right).$$ (4.2.10)

Note that although $\{\eta_{j,i}\}$ depend on $\Psi_{1,i}$ and $\Psi_{2,i}$, it can be shown that $\eta_{1,i}$ and $\eta_{2,i}$ are independent zero-mean complex Gaussian RVs with equal variance. Hence, we can express (4.2.8) compactly by redefining the sum indices as

$$\mathcal{I}_{u,v,u',v'}(n) = \Pr \left\{ \sum_{k=1}^{2N_R} \left\{ |\hat{g}_k|^2 \Re \left(B(n) - s_{u,v} \right) - \frac{1}{2} \hat{g}_k^* \eta_k - \frac{1}{2} \hat{g}_k \eta_k^* \right\} < 0 \right\},$$ (4.2.11)

where $k = 1, \ldots, N_R$ represents $\{j = 1, i = 1, \ldots, N_R\}$, and $k = N_R + 1, \ldots, 2N_R$ represents $\{j = 2, i = 1, \ldots, N_R\}$. The term $\eta_k \sim \mathcal{CN}\left(0, \sigma_w^2 + \sigma_\psi^2 \left(|s_{u,v}|^2 + |s_{u',v'}|^2 \right)\right)$ accounts for the joint effect of noise and block code interference due to ICSI.

This expression (4.2.11) can be seen as a particular case of quadratic form $D = \sum_{k=1}^{2N_R} \mathbf{x}_k^{\mathcal{H}} \mathbf{Q} \mathbf{x}_k$, where $^{\mathcal{H}}$ denotes complex conjugate transpose operation, and the quadratic form matrix $\mathbf{Q}$

and the random variable vector $\mathbf{x}_k$ are defined as

$$\mathbf{x}_k \triangleq \begin{bmatrix} \hat{g}_k \\ \eta_k \end{bmatrix}, \quad \mathbf{Q} \triangleq \begin{bmatrix} \mathcal{B}(n) - \Re\{s_{u,v}\} & -\frac{1}{2} \\ -\frac{1}{2} & 0 \end{bmatrix}. \tag{4.2.12}$$

Hence, in this scenario, the calculation of $\Pr\{D < 0\}$ can be performed either using analysis of complex Gaussian quadratic forms [6, eq. B-21], or the alternative expression (3.2.7). If the mean vector $\mathbf{m}_k \triangleq \mathrm{E}\{\mathbf{x}_k\}$ and the covariance matrix $\mathbf{R} \triangleq \mathrm{E}\{(\mathbf{x}_k - \mathbf{m}_k)(\mathbf{x}_k^{\mathcal{H}} - \mathbf{m}_k^{\mathcal{H}})\}$ are calculated as

$$\mathbf{m}_k = \begin{bmatrix} m_{g_k} \\ 0 \end{bmatrix}, \quad \mathbf{R} = \begin{bmatrix} \sigma_g^2 - \sigma_\psi^2 & 0 \\ 0 & \sigma_w^2 + \sigma_\psi^2 \left(|s_{u,v}|^2 + |s_{u',v'}|^2\right) \end{bmatrix}, \tag{4.2.13}$$

the component of error probability (4.2.7) can be expressed in exact closed-form as

$$\mathcal{I}_{u,v,u',v'}(n) = Q_1(\mu, \lambda\mu) + \sum_{m=0}^{2N_R-1} C_m(\lambda) I_m(\lambda\mu^2) \exp\left\{-\frac{\mu^2}{2}(1 + \lambda^2)\right\}, \tag{4.2.14}$$

where $Q_1(a, b)$ is the first order Marcum Q function, $I_m(x)$ is the m-th order modified Bessel function of first kind, and λ, μ, and $C_m(\lambda)$ are defined in Table 4.1. Note that λ and μ also depend on u, v, u', v' and n indices, although it is not explicitly stated for notational simplicity.

Finally, the exact expression for the BER is given in closed-form by

$$BER = \frac{1}{M} \sum_{\forall s_{u,v}, s_{u',v'} \in \mathcal{S}_M} \sum_{n=u}^{\sqrt{M}-1} \omega_u(n) \times$$

$$\left(Q_1(\mu, \lambda\mu) + \sum_{m=0}^{2N_R-1} C_m(\lambda) I_m(\lambda\mu^2) \exp\left\{-\frac{\mu^2}{2}(1 + \lambda^2)\right\}\right). \tag{4.2.15}$$

After some algebra, we can find a simple expression for κ (and hence, for λ) and μ as

$$\mu = \frac{1}{\lambda + 1} \sqrt{\left(1 - \frac{\sigma_\psi^2}{\sigma_g^2}\right)^{-1} 4N_R \bar{K}}, \tag{4.2.16}$$

$$\kappa = \frac{\left(\sigma_g^2 - \sigma_\psi^2\right) \Re\left(s_{u,v} - B(n)\right)^2}{\left(\sigma_w^2 + \sigma_\psi^2 \left(|s_{u,v}|^2 + |s_{u',v'}|^2\right)\right)}, \tag{4.2.17}$$

where $\bar{K} = \frac{1}{2N_R} \sum_{k=1}^{2N_R} \frac{|m_{gk}|^2}{\sigma_g^2}$ is the average Ricean K factor, which accounts for the power ratio between the LOS and non-LOS components of the channel gain, and κ is defined in Table 4.1.

Table 4.1: Probability computation of Gaussian quadratic form.

FUNCTIONS AND PARAMETERS	DEFINITIONS
κ	$\left\| \frac{tr(\mathbf{RQ})^2}{4\det(\mathbf{RQ})} \right\|$
λ	$1 + 2\kappa + 2\sqrt{\kappa(\kappa+1)}$
μ	$\frac{1}{\lambda+1}\sqrt{2\frac{\sum_{k=1}^{2N_R}\mathbf{m}_k^{\mathcal{H}}\mathbf{m}_k}{\mathbf{u}^t\mathbf{Ru}}}, \quad \mathbf{u}^t \triangleq [1,0].$
$C_m(\lambda)$	$\begin{cases} -1 + \frac{1}{(1+\lambda)^{4N_R-1}}\sum_{k=0}^{2N_R-1}\binom{4N_R-1}{k}\lambda^k, & m=0 \\ \frac{1}{(1+\lambda)^{4N_R-1}}\sum_{k=0}^{2N_R-1-m}\binom{4N_R-1}{k}\left[\lambda^{m+k}-\lambda_l^{4N_R-1-k-m}\right], & m\neq 0 \end{cases}$

The derived closed-form expression (4.2.15) for the BER is exact. However, it is possible to provide a simpler approximate expression for a particular scenario of interest by means of asymptotic analysis.

Approximate analysis: Strong LOS component.

From (4.2.16), it is noted that the arguments in Marcum Q function are directly proportional to $\sqrt{\bar{K}}$, i.e., $\mu = \alpha\sqrt{\bar{K}}$. Hence, assuming $\bar{K} \to \infty$ (due to a strong LOS component), we can use the Marcum Q function approximation in terms of the Gaussian Q function [5] given by

$$Q_1(\mu, \lambda\mu) \approx \sqrt{\lambda}Q\left((\lambda-1)\alpha\sqrt{\bar{K}}\right), \ \bar{K} \to \infty. \tag{4.2.18}$$

Otherwise, the m-th order Bessel functions of first kind are approximated by exponentials when its argument tends to infinity as

$$I_m(\alpha^2\lambda\bar{K}) \sim \frac{\exp\{\alpha^2\lambda\bar{K}\}}{\alpha\sqrt{2\pi\lambda\bar{K}}}, \ \bar{K} \to \infty. \tag{4.2.19}$$

This latter approximation, combined with the asymptotic relation for the Gaussian Q

function given by

$$\frac{\exp\left\{-\frac{(\lambda-1)^2\alpha\bar{K}}{2}\right\}}{\sqrt{2\pi\bar{K}}\,(\lambda-1)\,\alpha} \approx Q((\lambda-1)\,\alpha^2\sqrt{\bar{K}}), \quad \bar{K}\to\infty, \tag{4.2.20}$$

leads to an approximate expression for the component of error probability (4.2.7) in terms of the Gaussian Q function

$$\mathcal{I}_{u,v,u',v'}(n) \approx C_q(n)Q\left(\sqrt{\frac{\kappa}{\kappa+1}\left(1-\frac{\sigma_\psi^2}{\sigma_g^2}\right)^{-1}4N_R\bar{K}}\right), \tag{4.2.21}$$

where $C_q(n)$ coefficients are calculated as

$$C_q(n) \triangleq \sqrt{\lambda} + \frac{\lambda-1}{\sqrt{\lambda}}\sum_{m=0}^{2N_R-1}C_m(\lambda). \tag{4.2.22}$$

Substituting (4.2.17) into (4.2.21), the CEP can be finally expressed as

$$\mathcal{I}_{u,v,u',v'}(n) \approx C_q(n)Q\left(\sqrt{\frac{4N_R\bar{K}}{\Gamma_{NI}^{-1}+1-\Gamma_\psi^{-1}}}\right), \tag{4.2.23}$$

where the Γ_{NI} and Γ_ψ are defined as

$$\Gamma_{NI} = \frac{\sigma_g^2\Re\left(s_{u,v}-B(n)\right)^2}{\sigma_w^2+\sigma_\psi^2\left(|s_{u,v}|^2+|s_{u',v'}|^2\right)}, \tag{4.2.24}$$

$$\Gamma_\psi = \frac{\sigma_g^2}{\sigma_\psi^2}. \tag{4.2.25}$$

From (4.2.24), it is easy to see that Γ_{NI} depends on u, v, u', v' and n, although this dependence has been omitted for notational simplicity. Finally, the approximate BER expression for $\bar{K}\to\infty$ is obtained as

$$BER_{(\bar{K}\to\infty)} \approx \frac{1}{M}\sum_{\forall s_{u,v},s_{u',v'}\in\mathcal{S}_M}\sum_{n=u}^{\sqrt{M}-1}\omega_u(n)C_q(n)Q\left(\sqrt{\frac{4N_R\bar{K}}{\Gamma_{NI}^{-1}+1-\Gamma_\psi^{-1}}}\right). \tag{4.2.26}$$

4.2.4 Numerical Results

In this section, we evaluate how the BER is affected by the variation of the parameters in our system model. For simplicity, equal mean for the Ricean channel for all the k branches is assumed, i.e., $m_{g_k} = m_g$, $\forall k$. Besides, Gray mapping is considered for QAM constellations.

The signal-to-noise ratio (SNR) is defined as $\gamma = E_S/\sigma_w^2$, where E_S is the average transmitted symbol energy. In a similar way, we denote the signal-to-channel estimation error ratio (SCER) as $\gamma_\psi = E_S/\sigma_\psi^2$. We also define the Ricean K factor as $K = 10\log(|m_g|^2/\sigma_g^2)$.

Evaluation of exact expression

Fig. 4.8 illustrates the BER performance as function of γ, for different values of Ricean K factor and number of reception branches N_R. 4-QAM modulation is considered, and the channel estimation error is set to $\gamma_\psi = 20$dB. It is observed that a stronger LOS component results in a better BER performance. Similarly, it is appreciated that BER performance is improved when the number of reception branches N_R is increased. It is seen that the Monte Carlo simulations and the analytical results are in excellent agreement.
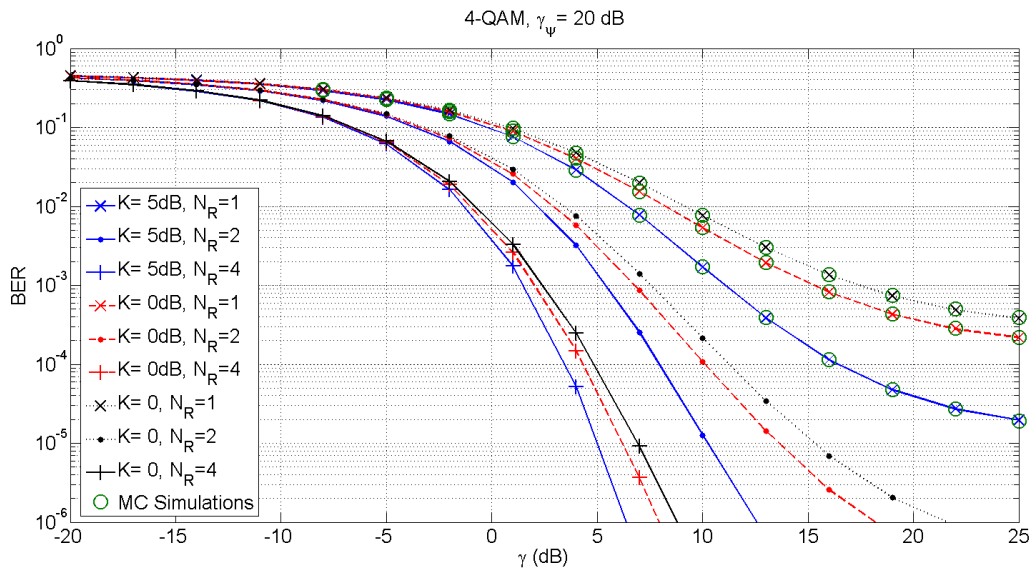
Figure 4.8: BER vs SNR for different values of Ricean K factor and number of reception branches N_R, 4-QAM constellation and $\gamma_\psi = 20$dB.

In Fig. 4.9, the BER for different constellation sizes and channel estimation error values γ_ψ is evaluated. Two reception branches and a $K = 5$dB Ricean factor are assumed. As expected, more dense constellations are more sensitive to channel estimation error. For 64-QAM, the minimum achievable BER is worse than 10^{-3} for the considered values of γ_ψ, due to the effect of ICSI.
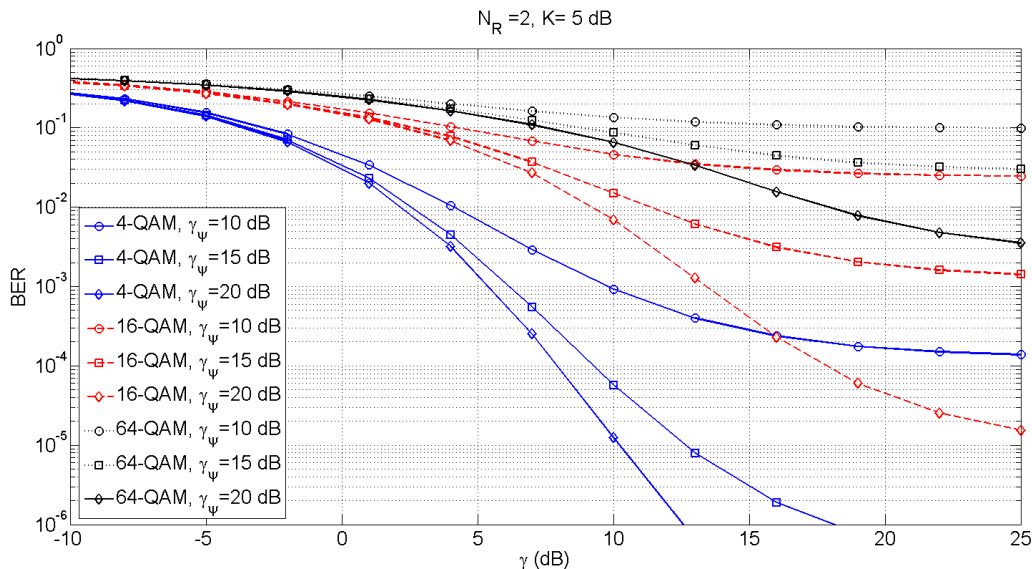
Figure 4.9: BER vs SNR for different values of γ_ψ and constellation sizes, $K = 5$dB Ricean factor and $N_R = 2$ reception branches.

Fig. 4.10 represents the BER as a function of γ_ψ, considering 16-QAM modulation, two reception branches, and different SNR constraints and K values. When the channel estimation error is under $10 - 12$dB, the BER performance is very similar and independent of the value of K.

It is observed that in the presence of a strong LOS component ($K = 5$dB), the BER performance ($\gamma = 20$dB) for high values of γ_ψ is under 10^{-6}, whereas it is over 10^{-5} when non-LOS is considered (i.e., Rayleigh channel). In the case of $\gamma \rightarrow \infty$, the BER values represent the irreducible BER floor due to ICSI.

In Fig. 4.11, the BER performance of the $2 \times N_R$ Alamouti-MRC scheme is compared to a conventional $1 \times 2N_R$ MRC system [9], in the presence of ICSI. It is appreciated that both systems have equal BER performance when perfect CSI is considered. However, Alamouti-MRC scheme suffers a more severe performance degradation due to the effect of ICSI, which causes a noise enhancement through block code interference. When the channel estimate becomes worse (i.e., lower values of γ_ψ), the performance gap is reduced, since the channel estimation error becomes the dominant factor in the BER, compared to equivalent noise.
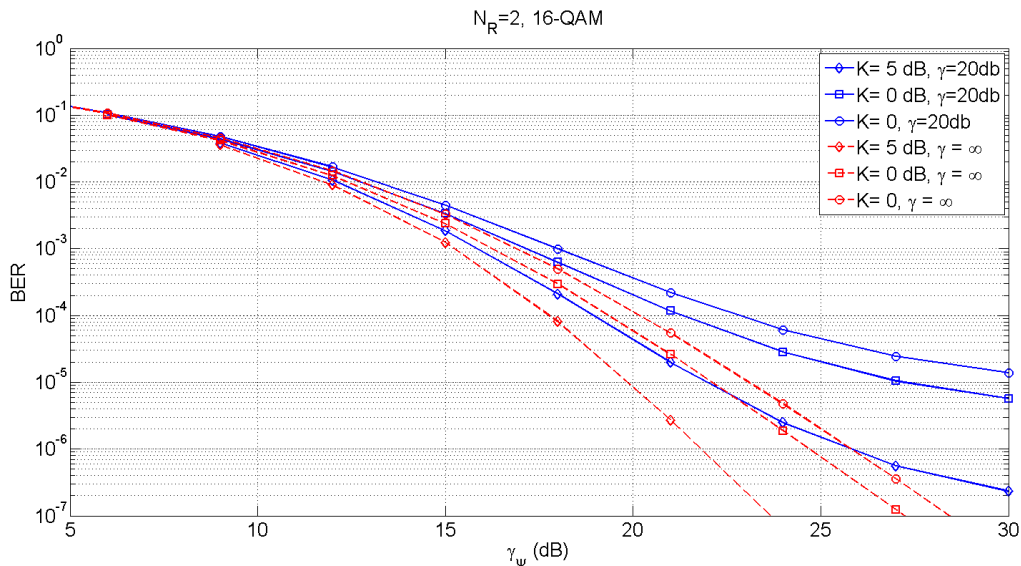
Figure 4.10: BER vs SCER for different values Ricean K factor and γ, N_R=2 reception branches and 16-QAM.

The different impact of ICSI in $2 \times N_R$ Alamouti-MRC and conventional $1 \times 2N_R$ MRC is also appreciated in Fig. 4.12, where the BER is evaluated as a function of γ_ψ, for a fixed value of SNR. In this figure, three different regions can be identified:

1. When the magnitude of the channel estimation error is considerable (i.e., low values of γ_ψ), both Alamouti-MRC and conventional MRC behave similarly, since the dominant effect in the BER is the error in the channel estimation.

2. When the channel estimation error decreases (i.e., $15dB < \gamma_\psi < \gamma$), a performance gap between Alamouti-MRC and conventional MRC is observed. This effect is provoked by the block code interference due to ICSI that appears in Alamouti-MRC scheme, which can be seen as an equivalent noise enhancement (see η_k term in Section 4.2.3). The magnitude of this gap grows in the presence of a LOS component, as well as when the number of receive antennas N_R is increased.

3. Finally, when the SNR is the dominant factor compared to γ_ψ (i.e., $\gamma_\psi > \gamma$), both schemes tend to behave similarly.
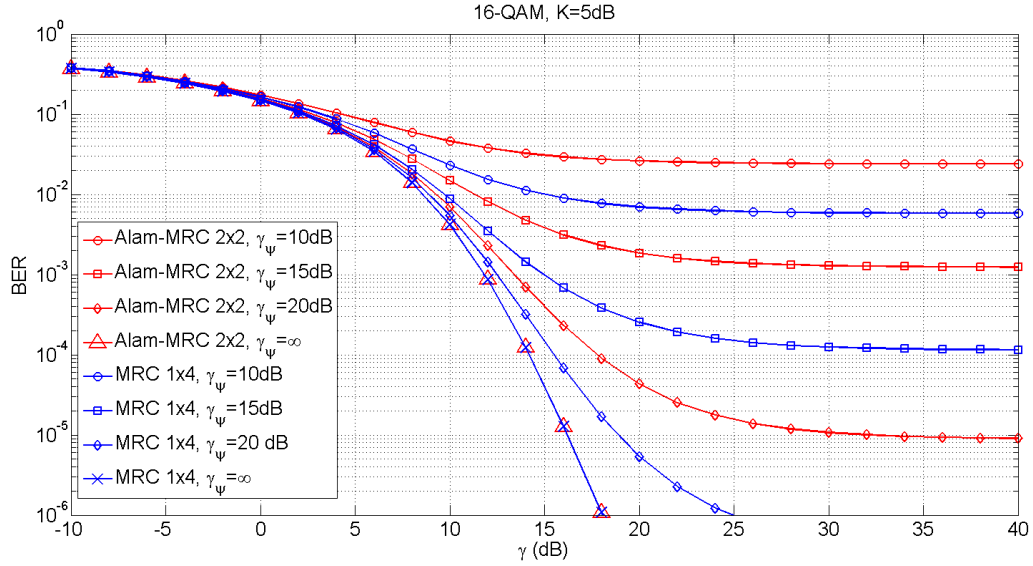
Figure 4.11: Comparison of $2 \times N_R$ Alamouti-MRC and $1 \times 2N_R$ MRC. BER vs SNR for different values of γ_ψ, $K = 5$dB Ricean factor and 16-QAM.
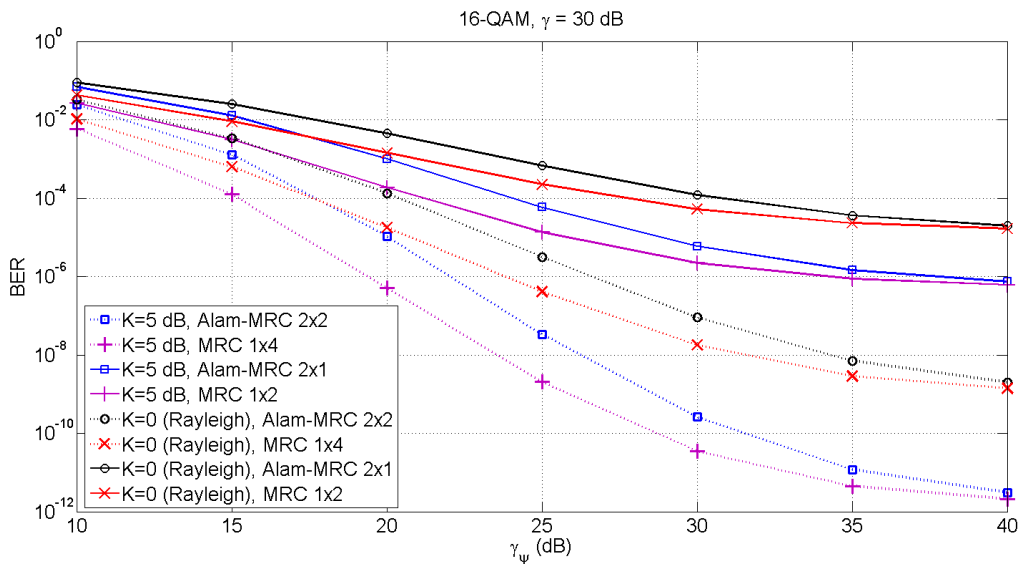
Figure 4.12: Comparison of $2 \times N_R$ Alamouti-MRC and $1 \times 2N_R$ MRC. BER vs SCER for different values of receive antennas N_R and Ricean K factor, $\gamma = 30$dB and 16-QAM.

Evaluation of approximate expression

The exact (4.2.15) and approximate (4.2.26) BER expressions are evaluated in Fig. 4.13, for different combinations of Ricean K factor, and number of reception branches N_R. It is observed that the approximate and exact curves become more similar when N_R and K are increased. In fact, for values of $K > 10dB$ the approximate expression provides an excellent match with the exact BER values.
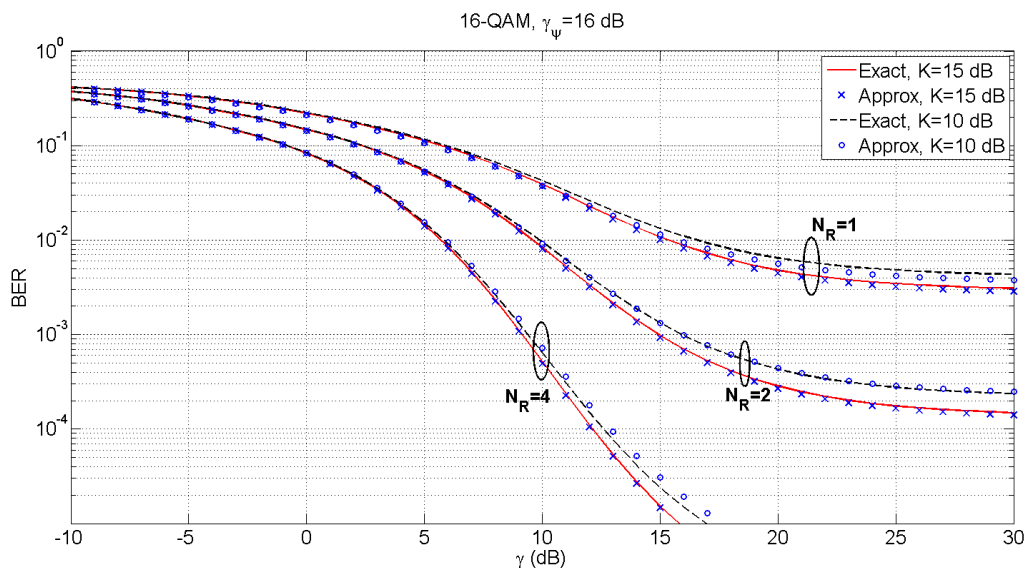
Figure 4.13: BER vs SNR (Exact and approximate) for different values of Ricean K factor and number of reception branches N_R, $\gamma_\psi = 16$dB, 16-QAM.

4.2.5 Discussion

Closed-form BER expressions have been obtained for a MIMO $2 \times N_R$ system that combines Alamouti transmission and MRC reception in Ricean fading channels, when imperfect channel estimation is considered. The exact expression is given in terms of a finite sum of special functions, which can be easily evaluated. Additionally, an approximate expression in terms of Gaussian Q function is provided for strong LOS scenarios.

Results show that an appreciable performance gap between the investigated configuration and the conventional $1 \times 2N_R$ MRC system is appeared due to the noise enhancement caused

by block code interference. Ir is also appreciated that the magnitude of this performance gap grows either when the diversity order is increased, or in the presence an stronger LOS component.

The main contributions of this section have been published in [21].

Chapter 5

Analysis of OFDM systems under RF impairments

This chapter is devoted to the performance analysis of OFDM systems affected by different non idealities. Particularly, we focus on two major impairments associated with direct conversion receivers (DCRs), which are being extensively used for the development of low-cost integrated radio front-ends in wireless communication systems: the direct-current (DC) offset and the in-phase/quadrature (IQ) imbalance.

First, we calculate an exact closed-form expression for the BER of OFDM systems with direct conversion that employ MRC reception in multipath Rayleigh fading channels, using binary phase-shift keying (BPSK) modulation. We assume a realistic system model where DC offset, carrier frequency offset (CFO) and ICSI are simultaneously considered.

Then, we analyze the effect of the transmit and receive IQ imbalances in OFDM systems that employ M-QAM modulation, when ICSI is considered in multipath Rayleigh fading channels. Since in this scenario the equivalent channel gain is modelled as a non circularly symmetric RV, the real and imaginary parts of the decision variable are not independent. Hence, this aspect must be taken into account for a proper analysis.

5.1 OFDM systems affected by DC-offset

5.1.1 Related Work

Direct conversion receivers have become the preferred solution for the implementation of low-cost wireless radio frequency (RF) integrated circuits [53]. Unlike heterodyne receivers, DCRs are not affected by image frequency problems, thus reducing the complexity in off-chip components. Besides, RF front-end in DCRs is suitable for the implementation of multi-standard software radios required in next generation wireless systems. However, DCRs are known to be affected by direct current (DC) offset due to the non ideal behaviour of analog components [54], among other impairments.

Most part of modern wireless communication systems use orthogonal frequency division multiplexing (OFDM) as transmission technique, thanks to its inherent ability to compensate the effects of multipath fading [55]. This performance is degraded in the presence of carrier frequency offset (CFO), which may cause inter carrier interference (ICI). Since the CFO compensation process requires a multiplication with a complex exponential, the DC offset is spread over all the OFDM subcarriers [56]. Hence, every data subcarrier is affected by a DC offset interference, whose value depends on the subcarrier index and the CFO.

Therefore, the CFO must be accurately estimated and compensated in the OFDM receiver. Although DC offset may affect the quality of CFO estimation through classical correlation algorithms [57], there exist different mechanisms to accurately estimate the CFO in the presence of DC offset [58, 59]. In many cases (e.g IEEE 802.16 [60], Long Term Evolution (LTE) [61] and others), DC subcarrier is not used for data transmission in OFDM systems since it is expected to be affected by DC offsets in the transceiver.

The analysis of non-ideal OFDM systems has been tackled in the literature from different perspectives. The effect of ICI [62] in the BER was studied in [63] and [64], both assuming perfect channel state information (PCSI). The effect of imperfect channel state information (ICSI) on the performance of OFDM systems was incorporated in [15] and [65]. Less literature is available when residual DC offset is considered: In [66], a bit error rate (BER) analysis of OFDM systems in the presence of DC offset and CFO under CLT approximation

was accomplished, for the particular case of binary phase-shift keying (BPSK) modulation, and was further extended to other modulation formats in [67]. However, the calculated expressions are not given in closed-form and assume PCSI in the receiver side, which is not a realistic approach since the estimate of the channel frequency response may be affected by the residual DC offset [68].

In this section, we derive an exact closed-form expression for the BER of a non-ideal OFDM system with residual DC offset, CFO and ICSI, for an arbitrary number of receive antennas and considering maximal ratio combining (MRC) reception. Therefore, the contribution of this work may be summarized as: (1) the final BER expression is exact and is given in closed-form, (2) the number of receive antennas is arbitrary, and (3) the effect of ICSI is included in our analysis. Additionally, (4) we obtain a simple yet accurate expression for the maximum allowable DC offset in a DCR, for a target signal-to-noise ratio (SNR).

5.1.2 System Model

Let us consider a discrete time OFDM system with N_R reception branches. The received baseband signal in the v-th branch $y_v[n]$ can be expressed as

$$y_v[n] = \frac{1}{\sqrt{N}} \sum_{m=-N/2}^{N/2-1} H_{v,m} X_m e^{\frac{j2\pi n(m+\varepsilon)}{N}} + \eta_v + w_v[n], \qquad (5.1.1)$$

where N is the number of OFDM subcarriers, $n = 0 \ldots N-1$ is the discrete time index of the OFDM symbol, X_m represents the BPSK symbol with energy E_s transmitted at the m-th OFDM subcarrier, η_v is the complex-valued DC offset, ϵ is the normalized CFO, $w_v[n]$ is the additive white Gaussian noise (AWGN) with zero mean and σ_w^2 variance and $H_{v,m}$ is the channel frequency response at the m-th subcarrier for the v-th reception branch.

In this model, we assume the length of the channel impulse response to be less than the cyclic prefix size and the $H_{v,m}$ coefficients of the channel frequency response are complex Gaussian RVs with zero mean and unity variance, independently distributed for every reception branch, i.e. $E\left\{H_{v_1,m}H_{v_2,m}^*\right\} = 0, \forall v_1 \neq v_2$, where $E\{\cdot\}$ denotes expectation operation. We also consider η_v to remain invariant within one OFDM symbol.

After the cyclic prefix removal and CFO compensation, the OFDM received signal is

passed back to frequency domain by means of a discrete Fourier transform (DFT). Mathematically, this process results in

$$Y_{v,k} = H_{v,k}X_k + W_{v,k} + \eta_v \zeta_k(\varepsilon), \tag{5.1.2}$$

where $k = -N/2...N/2 - 1$ is the subcarrier index, $\zeta_k(\varepsilon) = \sqrt{N} \frac{\mathrm{sinc}(k+\varepsilon)}{\mathrm{sinc}(\frac{k+\varepsilon}{N})} e^{-j\pi(k+\varepsilon)(N-1)/N}$, $\mathrm{sinc}(x) = \frac{\sin(\pi x)}{\pi x}$, and $W_{v,k}$ is the AWGN term.

In order to separate the effects of ICSI and ICI in our analysis, we assume perfect CFO estimation in the receiver side, which can be achieved considering the method proposed in [59]. However, the effect of ICI can be incorporated in our analysis through CLT approximation as in [63] and [65–67, 69].

5.1.3 BER analysis

In this subsection, we calculate an exact closed-form expression for the BER of an OFDM-MRC system impaired by DC-offset and ICSI, for an arbitrary number of receive antennas. Then, we particularize our results for the case of single branch reception and PCSI, in order to allow for a better insight into the effect of the DC-offset in the BER.

General case

When MRC is performed at the receiver, the decision metric r_k can be expressed as

$$r_k = \sum_{v=1}^{N_R} \left(\frac{H_{v,k}X_k\hat{H}_{v,k}^*}{||\hat{\mathbf{h}}||^2} + \frac{(W_{v,k} + \eta_v\zeta_k(\varepsilon))\hat{H}_{v,k}^*}{||\hat{\mathbf{h}}||^2} \right), \tag{5.1.3}$$

where $\hat{\mathbf{h}}$ is the channel estimation vector. Following the channel model introduced in [38], we denote the components of $\hat{\mathbf{h}}$ as $\hat{H}_v = H_v + \psi_v$, where ψ_v is the Gaussian error in channel estimation with zero mean and σ_ψ^2 variance, and ψ_v is independent of $\hat{H}_v$. In this scenario, the BER in the k-th subcarrier can be expressed as

$$P_k = \Pr\left\{\Re\{r_k\} > 0 | X_k = -\sqrt{E_s}\right\}. \tag{5.1.4}$$

Let us define a random variable D as a quadratic form

$$D = \sum_{v=1}^{N_R} \mathbf{x}_{v,k}^{\mathcal{H}} \mathbf{Q}\mathbf{x}_{v,k}. \tag{5.1.5}$$

The quadratic form matrix $\mathbf{Q}$ and the random variable vector $\mathbf{x}_{v,k}$ are defined as

$$\mathbf{x}_{v,k} \triangleq \left[\begin{array}{c} Y_{v,k} \\ \hat{H}_{v,k} \end{array} \right], \quad \mathbf{Q} \triangleq \left[\begin{array}{cc} 0 & -\frac{1}{2} \\ -\frac{1}{2} & 0 \end{array} \right]. \tag{5.1.6}$$

If we expand (5.1.5) and (5.1.6), we have

$$P_k = \Pr \left\{ \sum_{v=1}^{N_R} \left(Y_{v,k} \hat{H}_{v,k}^* + Y_{v,k}^* \hat{H}_{v,k} \right) < 0 | X_k = -\sqrt{E_s} \right\}. \tag{5.1.7}$$

The calculation of P_k can be tackled through Proakis' analysis of complex Gaussian quadratic forms [6, eq. B-21], or using the alternative expression given in (3.2.7). Here, the mean vector $\mathbf{m}_{v,k} \triangleq \mathrm{E}\{\mathbf{x}_{v,k}\}$ and the covariance matrix $\mathbf{R} \triangleq \mathrm{E}\left\{ (\mathbf{x}_{v,k} - \mathbf{m}_{v,k})(\mathbf{x}_{v,k}^{\mathcal{H}} - \mathbf{m}_{v,k}^{\mathcal{H}}) \right\}$ yield

$$\mathbf{m}_{v,k} = \eta_v \zeta_k(\varepsilon)\mathbf{u},$$
$$\mathbf{R} \triangleq \left[\begin{array}{cc} r_{11} & r_{12} \\ r_{21} & r_{22} \end{array} \right] = \left[\begin{array}{cc} |X_k|^2 + \sigma_w^2 & (1 - \sigma_\psi^2)X_k \\ (1 - \sigma_\psi^2)X_k^* & 1 - \sigma_\psi^2 \end{array} \right], \tag{5.1.8}$$

where $\mathbf{u}^t = [1, 0]$. According to the general expression (3.2.7), in this scenario we have $\alpha \triangleq a = b$. Hence, we can use the relationship between Marcum-Q function and the $v-th$ order modified Bessel function of the first kind $I_v(x)$ given in [4, eq. 4.17]

$$Q_1(\alpha, \alpha) = \frac{1 + \exp\left(-\alpha^2\right) I_0(\alpha^2)}{2}, \tag{5.1.9}$$

to express the BER in exact closed-form as

$$P_k = \frac{1}{2} + \sum_{v=0}^{N_R-1} C_v(\lambda) I_v(\bar{\eta}_\varepsilon^2 \alpha^2) \exp\left[-\bar{\eta}_\varepsilon^2 \alpha^2\right], \tag{5.1.10}$$

where $\bar{\eta}_\varepsilon = \sqrt{\Sigma_{v=1}^{N_R} |\eta_v \zeta_k(\varepsilon)|^2}$, and λ, α and $C_v(\lambda)$ are defined in Table 5.1.

After some algebra, we find an easy expression for λ and α in this scenario

$$\alpha = \frac{\Gamma}{\sqrt{2E_s}}, \quad \lambda = \frac{1+\Gamma\sqrt{\left(1-\sigma_\psi^2\right)}}{1-\Gamma\sqrt{\left(1-\sigma_\psi^2\right)}}, \tag{5.1.11}$$

where $\Gamma = \sqrt{\frac{\bar{\gamma}}{1+\bar{\gamma}}}$, and $\bar{\gamma} = E_s/\sigma_w^2$ is the average SNR. From expression (5.1.10) it is appreciated that the phase of η_v does not affect the BER, since H_k is a circularly symmetric random variable. Interestingly, it is observed that the effect of DC offset, and ICSI are separated: $\bar{\eta}_\epsilon$ term is only present in the argument of $I_v(\cdot)$ and exponential functions, whereas σ_ψ^2 only affects the $C_v(\cdot)$ coefficients through λ.

Table 5.1: Parameters and definitions for BER calculation.

PARAMETER	DEFINITION
λ	$\left\| \dfrac{\left(\mathrm{tr}(\mathbf{RQ}) + \sqrt{\mathrm{tr}(\mathbf{RQ})^2 - 4\det(\mathbf{RQ})} \right)}{\left(\mathrm{tr}(\mathbf{RQ}) - \sqrt{\mathrm{tr}(\mathbf{RQ})^2 - 4\det(\mathbf{RQ})} \right)} \right\|$
α	$\sqrt{\dfrac{1}{2} \dfrac{r_{22}}{\mathrm{tr}(\mathbf{RQ})^2 - 4\det(\mathbf{RQ})}}$
$C_v(\lambda)$	$\dfrac{\mathrm{K}}{(1+\lambda)^{2N_R-1}} \displaystyle\sum_{l=0}^{N_R-1-v} \binom{2N_R-1}{l} \left[\lambda^l - \lambda^{2N_R-1-l} \right]; \quad \mathrm{K} = \begin{cases} 1/2, & v = 0 \\ 1, & v \neq 0 \end{cases}$

Perfect CSI and single branch reception

Additional insights can be extracted for some scenarios of interest. In the particular case of $N_R = 1$ and PCSI, the BER can be expressed in the following compact form

$$P_k = \frac{1}{2} \left[1 - \Gamma I_0 \left(\Gamma^2 \frac{|\eta_v \zeta_k(\varepsilon)|^2}{2E_s} \right) \exp\left\{ -\Gamma^2 \frac{|\eta_v \zeta_k(\varepsilon)|^2}{2E_s} \right\} \right]. \tag{5.1.12}$$

Note that in the limit case of zero DC offset, the BER expression reduces to $P_k = \frac{1}{2}(1 - \Gamma)$ given in [6, Eq. 13.3-7]. From expression (5.1.12), considering a first order Taylor approximation, the irreducible BER floor due to CFO and residual DC offset in the k-th subcarrier can be easily calculated, i.e. considering $\bar{\gamma} \to \infty$ and $|\eta_v \zeta_k(\varepsilon)|^2 << E_s$

$$P_k \approx \frac{|\eta_v \zeta_k(\varepsilon)|^2}{4E_s}. \tag{5.1.13}$$

Hence, in this scenario the BER floor is approximately one quarter of the DC offset to signal ratio. Combining (5.1.13) and the BER expression in the absence of DC offset $P_k = \frac{1}{2}(1 - \Gamma)$, we can derive a rule of thumb for the maximum allowable residual DC offset in a receiver for a particular $\bar{\gamma}_{th}$ value,

$$|\eta_v(max)|^2 = \frac{2E_s}{\beta^2 |\zeta_k(\varepsilon)|^2} \left(1 - \sqrt{\frac{\bar{\gamma}_{th}}{1 + \bar{\gamma}_{th}}} \right), \tag{5.1.14}$$

where β is a constant value designed for a particular SNR degradation. If we consider a maximum degradation due to DC offset of $0.5dB$, we obtain $\beta \approx 4$.

5.1.4 Numerical Results

We use the expressions calculated in Section 5.1.3 to evaluate the BER in different particular scenarios. As in [66], we consider an OFDM system with $N=64$ subcarriers with BPSK modulation, and the same parameters for multipath Rayleigh fading. We assume that the channel does not vary within one OFDM symbol, and $k = 0$ subcarrier is not used for data transmission. For convenience of discussion, we assume equal DC offset in all the reception branches (i.e. $\eta_v = \eta$). In the following, we denote the signal-to-channel estimation error ratio (SCER) as $\gamma_{CE} = E_S/\sigma_\psi^2$.

Figure 5.1 illustrates the effect of DC offset in the BER for all subcarriers which compose the OFDM symbol, for different values of γ_{CE} and η_v. Two reception branches (i.e. $N_R=2$) are considered. As expected, the BER in the subcarriers near DC is worse than in higher frequencies ($|k| \to N/2$), since the DC offset leakage decays with $|k|$ index. When channel estimation error grows (i.e. lower γ_{CE} values), the BER in low and high frequencies tends to behave similarly, and the BER floor is increased.
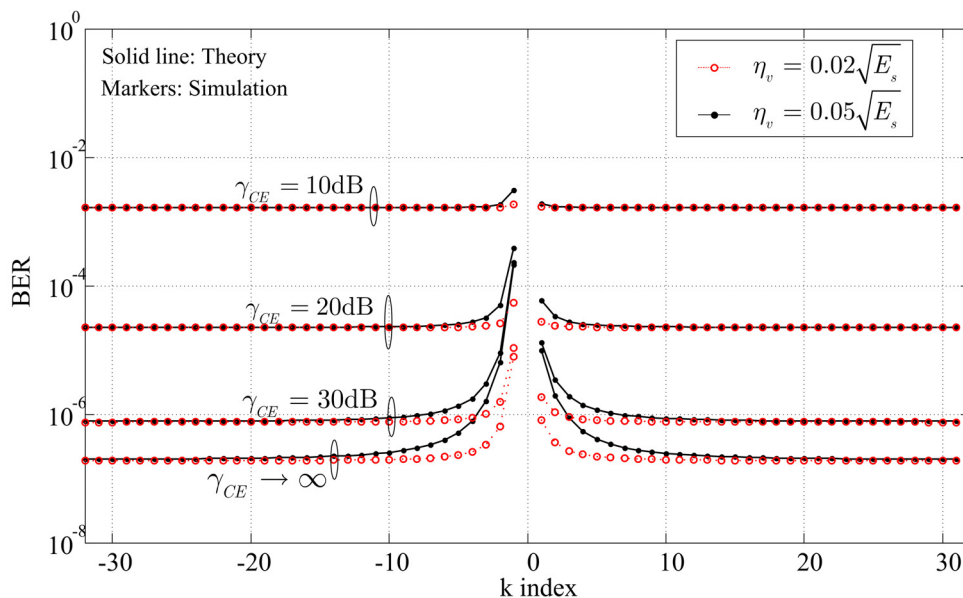
Figure 5.1: BER vs subcarrier index k, with $N_R=2$ receive antennas, BPSK modulation, $\varepsilon = 0.4$, and $\bar{\gamma} = 30$dB for different values of γ_{CE} and η_v.

Figure 5.2 shows the average BER for the OFDM symbol defined as

$$\overline{\overline{BER}} = \frac{1}{N-1} \sum_{k=-N/2, k \neq 0}^{k=N/2-1} P_k, \tag{5.1.15}$$

as a function of the SNR, for different scenarios in the case of a single reception branch. In the case of dominant channel estimation error, similar BER values are obtained independently of the DC offset η_v. When the SCER grows, a BER floor due to DC offset interference is appreciated. When PCSI is assumed, the BER floor due to DC offset is accurately calculated by (5.1.13).
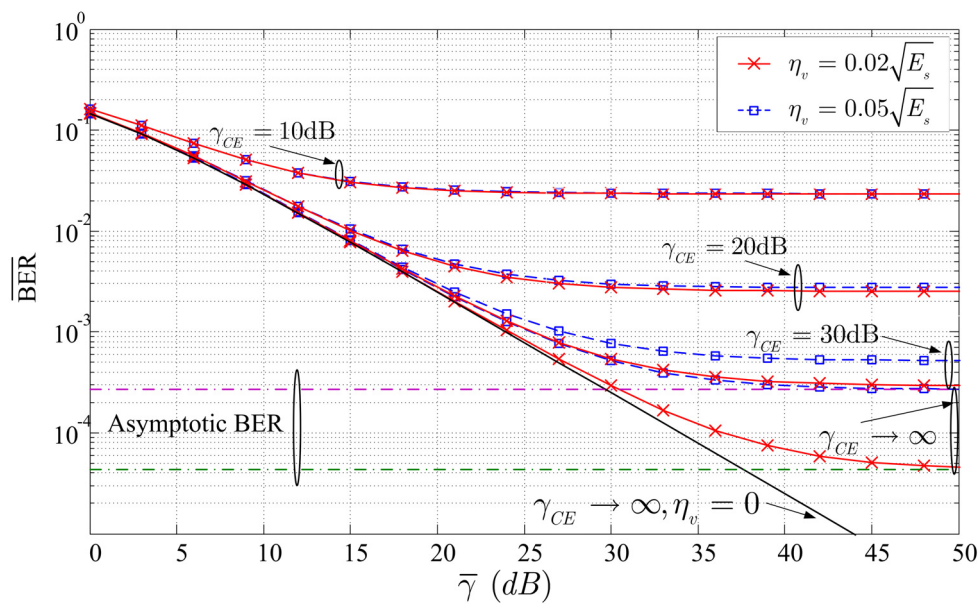
Figure 5.2: Average BER vs SNR, with N_R=1 receive antenna and BPSK modulation, for different values of η_v and γ_{CE}.

5.1.5 Discussion

We performed an exact closed-form BER analysis of an OFDM system with BPSK modulation, in the presence of CFO, DC offset and non-ideal channel estimation, for an arbitrary number of receive antennas, when multipath Rayleigh fading is considered. Results show

that channel estimation error in combination with DC offset and CFO provokes the appearance of an irreducible BER floor. Additionally, we provided a simple rule of thumb to determine the maximum allowable residual DC offset in a receiver for a target SNR.

The main contributions of this section have been published in [20]

5.2 OFDM systems affected by IQ-imbalance

5.2.1 Related Work

In section 5.1, it was stated that DCRs are a feasible alternative for the implementation of low-cost wireless radio RF front-ends. Despite its appealing characteristics, these structures are more sensitive to different impairments associated with a non ideal behaviour of analog components. One of the major impairments in DCRs is the enhancement of amplitude and phase mismatch between the in-phase (I) and quadrature (Q) carriers, usually referred to as IQ imbalance. The effect of these mismatches results on a performance degradation due to the appearance of an interference term due to the loss of orthogonality between I and Q components.

In the case of orthogonal frequency division multiplexing (OFDM) systems, the effect of IQ imbalance is the appearance of a mirror carrier interference (MCI), since the received signal at the frequency index k is both affected by the transmitted symbol z_{-k} and the channel frequency response H_{-k} at the mirror index. In the literature, the effects of IQ imbalance have been mostly addressed from the perspective of compensation schemes [70–77] or pilot design [78–80]. On the contrary, analytical results covering the impact of IQ imbalance in the system performance are much scarcer [81–83].

Particularly, the bit error rate of an OFDM system affected by IQ imbalance at the receiver side was treated in [81], assuming that the channel frequency responses H_k and H_{-k} were independent, as well as perfect channel state information (PCSI) at the receiver side. These results were further extended in [82] introducing some other receiver impairments in the analysis such as imperfect channel estimation, but the BER expression required a two-fold numerical integration. The effects of transmit (TX) and receive (RX) IQ imbalances

were tackled in [83], considering a multiple-input multiple-output (MIMO) OFDM system. However, the same assumptions that in [81] were taken, the closed-form results were approximate, and an expression accounting for the joint effect of TX and RX IQ imbalances was not provided.

A realistic system model of an OFDM system impaired by TX and RX IQ imbalances must consider that the equivalent channel gain is a complex random variable (RV) that lacks from circular symmetry, i.e., the real and imaginary parts of the equivalent channel gain are not independent and have different variances [12, 13]. Hence, the non-circular symmetry of the RVs involved in the process must be taken into account for an exact analysis.

In this section, we calculate an exact closed-form expression for the bit error rate (BER) of an OFDM system impaired by TX and RX IQ imbalances, when imperfect channel state information (ICSI) is considered, in Rayleigh fading channels. The probability calculation is accomplished by means of the general analysis of quadratic forms introduced in section 3.3, which considers complex-valued non-circularly symmetric zero-mean Gaussian RVs.

We demonstrate that the BER in this scenario can be expressed in terms of the Lauricella function $F_D(\cdot)$, which has recently been used in a great number of publications in the area of performance analysis of wireless communication systems [84–88]. Additionally, we derive two approximate yet accurate expressions for the BER: the first one is given in terms of the Appell hypergeometric function $F_1(\cdot)$, which is included in many mathematical packages such as Mathematica, and the second one does not require for the evaluation of special functions. The former approximation provides an excellent match with the exact BER values for a wide range of IQ imbalances, whereas the latter expression is very accurate for practical values of IQ imbalances.

Hence, the contribution of this work is twofold: First, an exact closed-form expression for the BER in the investigated scenario is obtained; and secondly, two approximate yet highly accurate expressions for the BER are provided.

5.2.2 Preliminaries

Proposition 1. *Let x and y be two correlated circularly-symmetric complex RVs with zero mean, σ^2 variance and $\rho \triangleq E\{xy^*\}$. The RV $z \triangleq ax + by^*$ is in general a non circularly*

symmetric RV, where $a, b \in \mathbb{C}$ are arbitrary constants values.

Proof. Using the definitions in (3.3.1) and (3.3.2), the terms in the real covariance matrix of $\check{z}$ can be calculated as

$$\sigma_{z_r}^2 = \frac{\sigma^2}{2} \left(|a|^2 + |b|^2 + 2\Re\{\rho ab\} \right), \tag{5.2.1}$$

$$\sigma_{z_i}^2 = \frac{\sigma^2}{2} \left(|a|^2 + |b|^2 - 2\Re\{\rho ab\} \right), \tag{5.2.2}$$

$$\sigma_{z_r z_i} = \sigma^2 \Im\{\rho ab\}. \tag{5.2.3}$$

Clearly, according to the circular symmetry condition given in section 3.3.1, z is a non circularly symmetric RV when a, b and ρ are different to zero. □

5.2.3 System Model

In the following, we consider an OFDM system where the cyclic prefix size is larger than the maximum delay spread. It is also assumed that time and frequency synchronization is perfectly accomplished at the receiver side. Hence, an equivalent frequency-domain system model as in [77, 83] can be used, where the received signal in the kth subcarrier r_k can be expressed as

$$r_k = g_k z_k + h_{-k} z_{-k} + w_k, \tag{5.2.4}$$

where $k \in \{-N/2, \ldots, N/2 - 1\}$, N is the number of subcarriers of the OFDM symbol, and z_k and z_{-k} represent the transmitted symbols in the kth and $-k^{th}$ subcarriers respectively (namely desired signal and MCI), belonging to an M-ary quadrature amplitude modulation (M-QAM) constellation. The set of M complex symbols is denoted as $\mathcal{S}_M \triangleq \{s_{u,v} \in \mathbb{C} \, / \, \Re\{s_{u,v}\} = (2u - \sqrt{M} - 1)d; \, \Im\{s_{u,v}\} = (2v - \sqrt{M} - 1)d; \, \{u, v\} \in 1, \ldots, \sqrt{M}\}$, where $2d$ is the minimum distance between symbols, and independent bit mapping is assumed for I and Q components.

The remainder terms in (5.2.4) g_k and h_{-k} represent the equivalent channel gains for the desired signal and the MCI respectively, whereas w_k is an equivalent noise term. These latter terms can be expressed as

$$g_k = K_1 G_1 H_k + K_2 G_2 H_{-k}^*, \tag{5.2.5}$$

$$h_{-k} = K_2 G_1^* H_{-k}^* + K_1 G_2^* H_k, \tag{5.2.6}$$

$$w_k = K_1 n_k + K_2 n_{-k}^*, \tag{5.2.7}$$

where H_k and H_{-k} are correlated complex Gaussian RVs with zero-mean and σ_g^2 variance which denote the channel frequency response in the kth and $-k^{th}$ subcarriers respectively, n_k and n_{-k} represent the additive white Gaussian noise with zero-mean and σ_n^2 variance, and the G_i and K_i terms ($i = 1, 2$) are used to model the TX and RX IQ imbalances respectively, through the following expressions

$$G_1 = \frac{1 + \alpha_t e^{j\varphi_t}}{2}, \qquad\qquad G_2 = \frac{1 - \alpha_t e^{-j\varphi_t}}{2}, \qquad (5.2.8)$$

$$K_1 = \frac{1 + \alpha_r e^{-j\varphi_r}}{2}, \qquad\qquad K_2 = \frac{1 - \alpha_r e^{j\varphi_r}}{2}. \qquad (5.2.9)$$

Hence, the amplitude and phase imbalances are given by α_t and φ_t at the transmitter side, and by α_r and φ_r at the receiver side, respectively.

According to proposition (1), the equivalent gain g_k in this system model is a non-circularly symmetric complex Gaussian RV with zero-mean, which can be characterized by a 2×2 covariance matrix [13] as

$$\mathbf{\Sigma}_{\breve{g}_k} \triangleq E \left\{ \begin{bmatrix} \Re(g_k) \\ \Im(g_k) \end{bmatrix} \begin{bmatrix} \Re(g_k) & \Im(g_k) \end{bmatrix} \right\} = \begin{bmatrix} \sigma^2_{\Re(g_k)} & \sigma^2_{\Re(g_k)\Im(g_k)} \\ \sigma^2_{\Re(g_k)\Im(g_k)} & \sigma^2_{\Im(g_k)} \end{bmatrix}. \qquad (5.2.10)$$

Note that in the absence of IQ imbalances (i.e., $\alpha_t = \alpha_r = 1$ and $\varphi_t = \varphi_r = 0$), we have $G_1 = K_1 = 1$ and $G_2 = K_2 = 0$, and the equivalent gain terms are expressed as $g_k = H_k$ and $h_{-k} = 0$. Therefore, this leads to circular symmetry in g_k RV, and $\mathbf{\Sigma}_{\breve{g}_k} = \mathbf{I}_{2\times 2}\frac{\sigma_g^2}{2}$., where $\mathbf{I}_{2\times 2}$ is the identity matrix.

We also denote the channel estimate at the receiver side as $\hat{g}_k = g_k + \Psi_k$, where Ψ_k is in general a non-circularly symmetric complex Gaussian RV that represents the channel estimation error, with zero-mean and covariance matrix $\mathbf{\Sigma}_{\breve{\Psi}_k}$. Finally, the decision metric after channel compensation is expressed as

$$y_k = \frac{r_k \hat{g}_k^*}{|\hat{g}_k|^2}. \qquad (5.2.11)$$

5.2.4 BER analysis

The probability calculation in this scenario is accomplished as follows: First, the BER is expressed as the average, over all the transmitted z_k and z_{-k} symbols, of a weighted sum of

components of error probability. These weights only depend on the constellation mapping, and their calculation is tackled in section 2.3. Then, the probability calculation for the investigated scenario is carried out by making use of a general analysis of non circularly-symmetric Gaussian quadratic forms in complex RVs.

According to these premises, the BER expression is hence given by

$$BER = \frac{1}{M^2 log_2 M} \sum_{\forall s_{u,v}, s_{u',v'} \in \mathcal{S}_M} \left[\sum_{n=1}^{u-1} \alpha_u^-(n) \mathcal{I}_{u,v}^-(n) + \sum_{n=u}^{\sqrt{M}-1} \alpha_u^+(n) \mathcal{I}_{u,v}^+(n) + \sum_{n=1}^{v-1} \beta_v^-(n) \mathcal{Q}_{u,v}^-(n) + \right.$$
$$\left. \sum_{n=v}^{\sqrt{M}-1} \beta_v^+(n) \mathcal{Q}_{u,v}^+(n) \right],$$

$$(5.2.12)$$

where the $\alpha_u^\pm(n)$ and $\beta_v^\pm(n)$ coefficients are defined in (2.3.2), and $\mathcal{I}_{u,v}^\pm(n)$ and $\mathcal{Q}_{u,v}^\pm(n)$ are the components of error probability (CEPs) conditioned on a particular value of z_k and z_{-k}, i.e.,

$$\mathcal{I}_{u,v}^\mp(n) = \Pr \left\{ \pm \Re \left\{ y_k - \mathcal{B}_{\mathcal{I}}(n) \right\} < 0 \middle| z_k = s_{u,v}; z_{-k} = s_{u',v'} \right\}, \qquad (5.2.13)$$

$$\mathcal{Q}_{u,v}^\mp(n) = \Pr \left\{ \pm \Im \left\{ y_k - \mathcal{B}_{\mathcal{Q}}(n) \right\} < 0 \middle| z_k = s_{u,v}; z_{-k} = s_{u',v'} \right\}. \qquad (5.2.14)$$

where $\mathcal{B}_{\mathcal{I}}(n) = (2n - \sqrt{M})d$ and $\mathcal{B}_{\mathcal{Q}}(n) = j(2n - \sqrt{M})d$ are the decision boundaries for the I and Q components in the M-QAM constellation, respectively.

With these definitions, we proceed to calculate $\mathcal{I}_{u,v}^-(n)$ probability. The remainder CEPs can be calculated using the same procedure. Combining (5.2.11) and (5.2.13), we have

$$\mathcal{I}_{u,v}^-(n) = \Pr \left\{ \frac{1}{2} r_k \hat{g}_k^* + \frac{1}{2} r_k^* \hat{g}_k - |\hat{g}_k|^2 B_I(n) < 0 \right\} = \Pr \left\{ D < 0 \right\}. \qquad (5.2.15)$$

In expression (5.2.15), D can be seen as a particular case of a general quadratic form denoted as $D = A |X|^2 + B |Y|^2 + CXY^* + C^*X^*Y$, where $A = 0$, $B = -B_I(n)$, $C = C_r + jC_i = 1/2$, $X = r_k$ and $Y = \hat{g}_k$. The values of A, B and C parameters for the remainder CEPs are given in Table 5.2.

Using the matrix expression of a quadratic form introduced in (3.2.1), and adopting the notation presented in (3.3.1), we can express

$$D = \breve{\mathbf{x}}_k^T \breve{\mathbf{Q}} \breve{\mathbf{x}}_k \qquad (5.2.16)$$

CEP	A	B	C
$\mathcal{I}^-(n)$	0	$-B_I(n)$	$1/2$
$\mathcal{I}^+(n)$	0	$B_I(n)$	$-1/2$
$\mathcal{Q}^-(n)$	0	$-B_Q(n)$	$j/2$
$\mathcal{Q}^+(n)$	0	$B_Q(n)$	$-j/2$

Table 5.2: Quadratic form matrices for the different CEPs

where

$$\check{\mathbf{x}}_k = \begin{bmatrix} \check{\mathbf{r}}_k \\ \check{\mathbf{g}}_k \end{bmatrix} ; \check{\mathbf{Q}} = \begin{bmatrix} \check{\mathbf{A}} & \check{\mathbf{C}} \\ \check{\mathbf{C}}^T & \check{\mathbf{B}} \end{bmatrix}. \tag{5.2.17}$$

Note that a simple rearrangement of rows and columns has been performed in $\check{\mathbf{x}}_k$ and $\check{\mathbf{Q}}$, in order to allow the covariance matrix of $\check{\mathbf{x}}_k$ to be expressed in terms of the individual covariance matrices of $\check{\mathbf{r}}_k$, $\check{\mathbf{g}}_k$, and its cross correlation matrix in Appendix 5.2.7.

For convenience of notation, we introduce a superindex where necessary to denote the corresponding CEP. The $\check{\mathbf{x}}_k$ vector is a real Gaussian RV, with zero mean and covariance matrix $\mathbf{R} \triangleq \mathrm{E}\left\{\check{\mathbf{x}}_k \check{\mathbf{x}}_k^T\right\}$. The covariance matrix $\mathbf{R}$ for this scenario is derived in Appendix 5.2.7. Finally, with $\mathbf{R}$ and $\check{\mathbf{Q}}$ matrices, the probability (5.2.15) is calculated using (3.3.19) as

$$\mathcal{I}_{u,v}^-(n) = \sqrt{\frac{\omega_1^{\mathcal{I}^-} \omega_2^{\mathcal{I}^-} \omega_4^{\mathcal{I}^-}}{d_{1,3}^{\mathcal{I}^-} d_{2,3}^{\mathcal{I}^-} \omega_3^{\mathcal{I}^-}}} F\left(\frac{d_{3,4}^{\mathcal{I}^-}}{\omega_3^{\mathcal{I}^-}}, -\frac{d_{3,4}^{\mathcal{I}^-}}{d_{1,3}^{\mathcal{I}^-}}, -\frac{d_{3,4}^{\mathcal{I}^-}}{d_{2,3}^{\mathcal{I}^-}}\right), \tag{5.2.18}$$

where $\omega_{i=1\ldots4}^{\mathcal{I}^-} = \frac{-1}{2\lambda_i}$ are the poles of the characteristic function of D, λ_i are the eigenvalues of $\mathbf{R}\check{\mathbf{Q}}^{\mathcal{I}^-}$ matrix, $d_{i,j} = \omega_i - \omega_j$, $F(\cdot,\cdot,\cdot) \triangleq F_D(\frac{1}{2}, 1, \frac{1}{2}, \frac{1}{2}; 1; \cdot, \cdot, \cdot)$ and F_D is the Lauricella function.

The calculation of $\mathcal{I}_{u,v}^+(n)$ and $\mathcal{Q}_{u,v}^\pm(n)$ can be performed following the same procedure, since it is only necessary to modify $\check{\mathbf{Q}}$ matrix according Table 5.2. Therefore, the exact

closed-form expression for the BER is given by

$$
\begin{aligned}
BER = \tfrac{1}{M^2 log_2 M} \sum_{\forall s_{u,v}, s_{u',v'} \in S_M} & \Bigg[\sum_{n=1}^{u-1} \alpha_u^-(n) \sqrt{\tfrac{\omega_1^{\mathcal{I}-}\omega_2^{\mathcal{I}-}\omega_4^{\mathcal{I}-}}{d_{1,3}^{\mathcal{I}-} d_{2,3}^{\mathcal{I}-} \omega_3^{\mathcal{I}-}}} F\left(\tfrac{d_{3,4}^{\mathcal{I}-}}{\omega_3^{\mathcal{I}-}}, -\tfrac{d_{3,4}^{\mathcal{I}-}}{d_{1,3}^{\mathcal{I}-}}, -\tfrac{d_{3,4}^{\mathcal{I}-}}{d_{2,3}^{\mathcal{I}-}} \right) + \\
& \sum_{n=u}^{\sqrt{M}-1} \alpha_u^+(n) \sqrt{\tfrac{\omega_1^{\mathcal{I}+}\omega_2^{\mathcal{I}+}\omega_4^{\mathcal{I}+}}{d_{1,3}^{\mathcal{I}+} d_{2,3}^{\mathcal{I}+} \omega_3^{\mathcal{I}+}}} F\left(\tfrac{d_{3,4}^{\mathcal{I}+}}{\omega_3^{\mathcal{I}+}}, -\tfrac{d_{3,4}^{\mathcal{I}+}}{d_{1,3}^{\mathcal{I}+}}, -\tfrac{d_{3,4}^{\mathcal{I}+}}{d_{2,3}^{\mathcal{I}+}} \right) + \\
& \sum_{n=1}^{v-1} \beta_v^-(n) \sqrt{\tfrac{\omega_1^{\mathcal{Q}-}\omega_2^{\mathcal{Q}-}\omega_4^{\mathcal{Q}-}}{d_{1,3}^{\mathcal{Q}-} d_{2,3}^{\mathcal{Q}-} \omega_3^{\mathcal{Q}-}}} F\left(\tfrac{d_{3,4}^{\mathcal{Q}-}}{\omega_3^{\mathcal{Q}-}}, -\tfrac{d_{3,4}^{\mathcal{Q}-}}{d_{1,3}^{\mathcal{Q}-}}, -\tfrac{d_{3,4}^{\mathcal{Q}-}}{d_{2,3}^{\mathcal{Q}-}} \right) + \\
& \sum_{n=v}^{\sqrt{M}-1} \beta_v^+(n) \sqrt{\tfrac{\omega_1^{\mathcal{Q}+}\omega_2^{\mathcal{Q}+}\omega_4^{\mathcal{Q}+}}{d_{1,3}^{\mathcal{Q}+} d_{2,3}^{\mathcal{Q}+} \omega_3^{\mathcal{Q}+}}} F\left(\tfrac{d_{3,4}^{\mathcal{Q}+}}{\omega_3^{\mathcal{Q}+}}, -\tfrac{d_{3,4}^{\mathcal{Q}+}}{d_{1,3}^{\mathcal{Q}+}}, -\tfrac{d_{3,4}^{\mathcal{Q}+}}{d_{2,3}^{\mathcal{Q}+}} \right) \Bigg],
\end{aligned}
\tag{5.2.19}
$$

where $\alpha_u^{\pm}(n)$ and $\beta_v^{\pm}(n)$ coefficients are calculated in (2.3.2) for an arbitrary bit-mapping, and in (2.3.7) for the particular case of Gray mapping.

The calculated expression (5.2.19) is exact, and consists of a finite sum of Lauricella functions. However, it is possible to simplify this expression by means of some considerations in (5.2.19).

Using the results of expression (3.3.24), the BER can be approximated by the following expression

$$
\begin{aligned}
BER = \tfrac{1}{M^2 log_2 M} \sum_{\forall s_{u,v}, s_{u',v'} \in S_M} & \Bigg[\sum_{n=1}^{u-1} \alpha_u^-(n) \sqrt{\tfrac{\omega_1^{\mathcal{I}-}\omega_2^{\mathcal{I}-}\omega_4^{\mathcal{I}-}}{d_{1,3}^{\mathcal{I}-} d_{2,3}^{\mathcal{I}-} \omega_3^{\mathcal{I}-}}} G\left(\tfrac{d_{3,4}^{\mathcal{I}-}}{\omega_3^{\mathcal{I}-}}, -\tfrac{d_{3,4}^{\mathcal{I}-}}{\bar{d}^{\mathcal{I}-}} \right) + \\
& \sum_{n=u}^{\sqrt{M}-1} \alpha_u^+(n) \sqrt{\tfrac{\omega_1^{\mathcal{I}+}\omega_2^{\mathcal{I}+}\omega_4^{\mathcal{I}+}}{d_{1,3}^{\mathcal{I}+} d_{2,3}^{\mathcal{I}+} \omega_3^{\mathcal{I}+}}} G\left(\tfrac{d_{3,4}^{\mathcal{I}+}}{\omega_3^{\mathcal{I}+}}, -\tfrac{d_{3,4}^{\mathcal{I}+}}{\bar{d}^{\mathcal{I}+}} \right) + \\
& \sum_{n=1}^{v-1} \beta_v^-(n) \sqrt{\tfrac{\omega_1^{\mathcal{Q}-}\omega_2^{\mathcal{Q}-}\omega_4^{\mathcal{Q}-}}{d_{1,3}^{\mathcal{Q}-} d_{2,3}^{\mathcal{Q}-} \omega_3^{\mathcal{Q}-}}} G\left(\tfrac{d_{3,4}^{\mathcal{Q}-}}{\omega_3^{\mathcal{Q}-}}, -\tfrac{d_{3,4}^{\mathcal{Q}-}}{\bar{d}^{\mathcal{Q}-}} \right) + \\
& \sum_{n=v}^{\sqrt{M}-1} \beta_v^+(n) \sqrt{\tfrac{\omega_1^{\mathcal{Q}+}\omega_2^{\mathcal{Q}+}\omega_4^{\mathcal{Q}+}}{d_{1,3}^{\mathcal{Q}+} d_{2,3}^{\mathcal{Q}+} \omega_3^{\mathcal{Q}+}}} G\left(\tfrac{d_{3,4}^{\mathcal{Q}+}}{\omega_3^{\mathcal{Q}+}}, -\tfrac{d_{3,4}^{\mathcal{Q}+}}{\bar{d}^{\mathcal{Q}+}} \right) \Bigg],
\end{aligned}
\tag{5.2.20}
$$

where $G(\cdot, \cdot) \triangleq F_1(\tfrac{1}{2}, 1, 1; 1; \cdot, \cdot)$, and $\bar{d} \triangleq \tfrac{d_{1,3} + d_{2,3}}{2}$. The only assumptions in (3.3.24) can be summarized as

- The magnitudes of the distances between ω_i, ω_j with equal sign are much lower than the magnitudes of the distances between ω_i, ω_j with different sign 3.3.21.

- The magnitudes of the distances between ω_i, ω_j with equal sign are much lower than the magnitudes of the ω_i 3.3.22.

Another approximate expression can be obtained according (3.3.26), as follows

$$BER = \frac{1}{M^2 log_2 M} \sum_{\forall s_{u,v}, s_{u',v'} \in S_M} \left[\sum_{n=1}^{u-1} \alpha_u^-(n) \frac{\sqrt{\omega_1^{\mathcal{I}-} \omega_2^{\mathcal{I}-}}}{\omega_3^{\mathcal{I}-} - \frac{\omega_1^{\mathcal{I}-} + \omega_2^{\mathcal{I}-}}{2}} + \sum_{n=u}^{\sqrt{M}-1} \alpha_u^+(n) \frac{\sqrt{\omega_1^{\mathcal{I}+} \omega_2^{\mathcal{I}+}}}{\omega_3^{\mathcal{I}+} - \frac{\omega_1^{\mathcal{I}+} + \omega_2^{\mathcal{I}+}}{2}} + \right.$$
$$\left. \sum_{n=1}^{v-1} \beta_v^-(n) \frac{\sqrt{\omega_1^{\mathcal{Q}-} \omega_2^{\mathcal{Q}-}}}{\omega_3^{\mathcal{Q}-} - \frac{\omega_1^{\mathcal{Q}-} + \omega_2^{\mathcal{Q}-}}{2}} + \sum_{n=v}^{\sqrt{M}-1} \beta_v^+(n) \frac{\sqrt{\omega_1^{\mathcal{Q}+} \omega_2^{\mathcal{Q}+}}}{\omega_3^{\mathcal{Q}+} - \frac{\omega_1^{\mathcal{Q}+} + \omega_2^{\mathcal{Q}+}}{2}} \right].$$

$$(5.2.21)$$

In this case, we assumed that the values of IQ imbalances are moderate, which means that the non-circular symmetry in g_k is reduced. Since the ω_i are double in the case of circularly symmetric RVs (see section 3.3.2), ω_3 and ω_4 are close to each other as the non-circular symmetry is reduced. This implies, in conjunction with (3.3.21) and (3.3.22), that $\frac{d_{3,4}}{\check{d}}$ tends to zero more rapidly than $\frac{d_{3,4}}{\omega_3}$ when moderate IQ imbalances are considered.

5.2.5 Numerical Results

In this section, we use the closed-form expressions obtained in section 5.2.4 to evaluate the BER performance in different scenarios. Gray mapping is considered for the M-QAM constellations. We define the signal-to-noise ratio (SNR) as $\gamma = E_s/\sigma_n^2$, where E_s is the average transmitted constellation energy. Similarly, we denote the signal-to-channel estimation error ratio as $\gamma_\psi = E_s/\sigma_\psi^2$, where $\sigma_{\psi_k}^2 = \text{tr}(\mathbf{\Sigma}_{\check{\Psi}_k})$ and $\mathbf{\Sigma}_{\check{\Psi}_k} \triangleq \text{E}\{\check{\mathbf{\Psi}}_k \check{\mathbf{\Psi}}_{-k}^T\} = 0.5\sigma_{\psi_k}^2 \mathbf{I_{2 \times 2}}$, according to the channel estimation model given in [38]. We also define the correlation between the channel frequency response H_k and the mirror index H_{-k} as $\rho = \text{E}\{\check{\mathbf{H}}_k \check{\mathbf{H}}_{-k}^T\}/\sigma_g^2$.

Fig. 5.3 illustrates the BER as a function of γ, for a general scenario including TX and RX IQ imbalances, imperfect channel estimation, non-independent channel frequency responses at k and $-k$ indices, as well as different modulation schemes. Monte Carlo simulations have been included in order to show the validity of the calculated expression (5.2.19). It is appreciated the appearance of a irreducible error floor due to ICSI, for the different constellations. When perfect channel estimation is considered, an error floor is still appreciated due to the effect of IQ imbalances.

For convenience of discussion, in order to separate the effects of ICSI and IQ imbalances we will assume PCSI in the forthcoming figures. In Fig. 5.4 and 5.5, it is investigated the effect of transmit and receive IQ imbalances, respectively.
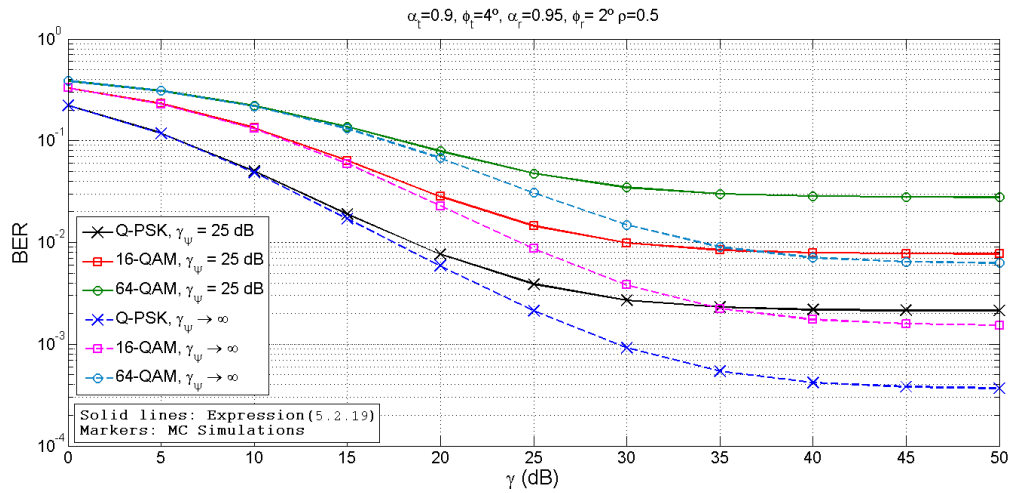
Figure 5.3: BER vs SNR for different values of channel estimation error and constellation sizes, $\alpha_t = 0.9, \phi_t = 4$, $\alpha_r = 0.95, \phi_r = 2$, $\rho = 0.5$.
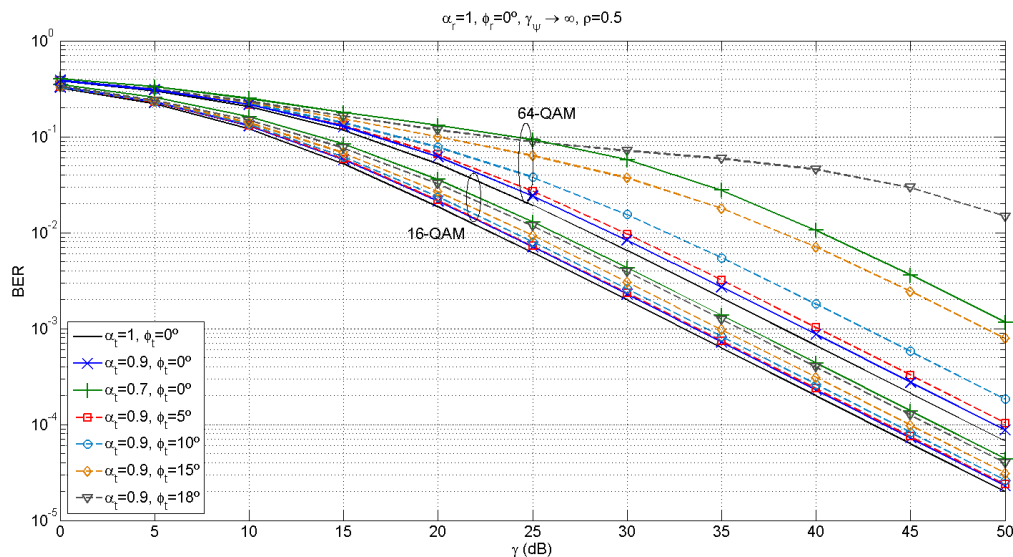
Figure 5.4: BER vs SNR for different values of TX IQ imbalance and constellation sizes, $\alpha_r = 1, \phi_r = 0$, $\rho = 0.5$, PCSI.

It is observed in Fig. 5.4 that the effect of TX IQ imbalance, either in amplitude or phase, does not severely degrade the BER performance. In fact, an irreducible BER floor is not appreciated for the considered SNR values, even for large values of phase IQ imbalances. It can also be stated how denser constellations (i.e., 64-QAM) suffer from a more important performance degradation in the presence of TX IQ imbalance.

On the contrary, the effect of RX IQ imbalance results in the appearance of an irreducible floor in the BER, as observed in Fig. 5.5. For the particular case of amplitude RX IQ imbalance (e.g., $\alpha_r = 0.9$), it is appreciated how the performance is dramatically reduced, leading to BER floors above 10^{-3} and 10^{-2} when 16-QAM and 64-QAM are considered, respectively. Similarly, the phase RX IQ imbalance also leads to an irreducible BER, even when low imbalances are considered.
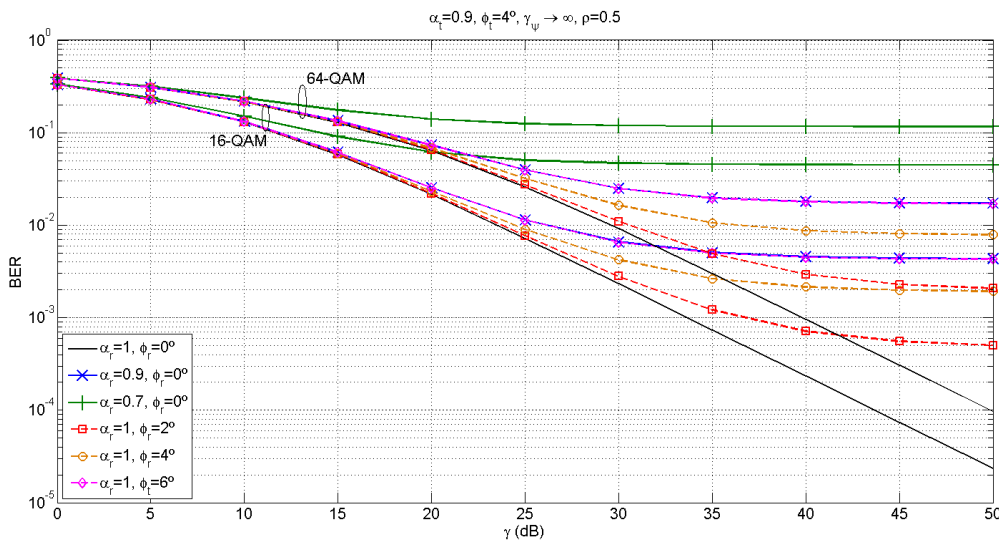
Figure 5.5: BER vs SNR for different values of RX IQ imbalance and constellation sizes, $\alpha_t = 0.9, \phi_t = 4$, $\rho = 0.5$, PCSI.

The effect of the correlation between the channel frequency response at the desired frequency index H_k and the mirror index H_{-k} is studied in Fig. 5.6. It is observed that the effect of IQ imbalance varies depending on the magnitude of the correlation ρ, resulting in a better performance when the correlation between the desired and mirror carrier frequency

responses grows. Hence, the assumption of statistical independence between H_k and H_{-k} [81, 83] leads to a considerable underestimation in the achievable BER. In the limit case of $\rho = 1$, it is interesting to remark that TX and RX IQ imbalances become mathematically equivalent, which can be extracted from (5.2.5) and (5.2.6) by considering $H_k = H_{-k}$.
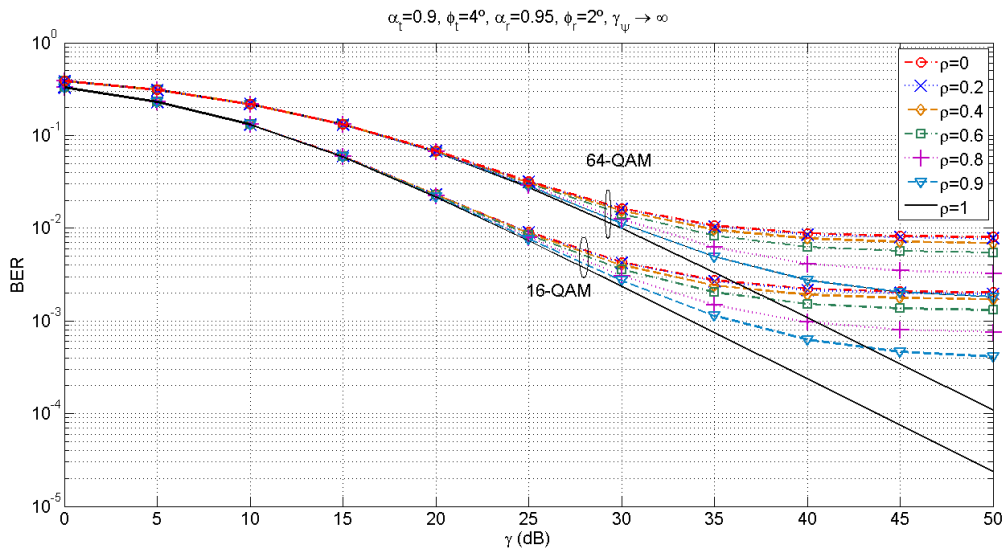
Figure 5.6: BER vs SNR, for different values of correlation and constellation sizes, $\alpha_t = 0.9, \phi_t = 4$, $\alpha_r = 0.95, \phi_r = 2$, PCSI.

In Fig. 5.7, we compare the accuracy of the approximated BER expressions (5.2.20) and (5.2.21) with the exact BER expression given by (5.2.19). It is observed that when the IQ imbalance is moderate, both approximations provide an excellent match with the exact expressions. As the IQ imbalance is increased, the accuracy of approximation (5.2.20) is still excellent, whereas the differences between the approximation (5.2.21) and the exact expression become more appreciable. For 64-QAM it is observed that the differences between the exact and approximate expression (5.2.21) grow. In this case, the decision regions are smaller and therefore the different contributions in the BER of the real and imaginary parts of the decision statistic (due to non-circular symmetry) are more evident.
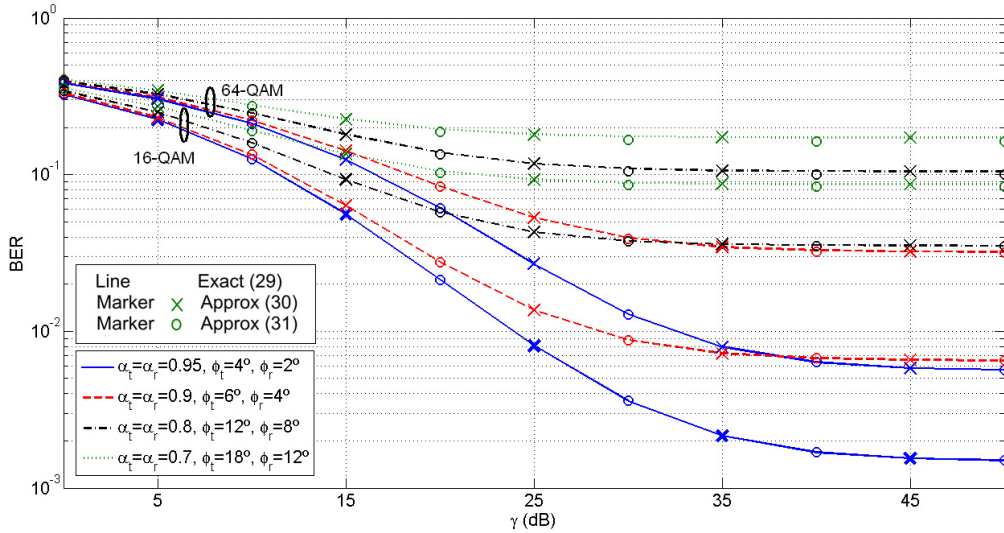
Figure 5.7: BER vs SNR (exact and approximate) for different values of TX-RX IQ imbalances and constellation sizes, $\rho = 0.5$, PCSI.

5.2.6 Discussion

An exact BER analysis of OFDM systems impaired by transmit and receive IQ imbalances has been presented, when ICSI is considered under Rayleigh fading. The calculated expression is obtained using a novel general analysis of quadratic forms in complex-valued non-circularly symmetric Gaussian RVs with zero mean, and is given in terms of a weighted sum of Lauricella F_D functions. Two additional BER expressions are provided, which allow for accurately calculating the BER for a wide range of IQ imbalances, even preventing the need of evaluating special functions when moderate IQ imbalances are considered. Results show that performance loss due to RX IQ imbalance is in general more severe, compared to TX IQ imbalance. This degradation becomes more important when denser constellations are considered, and when the correlation between the desired and the mirror channel frequency responses is decreased.

The main contributions of this section have been published in [22].

5.2.7 Appendix: Calculation of the covariance matrix R

Let $\mathbf{R}$ be the covariance matrix defined as $\mathrm{E}\left\{\breve{\mathbf{x}}\breve{\mathbf{x}}^T\right\}$, where $\breve{\mathbf{x}}$ vector is

$$\breve{\mathbf{x}}^T = \left[\begin{array}{cccc} \Re\{y_1\} & \Im\{y_1\} & \Re\{y_2\} & \Im\{y_2\} \end{array}\right], \tag{5.2.22}$$

and y_1, y_2 are complex-valued non-circularly symmetric Gaussian RVs, with zero-mean, covariance matrices $\boldsymbol{\Sigma}_{\breve{\mathbf{y}}_1}$ and $\boldsymbol{\Sigma}_{\breve{\mathbf{y}}_2}$, and cross covariance matrix $\boldsymbol{\Sigma}_{\breve{\mathbf{y}}_1\breve{\mathbf{y}}_2}$. Hence, $\mathbf{R}$ can be expressed as

$$\mathbf{R} = \left[\begin{array}{cc} \boldsymbol{\Sigma}_{\breve{\mathbf{y}}_1} & \boldsymbol{\Sigma}_{\breve{\mathbf{y}}_1\breve{\mathbf{y}}_2} \\ \boldsymbol{\Sigma}_{\breve{\mathbf{y}}_1\breve{\mathbf{y}}_2}^T & \boldsymbol{\Sigma}_{\breve{\mathbf{y}}_2} \end{array}\right]. \tag{5.2.23}$$

The complex-valued RVs y_1 and y_2 are identified with r_k and $\hat{g}_k$ in our system model, respectively. If we re-elaborate the expressions for r_k and $\hat{g}_k$ from Section 5.2.3, we have

$$r_k = \Delta_1 H_k + \Delta_2 H_{-k}^* + w_k; \tag{5.2.24}$$

$$\hat{g}_k = \Delta_3 H_k + \Delta_4 H_{-k}^* + \psi_k, \tag{5.2.25}$$

where Δ_i parameters are defined as

$$\Delta_1 = K_1 G_1 z_k + K_1 G_2^* z_{-k}; \qquad\qquad \Delta_3 = K_1 G_1; \tag{5.2.26}$$

$$\Delta_2 = K_2 G_2 z_k + K_2 G_1^* z_{-k}; \qquad\qquad \Delta_4 = K_2 G_2. \tag{5.2.27}$$

After some algebra, the following expressions for the correlation matrices are obtained

$$\boldsymbol{\Sigma}_{\breve{\mathbf{y}}_1} = \left[\begin{array}{cc} \breve{\boldsymbol{\Delta}}_1 & \breve{\boldsymbol{\Delta}}_2\boldsymbol{\Phi} \end{array}\right] \left[\begin{array}{cc} \boldsymbol{\Sigma}_{\breve{\mathbf{H}}} & \boldsymbol{\Sigma}_\rho \\ \boldsymbol{\Sigma}_\rho^T & \boldsymbol{\Sigma}_{\breve{\mathbf{H}}} \end{array}\right] \left[\begin{array}{c} \breve{\boldsymbol{\Delta}}_1^T \\ \boldsymbol{\Phi}\breve{\boldsymbol{\Delta}}_2^T \end{array}\right] + \boldsymbol{\Sigma}_{\breve{\mathbf{w}}}, \tag{5.2.28}$$

$$\boldsymbol{\Sigma}_{\breve{\mathbf{y}}_1\breve{\mathbf{y}}_2} = \left[\begin{array}{cc} \breve{\boldsymbol{\Delta}}_1 & \breve{\boldsymbol{\Delta}}_2\boldsymbol{\Phi} \end{array}\right] \left[\begin{array}{cc} \boldsymbol{\Sigma}_{\breve{\mathbf{H}}} & \boldsymbol{\Sigma}_\rho \\ \boldsymbol{\Sigma}_\rho^T & \boldsymbol{\Sigma}_{\breve{\mathbf{H}}} \end{array}\right] \left[\begin{array}{c} \breve{\boldsymbol{\Delta}}_3^T \\ \boldsymbol{\Phi}\breve{\boldsymbol{\Delta}}_4^T \end{array}\right] + \breve{\boldsymbol{\Delta}}_1\boldsymbol{\Sigma}_{\mathrm{H}\Psi} + \breve{\boldsymbol{\Delta}}_2\boldsymbol{\Phi}\boldsymbol{\Sigma}_M, \tag{5.2.29}$$

$$\boldsymbol{\Sigma}_{\breve{\mathbf{y}}_2} = \left[\begin{array}{cc} \breve{\boldsymbol{\Delta}}_3 & \breve{\boldsymbol{\Delta}}_4\boldsymbol{\Phi} \end{array}\right] \left[\begin{array}{cc} \boldsymbol{\Sigma}_{\breve{\mathbf{H}}} & \boldsymbol{\Sigma}_\rho \\ \boldsymbol{\Sigma}_\rho^T & \boldsymbol{\Sigma}_{\breve{\mathbf{H}}} \end{array}\right] \left[\begin{array}{c} \breve{\boldsymbol{\Delta}}_3^T \\ \boldsymbol{\Phi}\breve{\boldsymbol{\Delta}}_4^T \end{array}\right] + \boldsymbol{\Theta} + \boldsymbol{\Theta}^T + \boldsymbol{\Sigma}_{\breve{\Psi}}, \tag{5.2.30}$$

where $\breve{\boldsymbol{\Delta}}_{\mathbf{i}}$ matrices are defined from Δ_i according to the mapping defined in section 3.3.1, and some auxiliary matrices have been used

$$\boldsymbol{\Phi} = \left[\begin{array}{cc} 1 & 0 \\ 0 & -1 \end{array}\right]; \boldsymbol{\Theta} = \left[\breve{\boldsymbol{\Delta}}_3, \breve{\boldsymbol{\Delta}}_4\boldsymbol{\Phi}\right] \left[\begin{array}{c} \boldsymbol{\Sigma}_{\mathrm{H}\Psi} \\ \boldsymbol{\Sigma}_M \end{array}\right] \tag{5.2.31}$$

and

$$\boldsymbol{\Sigma}_{\breve{\mathbf{H}}} = E\left\{\breve{\mathbf{H}}_k \breve{\mathbf{H}}_k^T\right\}; \boldsymbol{\Sigma}_\rho = E\left\{\breve{\mathbf{H}}_k \breve{\mathbf{H}}_{-k}^T\right\}; \boldsymbol{\Sigma}_{\breve{\mathbf{w}}} = E\left\{\breve{\mathbf{w}}_k \breve{\mathbf{w}}_k^T\right\};$$
$$\boldsymbol{\Sigma}_{\breve{\boldsymbol{\Psi}}} = E\left\{\breve{\boldsymbol{\Psi}}_k \breve{\boldsymbol{\Psi}}_k^T\right\}; \boldsymbol{\Sigma}_{\mathrm{H}\Psi} = E\left\{\breve{\mathbf{H}}_k \breve{\boldsymbol{\Psi}}_k^T\right\}; \boldsymbol{\Sigma}_M = E\left\{\breve{\mathbf{H}}_{-k} \breve{\boldsymbol{\Psi}}_k^T\right\} \tag{5.2.32}$$

In the particular case of PCSI, the expressions for the correlation matrices are simplified,

$$\boldsymbol{\Sigma}_{\breve{\mathbf{y}}_1} = \left[\begin{array}{cc} \breve{\boldsymbol{\Delta}}_1 & \breve{\boldsymbol{\Delta}}_2 \boldsymbol{\Phi} \end{array}\right] \left[\begin{array}{cc} \boldsymbol{\Sigma}_{\breve{\mathbf{H}}} & \boldsymbol{\Sigma}_\rho \\ \boldsymbol{\Sigma}_\rho^T & \boldsymbol{\Sigma}_{\breve{\mathbf{H}}} \end{array}\right] \left[\begin{array}{c} \breve{\boldsymbol{\Delta}}_1^T \\ \boldsymbol{\Phi} \breve{\boldsymbol{\Delta}}_2^T \end{array}\right] + \boldsymbol{\Sigma}_{\breve{\mathbf{w}}}, \tag{5.2.33}$$

$$\boldsymbol{\Sigma}_{\breve{\mathbf{y}}_1 \breve{\mathbf{y}}_2} = \left[\begin{array}{cc} \breve{\boldsymbol{\Delta}}_1 & \breve{\boldsymbol{\Delta}}_2 \boldsymbol{\Phi} \end{array}\right] \left[\begin{array}{cc} \boldsymbol{\Sigma}_{\breve{\mathbf{H}}} & \boldsymbol{\Sigma}_\rho \\ \boldsymbol{\Sigma}_\rho^T & \boldsymbol{\Sigma}_{\breve{\mathbf{H}}} \end{array}\right] \left[\begin{array}{c} \breve{\boldsymbol{\Delta}}_3^T \\ \boldsymbol{\Phi} \breve{\boldsymbol{\Delta}}_4^T \end{array}\right], \tag{5.2.34}$$

$$\boldsymbol{\Sigma}_{\breve{\mathbf{y}}_2} = \left[\begin{array}{cc} \breve{\boldsymbol{\Delta}}_3 & \breve{\boldsymbol{\Delta}}_4 \boldsymbol{\Phi} \end{array}\right] \left[\begin{array}{cc} \boldsymbol{\Sigma}_{\breve{\mathbf{H}}} & \boldsymbol{\Sigma}_\rho \\ \boldsymbol{\Sigma}_\rho^T & \boldsymbol{\Sigma}_{\breve{\mathbf{H}}} \end{array}\right] \left[\begin{array}{c} \breve{\boldsymbol{\Delta}}_3^T \\ \boldsymbol{\Phi} \breve{\boldsymbol{\Delta}}_4^T \end{array}\right]. \tag{5.2.35}$$

Chapter 6

Analysis of MIMO-OFDM systems with transmit beamforming

$\mathbf{I}$N this chapter, it is analyzed the effect of ICSI in a MIMO-OFDM system that employs transmit beamforming and MRC reception. Since in this scheme it is required the knowledge of the CSI at both the transmitter and receiver sides, the objective of this analysis is to determine the degradation in the system performance due to ICSI.

6.1   Related Work

In the previous chapters, the performance analysis of MIMO (chapter 3) and OFDM (chapter 4) systems using quadratic forms was accomplished. Finally, in this chapter we proceed to apply the mathematical tools derived in this thesis to the analysis of a MIMO-OFDM system. It is known that when MIMO techniques are used in conjunction with orthogonal frequency division multiplexing (OFDM), the benefits of employing multiple antennas are extended to multipath environments. Clearly, the performance of a MIMO-OFDM system depends on the accuracy in the estimation of the channel response, in order to compensate the effects of the frequency-selective time-varying channel for every frequency subcarrier at every symbol time.

The effect of channel estimation errors on the bit error rate (BER) performance in fading channels has been widely studied by many authors. Since the analysis of pilot symbol assisted modulation (PSAM) was introduced in [89], different analyses have been done: approximate

BER expressions in Rayleigh fading channels with imperfect channel estimation for quadrature amplitude modulation (QAM) were given in [14], and exact closed-form expressions for QAM systems with antenna diversity in Rayleigh [90] and Ricean fading channels were obtained in [9, 17].

When OFDM is used, several strategies can be used for channel estimation [91], but the most extended mechanisms are based on pilot arrangement [92]. In [15], an exact BER analysis for OFDM systems under imperfect channel state information (CSI) in Ricean fading channels is performed, considering different reception branches for maximal ratio combining (MRC).

For the general case of precoded multiple antenna systems, exact closed-form BER expressions which account for the effect of channel estimation errors have recently been obtained in different scenarios: transmit beamforming and MRC with channel prediction errors with fixed [10] and adaptive modulation [93] in Rayleigh fading, and singular value decomposition (SVD) MIMO systems [27] with channel estimation error and feedback delay in Ricean fading channels.

In the case of precoded MIMO-OFDM systems, less analyses are available in the literature. Recently, a lower bound for channel prediction and interpolation errors has been proposed in [94]. Under the assumption of perfect CSI knowledge in both the transmitter and receiver sides, a performance analysis of coded MIMO-OFDM systems over Ricean fading channels was tackled in [95]. In [96], space-frequency block coded OFDM (SFBC-OFDM) systems are analyzed, considering the effects of channel estimation errors only in the receiver side. A closed form analysis covering the effect of channel estimation errors in both transmitter and receiver sides has not been accomplished yet, to the author's knowledge. In this chapter, exact closed-form BER expressions for MIMO-OFDM beamforming with MRC under imperfect CSI due to prediction and interpolation errors are derived. Particularly, our analysis is valid for any square M-ary QAM constellation to be mapped onto the OFDM subcarriers.

The remainder of this section is organized as follows. Section 6.2 describes the system model considered in our analysis. In Section 6.3 exact closed-form BER expressions are
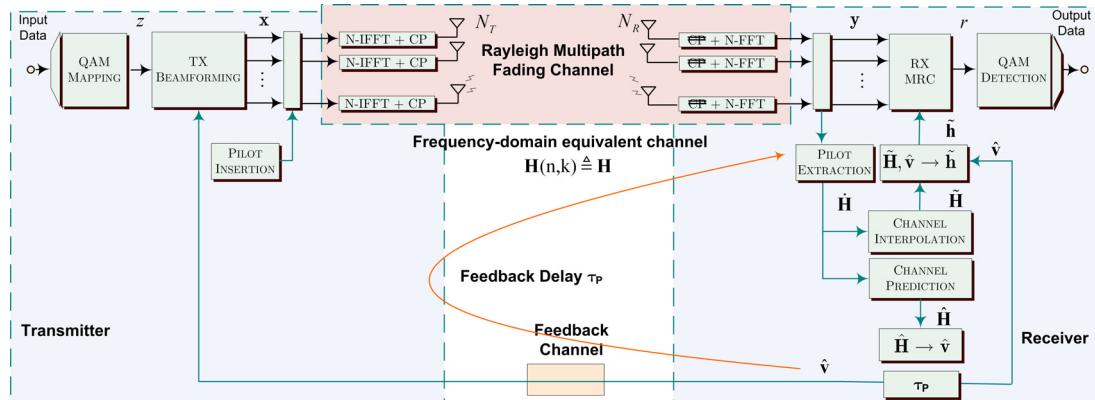
Figure 6.1: System model for MIMO-OFDM Beamforming with MRC and imperfect CSI

derived. Section 6.4 presents some numerical results which exploit the analytical expressions derived in previous section. Finally, main conclusions are exposed in Section 6.5.

6.2 System Model

Figure 6.1 shows the system model for MIMO-OFDM beamforming with MRC assumed in this work. We consider N_T transmit antennas and N_R receive antennas. In this system model, the symbol z is spread among the set of transmit antennas by means of a beamforming vector $\hat{\mathbf{v}}$, which is retrieved from the receiver using a feedback channel with τ_P delay.

For every signal path between transmitter and receiver, we assume a channel impulse response (CIR) with exponential multipath profile, mean delay spread denoted as τ, normalized gain, and time variation according to Jakes' correlation model [97], with maximum Doppler shift f_D.

For this analysis, we consider the following usual assumptions [15, 98] with respect to the OFDM transmission:

1. Channel state changes from symbol to symbol, but it does not significantly change within one OFDM symbol period T.

2. CIR length L is shorter than cyclic prefix (CP) size

3. Time and frequency synchronization is perfectly accomplished in the receiver side.

Therefore, the effect of intersymbolic interference (ISI) and intercarrier interference (ICI) are neglected. Under these assumptions, we can consider an equivalent channel model in the frequency domain so that the received signal, for the k*th* subcarrier of the n*th* OFDM symbol, can be expressed as

$$\mathbf{y}(n,k) = \mathbf{H}(n,k)\mathbf{x}(n,k) + \mathbf{w}(n,k), \tag{6.2.1}$$

where the transmitted signal after beamforming $\mathbf{x}(n,k)$ is an $N_T \times 1$ vector, the received signal before MRC $\mathbf{y}(n,k)$ is an $N_R \times 1$ vector, $\mathbf{w}(n,k)$ is an $N_R \times 1$ vector representing noise, and the channel gain is modelled by an $N_R \times N_T$ complex matrix $\mathbf{H}(n,k)$, so that each entry $H_{i,j}(n,k)$ is the channel gain between the jth transmit and the ith receive antennas. For simplicity, in the following analysis we omit indices n,k unless they are necessary.

The entries $\mathrm{H}_{i,j}$ are assumed independent identically distributed (i.i.d) complex circularly symmetric normal RVs, with zero-mean and unity-variance, i.e. $H_{i,j} \sim \mathcal{CN}(0,1)$, where the symbol $\sim$ means *statistically distributed as*. The entries of noise vector, namely w_m, are i.i.d. complex circularly symmetric normal RVs $\sim \mathcal{CN}(0, N_0)$.

Since we assume an exponential distribution of the multipath time delay, the two-dimensional correlation function of $\mathrm{H}_{i,j}$ entries is given in [15, 98] as

$$\rho_H(\Delta n, \Delta k) \triangleq \mathbf{E}[H_{i,j}(n,k)H_{i,j}^*(n+\Delta n, k+\Delta k)] = \frac{J_0[2\pi\epsilon_F(\Delta n)]}{1 - j2\pi\epsilon_T(\Delta k)}, \tag{6.2.2}$$

where $*$ denotes complex conjugation, J_0 is the zero*th* order Bessel function of the first kind, $\epsilon_F = f_D T$ represents the maximum Doppler shift f_D normalized to the OFDM symbol period T, and $\epsilon_T = \tau/T$ represents the normalized mean delay spread.

In the transmitter side, pilot subcarriers with energy E_p are transmitted on certain positions within the OFDM discrete time-frequency grid [92], in order to facilitate the estimation of the channel frequency response. These pilot subcarriers are uniformly distributed along this grid, with spacing ΔN in the discrete time-domain and spacing ΔK in the discrete frequency-domain. Hence, an initial channel estimate $\dot{\mathbf{H}}$ at pilot positions is obtained, since both the value and position of pilot subcarriers is known in the receiver side.

The predicted channel $\hat{\mathbf{H}}$ is employed to obtain the beam-steering vector $\hat{\mathbf{v}}$ which must be fed back to the transmitter, and can be expressed as

$$\hat{\mathbf{H}}(n + n_0, k + k_0) \triangleq \sum_{i=0}^{N_P-1} c_{P_i} \dot{\mathbf{H}}(n - \Delta N(i + \tau_P), k), \qquad (6.2.3)$$

where N_P is the number of taps of the prediction filter, c_{P_i} are the coefficients of the prediction filter, $n_0 = 0 \ldots \Delta N - 1$ indicates a shift from the position where the pilot is allocated in the symbol index, $k_0 = 0 \ldots \Delta K - 1$ denotes a shift in the discrete frequency grid, relative to the position of pilot subcarriers, and τ_P is the feedback delay expressed in units of discrete time intervals between pilots. Note that, in order to reduce feedback information, c_{P_i} are considered independent of n_0 and k_0.

The interpolated channel $\tilde{\mathbf{H}}$ is needed to carry out the MRC at the receiver, and is given by

$$\tilde{\mathbf{H}}(n + n_0, k + k_0) \triangleq \sum_{i=-(N_I-1)/2}^{(N_I-1)/2} c_{I_i} \dot{\mathbf{H}}(n, k - i\Delta K), \qquad (6.2.4)$$

where N_I is the number of taps of the interpolation filter, c_{I_i} are the coefficients of the interpolation filter. Note that in this case, since channel interpolation is needed to be accurately calculated for every frequency subcarrier, the value of c_{I_i} varies for every k_0 although for notational simplicity this dependence has not been stated.

Both channel estimates are obtained by filtering the previous channel estimate $\dot{\mathbf{H}}$. In our receiver model, we define the estimation $\dot{\boldsymbol{\Xi}}$, prediction $\hat{\boldsymbol{\Xi}}$ and the interpolation $\tilde{\boldsymbol{\Xi}}$ error matrices as

$$\dot{\boldsymbol{\Xi}} \triangleq \mathbf{H} - \dot{\mathbf{H}}; \quad \hat{\boldsymbol{\Xi}} \triangleq \mathbf{H} - \hat{\mathbf{H}}; \quad \tilde{\boldsymbol{\Xi}} \triangleq \mathbf{H} - \tilde{\mathbf{H}}, \qquad (6.2.5)$$

where the prediction and interpolation errors depend on the magnitude of the estimation error $\dot{\boldsymbol{\Xi}}$, and the coefficients of the prediction and interpolation filters, respectively.

Using the predicted channel $\hat{\mathbf{H}}$, the optimal beam-steering vector $\hat{\mathbf{v}}$ is the N_T-dimensional unitary eigenvector corresponding to the largest eigenvalue $\hat{\lambda}$ of matrix $\hat{\mathbf{H}}^{\mathcal{H}}\hat{\mathbf{H}}$ [99], which is given by $\hat{\lambda} = \hat{\mathbf{v}}^{\mathcal{H}}\hat{\mathbf{H}}^{\mathcal{H}}\hat{\mathbf{H}}\hat{\mathbf{v}}$. The receiver feeds vector $\hat{\mathbf{v}}$ back to the transmitter to perform beamforming, so that the transmitted vector becomes $\mathbf{x} = \hat{\mathbf{v}}z$. The effective channel gain is an N_R-dimensional vector defined as $\mathbf{h} \triangleq \mathbf{H}\hat{\mathbf{v}}$ and the predicted effective channel gain is the

vector $\hat{\mathbf{h}} \triangleq \hat{\mathbf{H}}\hat{\mathbf{v}}$, whose square Euclidean norm is $||\hat{\mathbf{h}}||^2 = \hat{\lambda}$. The effective channel gain can also be expressed as $\mathbf{h} \triangleq \mathbf{H}\hat{\mathbf{v}} = (\hat{\mathbf{H}} + \hat{\mathbf{\Xi}})\hat{\mathbf{v}} = \hat{\mathbf{h}} + \hat{\boldsymbol{\psi}}$, where $\hat{\boldsymbol{\psi}}$ is the channel gain prediction error.

At the receiver, the effective channel gain vector $\mathbf{h}$ is estimated to perform MRC. Using the interpolated channel $\tilde{\mathbf{H}}$ and the beam-steering vector $\hat{\mathbf{v}}$ sent to the transmitter, according to our system model, the estimation of $\mathbf{h}$ is

$$\tilde{\mathbf{h}} \triangleq \tilde{\mathbf{H}}\hat{\mathbf{v}} = (\mathbf{H} - \tilde{\mathbf{\Xi}})\hat{\mathbf{v}} = (\hat{\mathbf{H}} + \hat{\mathbf{\Xi}} - \tilde{\mathbf{\Xi}})\hat{\mathbf{v}} = \hat{\mathbf{h}} + \hat{\boldsymbol{\psi}} - \tilde{\boldsymbol{\psi}}, \tag{6.2.6}$$

where $\tilde{\boldsymbol{\psi}}$ is the channel gain interpolation error.

The symbol r which results from applying MRC to received vector $\mathbf{y}$ is given by

$$r \triangleq \frac{\tilde{\mathbf{h}}^{\mathcal{H}}\mathbf{y}}{||\tilde{\mathbf{h}}||^2} = \frac{\tilde{\mathbf{h}}^{\mathcal{H}}\mathbf{h}}{||\tilde{\mathbf{h}}||^2}z + \frac{\tilde{\mathbf{h}}^{\mathcal{H}}\mathbf{w}}{||\tilde{\mathbf{h}}||^2} = gz + w', \tag{6.2.7}$$

where z is the transmitted symbol with average energy E_S, g is the gain mismatch and w' is the resultant noise after MRC, whose pdf is circularly symmetric since $\mathbf{w}$ is a vector whose entries are circularly symmetric and independent of $\tilde{\mathbf{h}}$.

6.3 BER analysis

We consider square M-QAM modulation with independent bit mapping for the in-phase (I) and quadrature (Q) components for every OFDM subcarrier, so that the set of complex symbols of the constellation is $\{s_{u,v} = (2u - \sqrt{M} - 1)d + j(2v - \sqrt{M} - 1)d\}_{u,v=1,\ldots,\sqrt{M}}$, where $2d$ is the minimum distance between symbols.

In this scenario, taking advantage of the circular symmetry in the pdf of the noise, the BER can be expressed as

$$BER = \sum_{u=1}^{\sqrt{M}} \sum_{v=1}^{\sqrt{M}} \sum_{m=u}^{\sqrt{M}-1} \omega_u(m) \cdot \mathcal{I}_{u,v}(m), \tag{6.3.1}$$

where $\omega_u(m)$ coefficients are constant values given in [17] for the case of Gray mapping, and $\mathcal{I}_{u,v}(m)$ are called *components of error probability* (CEP), according to the notation introduced in [10]. These CEP are defined as the probability of the received symbol to

be above a decision boundary $\{\mathcal{B}(m) = (2m - \sqrt{M})d\}_{m=1,\dots,\sqrt{M}-1}$, when $z = s_{u,v}$ was transmitted, i.e.

$$\mathcal{I}_{u,v}(m) = \Pr\{\Re\{r\} - \mathcal{B}(m) > 0 \mid z = s_{u,v}\}. \tag{6.3.2}$$

In the forthcoming analysis, we calculate the CEP conditioned to a predicted channel state $\hat{\mathbf{H}}$ (section 6.3.1), and then we obtain both the conditional BER and the BER averaged over all the predicted channel states (section 6.3.2).

6.3.1 Conditional CEP

In this section we derive, for our system model, the CEP of the n*th* symbol in the k*th* subcarrier, conditioned on a predicted channel state (CCEP), i.e.

$$\mathcal{I}_{u,v}(m; \hat{\mathbf{H}}) = \Pr\left\{\Re\{r\} - \mathcal{B}(m) > 0 \mid \hat{\mathbf{H}}, z = s_{u,v}\right\}. \tag{6.3.3}$$

The calculation of CCEP is performed in two steps: firstly, we obtain the joint Gaussian pdf of channel gain prediction and interpolation error conditioned on the predicted channel. Then, analysis of complex Gaussian quadratic forms [6] is used for the derivation of the CCEP; more specifically, the compact expressions presented in [10] are adopted. Let $\boldsymbol{\varphi}$ be a random variable defined as

$$\boldsymbol{\varphi} \triangleq \left[\begin{array}{cc} \varphi_1 & \boldsymbol{\varphi}_2 \end{array}\right]^t, \tag{6.3.4}$$

where

$$\varphi_1 \overset{\triangle}{=} \hat{H}_{i,j} \;, \quad \boldsymbol{\varphi}_2 \overset{\triangle}{=} \left[\begin{array}{cc} \hat{\tilde{\Xi}}_{i,j} & \tilde{\Xi}_{i,j} \end{array}\right]. \tag{6.3.5}$$

Since the entries of the channel matrix $\mathbf{H}$ and the estimation error matrix $\dot{\bar{\Xi}}$ are circularly symmetric Gaussian variables i.i.d. with zero mean, it can be shown that $\boldsymbol{\varphi} \sim \mathcal{CN}(0, \mathbf{C}_{\boldsymbol{\varphi}})$, whose covariance matrix is

$$\mathbf{C}_{\boldsymbol{\varphi}} \triangleq \mathrm{E}\left[\boldsymbol{\varphi}\boldsymbol{\varphi}^H\right] = \left[\begin{array}{cc} C_{11} & \mathbf{C}_{12} \\ \mathbf{C}_{21} & \mathbf{C}_{22} \end{array}\right], \tag{6.3.6}$$

where the elements of the covariance matrix depend on the prediction and interpolation filter coefficients, the correlation function of the channel ρ_H in (6.2.2), and the power of

the estimation error $\dot{\boldsymbol{\Xi}}$. In expression (6.3.6), the matrix $\mathbf{C}_{\boldsymbol{\varphi}}$ is partitioned into four submatrices as depicted in (6.3.7), in order to facilitate the next calculations. The prediction and interpolation filter coefficients are expressed in vector notation, denoted as $\mathbf{c_P}$ and $\mathbf{c_I}$, respectively.

$$
\begin{aligned}
C_{11} &\triangleq \mathrm{c}_{\mathrm{P}}^t \hat{\mathbf{W}} \mathrm{c_P}, \\
\mathbf{C}_{12} &\triangleq \left[\begin{array}{cc} \hat{\mathbf{w}} \mathrm{c_P} - \mathrm{c}_{\mathrm{P}}^t \hat{\mathbf{W}} \mathrm{c_P} & \hat{\mathbf{w}} \mathrm{c_P} - \mathrm{c}_{\mathrm{P}}^t \breve{\mathbf{W}} \mathrm{c_I} \end{array} \right] \triangleq \mathbf{C}_{21}^H, \\
\mathbf{C}_{22} &\triangleq \left[\begin{array}{cc} 1 + \mathrm{c}_{\mathrm{P}}^t \hat{\mathbf{W}} \mathrm{c_P} - 2\hat{\mathbf{w}} \mathrm{c_P} & 1 + \mathrm{c}_{\mathrm{P}}^t \breve{\mathbf{W}} \mathrm{c_I} - \tilde{\mathbf{w}} \mathrm{c_I} - \hat{\mathbf{w}} \mathrm{c_P} \\ 1 + \mathrm{c}_{\mathrm{P}}^t \breve{\mathbf{W}} \mathrm{c_I} - \tilde{\mathbf{w}} \mathrm{c_I} - \hat{\mathbf{w}} \mathrm{c_P} & 1 + \mathrm{c}_{\mathrm{I}}^t \tilde{\mathbf{W}} \mathrm{c_I} - 2\tilde{\mathbf{w}} \mathrm{c_I}, \end{array} \right], \\
\hat{w}_m &= \rho_H((m + \tau_P)\Delta N - n_0, 0), \\
\tilde{w}_m &= \rho_H(0, (m + (N_I - 1)/2)\Delta K - k_0), \\
\hat{W}_{l,m} &= \rho_H((m - l)\Delta N, 0) + (N_0/E_P)\, \delta[m - l], \\
\tilde{W}_{l,m} &= \rho_H(0, (m - l)\Delta K) + (N_0/E_P)\, \delta[m - l], \\
\breve{W}_{l,m} &= \rho_H((l + \tau_P)\Delta N, (m + \tfrac{N_I-1}{2})\Delta K) + (N_0/E_P)\, \delta[l + \tau_P] \cdot \delta[m + \tfrac{N_I-1}{2}].
\end{aligned}
\tag{6.3.7}
$$

Conditioning on the predicted channel matrix $\hat{\mathbf{H}}$, we obtain a new circularly symmetric Gaussian variable $\boldsymbol{\theta}_{i,j} \triangleq \boldsymbol{\varphi}_2^t \mid \varphi_1 = \left[\hat{\dot{\Xi}}_{i,j}, \tilde{\dot{\Xi}}_{i,j} \right]^t \mid \hat{H}_{i,j}$, whose mean and covariance matrix can be calculated from $\mathbf{C}_{\boldsymbol{\varphi}}$

Taking into account that $\hat{\boldsymbol{\psi}} = \hat{\dot{\boldsymbol{\Xi}}}\hat{\mathbf{v}}$, $\tilde{\boldsymbol{\psi}} = \tilde{\dot{\boldsymbol{\Xi}}}\hat{\mathbf{v}}$ and $\hat{\mathbf{v}}$ is a unitary vector that remains constant conditioned on $\hat{\mathbf{H}}$, we can define an equivalent circularly symmetric Gaussian variable defined as the vector $\boldsymbol{\vartheta}_i = \left[\hat{\psi}_i, \tilde{\psi}_i \right] \Big| \hat{\mathbf{H}}$, representing the channel gain prediction and interpolation error, conditioned on the predicted channel. Using the analysis presented in [100] for conditioned Gaussian random variables, the mean and covariance matrix of $\boldsymbol{\vartheta}_i$ can be expressed as

$$
\mathbf{m}_{\boldsymbol{\vartheta}_i} \triangleq \mathrm{E}\left[\boldsymbol{\vartheta}_i \right] = \hat{h}_i C_{11}^{-1} \mathbf{C}_{21}, \tag{6.3.8}
$$

$$
\mathbf{C}_{\boldsymbol{\vartheta}_i} \triangleq \mathbf{C}_{22} - C_{11}^{-1} \mathbf{C}_{21} \mathbf{C}_{12} = \mathbf{C}_{\boldsymbol{\vartheta}}. \tag{6.3.9}
$$

Once the joint Gaussian pdf of channel gain prediction and interpolation error conditioned on the predicted channel is obtained, the second step is the calculation of the CCEP.

Table 6.1: Probability computation of Gaussian quadratic form.

PARAMETER	DEFINITION
$\{\delta_i\}_{i=1,2}$	$\frac{1}{2}\operatorname{tr}(\mathbf{C}_x\mathbf{Q}_m) \pm \sqrt{\left(\frac{1}{2}\operatorname{tr}(\mathbf{C}_x\mathbf{Q}_m)\right)^2 - \det(\mathbf{C}_x\mathbf{Q}_m)}$
η	$\left\|\dfrac{\delta_1}{\delta_2}\right\|$
a	$\sqrt{\dfrac{2\delta_2\left(\Sigma_{i=1}^{N_R}\mathbf{m}_{x_i}^{\mathcal{H}}\left[\mathbf{Q}_m - \delta_1\mathbf{C}_x^{-1}\right]\mathbf{m}_{x_i}\right)}{(\delta_1 - \delta_2)^2}}$
b	$\sqrt{\dfrac{2\delta_1\left(\Sigma_{i=1}^{N_R}\mathbf{m}_{x_i}^{\mathcal{H}}\left[\mathbf{Q}_m - \delta_2\mathbf{C}_x^{-1}\right]\mathbf{m}_{x_i}\right)}{(\delta_1 - \delta_2)^2}}$
$\Pr\{D < 0\}$	$Q_1(a,b) + \displaystyle\sum_{p=0}^{N_R-1} C_p(a,b,\eta)\,I_p(ab)\exp\left\{-\frac{1}{2}(a^2+b^2)\right\}$
$C_p(a,b,\eta)$	$\begin{cases} -1 + \dfrac{1}{(1+\eta)^{2N_R-1}}\displaystyle\sum_{k=0}^{N_R-1}\binom{2N_R-1}{k}\eta^k, & p=0 \\[2em] \dfrac{1}{(1+\eta)^{2N_R-1}}\displaystyle\sum_{k=0}^{N_R-1-p}\binom{2N_R-1}{k}\left[\left(\frac{b}{a}\right)^p\eta^k - \left(\frac{a}{b}\right)^p\eta^{2N_R-1-k}\right], & p\neq 0 \end{cases}$

Let us define a random variable D as a quadratic form

$$D = \sum_{i=1}^{N_R} \mathbf{x_i}^H \mathbf{Q}_m \mathbf{x_i}, \tag{6.3.10}$$

where N_R is the number of diversity branches in the receiver side. The quadratic form matrix $\mathbf{Q}_m$ and the random variable vector $\mathbf{x_i}$ are defined as:

$$\mathbf{x_i} \triangleq \begin{bmatrix} y_i \\ \tilde{h}_i \end{bmatrix} \quad \mathbf{Q}_m \triangleq \begin{bmatrix} 0 & -\frac{1}{2} \\ -\frac{1}{2} & \mathcal{B}(m) \end{bmatrix}, \tag{6.3.11}$$

where $\mathcal{B}(m)$ are the decision boundaries. Thus, if we expand (6.3.10) and (6.3.11), we have

$$D = \sum_{i=1}^{N_R} \left\{ \left|\tilde{h}_i\right|^2 \mathcal{B}(m) - \Re\left(y_i\tilde{h}_i^*\right) \right\}. \tag{6.3.12}$$

Therefore, from (6.3.12) and (6.3.3) we find the equivalence between the CCEP and the

quadratic form as

$$\mathcal{I}_{u,v}(m; \hat{\mathbf{H}}) = \Pr\left\{ D < 0 \,\middle|\, \hat{\mathbf{H}}, z = s_{u,v} \right\}, \tag{6.3.13}$$

The calculation of this probability (6.3.13) can be tackled through Proakis' analysis of complex Gaussian quadratic forms [6, eq. B-21], or using the alternative expression used in (3.2.7) and restated in table 6.1. According to our system model, the entries of received vector y_i and the entries of interpolated effective channel gain vector $\tilde{h}_i$ can be expressed as

$$\begin{aligned} y_i &= h_i z + w_i = (\hat{h}_i + \hat{\psi}_i)z + w_i, \\ \tilde{h}_i &= \hat{h}_i + \hat{\psi}_i + \tilde{\psi}_i, \end{aligned} \tag{6.3.14}$$

Thus, $\mathbf{x_i}$ conditioned on a certain transmitted symbol $z = s_{u,v}$ and a predicted channel matrix $\hat{\mathbf{H}}$, can be expressed as a linear combination of the complex and jointly normal variables $\hat{\psi}_i$ and $\tilde{\psi}_i$ and the independent complex normal variable w_i. Hence, $\mathbf{x_i}$ is a complex normal vector whose mean vector and covariance matrix are

$$\mathbf{m}_{\mathbf{x}_i} \triangleq \mathrm{E}\left[\mathbf{x}_i\right] = \hat{h}_i \boldsymbol{\mu} = \hat{h}_i \left(\boldsymbol{\Delta} + \boldsymbol{\Theta} C_{11}^{-1} \mathbf{C}_{21} \right), \tag{6.3.15}$$

$$\mathbf{C}_{\mathbf{x}} \triangleq \mathrm{E}\left[(\mathbf{x}_i - \mathbf{m}_{\mathbf{x}_i})(\mathbf{x}_i - \mathbf{m}_{\mathbf{x}_i})^{\mathcal{H}} \right] = \boldsymbol{\Theta} \mathbf{C}_{\boldsymbol{\vartheta}} \boldsymbol{\Theta}^{\mathcal{H}} + \boldsymbol{\Phi} N_0, \tag{6.3.16}$$

where $\boldsymbol{\mu} = \boldsymbol{\Delta} + \boldsymbol{\Theta} C_{11}^{-1} \mathbf{C}_{21}$ and

$$\boldsymbol{\Delta} \triangleq \begin{bmatrix} s_{u,v} \\ 1 \end{bmatrix}, \boldsymbol{\Theta} \triangleq \begin{bmatrix} s_{u,v} & 0 \\ 1 & -1 \end{bmatrix}, \boldsymbol{\Phi} \triangleq \begin{bmatrix} 1 & 0 \\ 0 & 0 \end{bmatrix}. \tag{6.3.17}$$

With the mean vector in (6.3.15), the covariance matrix in (6.3.16) and the quadratic form matrix in (6.3.11), we can calculate the CCEP by using the expressions in table 6.1 as

$$\mathcal{I}_{u,v}(m; \hat{\mathbf{H}}) = Q_1(a, b) + \sum_{p=0}^{N_R - 1} C_p(a, b, \eta) I_p(ab) e^{-\frac{a^2 + b^2}{2}}, \tag{6.3.18}$$

where $Q_1(\cdot)$ is the Marcum Q function, $I_p(\cdot)$ is the modified Bessel function, and the parameters a, b, η and C_p are obtained using the expressions that appear in table 6.1, where δ_1 and δ_2 are the eigenvalues of the matrix $\mathbf{C_x Q}_m$ and $\delta_1 > \delta_2$ by definition.

The CCEP dependence on $\hat{\mathbf{H}}$ in expression (6.3.18) is contained in the parameters a and b, specifically, in the term $\hat{h}_i$ that appears in the expression of $\mathbf{m}_{\mathbf{x}_i}$ (6.3.15). Substituting

expression (6.3.15) in the expression in table (6.1), the parameter a results

$$a = \sqrt{\frac{2\delta_2 \left(\sum_{i=1}^{N_R} \left|\hat{h}_i\right|^2\right) \left(\boldsymbol{\mu}^H \left(\mathbf{Q}_m - \delta_1 \mathbf{C_x}^{-1}\right) \boldsymbol{\mu}\right)}{(\delta_1 - \delta_2)^2}} = \sqrt{\frac{2\delta_2 \hat{\lambda} \left(\boldsymbol{\mu}^H \left(\mathbf{Q}_m - \delta_1 \mathbf{C_x}^{-1}\right) \boldsymbol{\mu}\right)}{(\delta_1 - \delta_2)^2}} = a_{u,v}(m)\sqrt{\hat{\lambda}}. \tag{6.3.19}$$

In (6.3.19), $\hat{\lambda}$ represents the largest eigenvalue of the matrix $\hat{\mathbf{H}}\hat{\mathbf{H}}^{\mathcal{H}}$. Since the elements of $\hat{\mathbf{H}}\hat{\mathbf{H}}^{\mathcal{H}}$ are complex Gaussian RVs, it is said to be a Wishart matrix [101].

In the same way, the parameter b can be expressed as

$$b = b_{u,v}(m)\sqrt{\hat{\lambda}}, \tag{6.3.20}$$

Therefore, it is shown that the CCEP dependence on $\hat{\lambda}$, so $\hat{\mathbf{H}}$ can be expressed as a CCEP dependence on $\hat{\lambda}$, i.e.

$$\mathcal{I}_{u,v}^+(m; \hat{\mathbf{H}}) = \mathcal{I}_{u,v}^+(m; \hat{\lambda}). \tag{6.3.21}$$

6.3.2 Conditional and average BER expressions

The CCEP calculated in the previous section allows for the derivation of the conditional BER (CBER). This probability represents the BER conditioned on the predicted effective channel gain $\hat{\lambda}$, i.e, the BER under imperfect channel state information (CSI). This CBER can be expressed as

$$CBER(\hat{\lambda}) = \sum_{u=1}^{\sqrt{M}} \sum_{v=1}^{\sqrt{M}} \sum_{m=u}^{\sqrt{M}-1} \omega_{u,v}(m) \cdot \mathcal{I}_{u,v}(m; \hat{\lambda}). \tag{6.3.22}$$

The BER is obtained by averaging the CBER over the predicted eigenvalue $\hat{\lambda}$ as

$$BER = \sum_{u=1}^{\sqrt{M}} \sum_{v=1}^{\sqrt{M}} \sum_{m=u}^{\sqrt{M}-1} \omega_{u,v}(m) \int_0^\infty \mathcal{I}_{u,v}(m; \hat{\lambda}) p(\hat{\lambda}) d\hat{\lambda}. \tag{6.3.23}$$

Using the fact that the pdf of the largest eigenvalue of the complex Wishart matrices can be expressed as a weighted sum of elementary Gamma pdfs [102], the pdf of $\hat{\lambda}$ is given by

$$p(\hat{\lambda}) = \sum_{l=1}^{N_1} \sum_{r=N_2-N_1}^{(N_2+N_1-2m)m} B_{l,r} \frac{\hat{\lambda}^r}{(C_{11})^{r+1}} \exp\left(\frac{-l\hat{\lambda}}{C_{11}}\right), \tag{6.3.24}$$

where $N_1 \triangleq \min\{N_T, N_R\}$, $N_2 \triangleq \max\{N_T, N_R\}$, $C_{11} = E[|\hat{H}_{i,j}|^2]$ is defined in (6.3.6), and the constants $B_{l,r}$ are

$$B_{l,r}(N_1, N_2) \triangleq \frac{A_{l,r}}{\prod_{l=1}^{N_1}(N_1 - l)! \prod_{l=1}^{N_1}(N_2 - l)!}, \tag{6.3.25}$$

and coefficients $A_{l,r}$ can be exactly computed by the algorithm proposed in [102].

Substituting (6.3.24) and (6.3.25) in expression (6.3.23), and using the expressions and integrals given in [33, 103], a final expression for the BER is given as

$$
\begin{aligned}
BER = &\sum_{u=1}^{\sqrt{M}} \sum_{v=1}^{\sqrt{M}} \sum_{m=u}^{\sqrt{M}-1} \sum_{l=1}^{N_1} \sum_{r=N_2-N_1}^{(N_2+N_1-2m)m} \frac{\omega_{u,v}(m) B_{l,r}}{l^{r+1}} \left\{ \frac{r!}{l^{1+r}} \left\{ 1 + \frac{b_{u,v}^2(m)}{e_{u,v}(m)} \sum_{l=0}^{r} (l+1) \left(\frac{2l}{e_{u,v}(m)} \right)^l \times \right. \right. \\
&\left[\frac{a_{u,v}^2(m)}{e_{u,v}(m)} {}_2F_1 \left(\frac{l+2}{2}, \frac{l+3}{2}; 2; \frac{4a_{u,v}^2(m) b_{u,v}^2(m)}{e_{u,v}^2(m)} \right) - \frac{1}{1+l} {}_2F_1 \left(\frac{l+1}{2}, \frac{l+2}{2}; 1; \frac{4a_{u,v}^2(m) b_{u,v}^2(m)}{e_{u,v}^2(m)} \right) \right] \right\} \\
&+ \frac{(r+l)!}{(a_{u,v}(m) b_{u,v}(m))^{r+1}} \frac{1}{l!} \left(\frac{p_{u,v}(m)-1}{p_{u,v}(m)+1} \right)^{l/2} \left(\frac{p_{u,v}(m)+1}{2} \right)^r \times \\
&{}_2F_1 \left(-r, -r+l; l+1; \frac{p_{u,v}(m)-1}{p_{u,v}(m)+1} \right) \sqrt{(p_{u,v}^2(m)-1)^{r+1}} \right\},
\end{aligned}
\tag{6.3.27}
$$

where ${}_2F_1$ is the Gauss hypergeometric function and

$$e_{u,v}(m) = a_{u,v}^2(m) + b_{u,v}^2(m) + 2m, \tag{6.3.28}$$

$$p_{u,v}(m) = \left(1 - \frac{4a_{u,v}^2(m) b_{u,v}^2(m)}{e_{u,v}^2(m)} \right)^{-1/2}. \tag{6.3.29}$$

Note that function ${}_2F_1$ in (6.3.27) can be expressed as a finite sum of elementary functions for the values of its arguments, although it is not shown here for compactness reasons.

6.4 Numerical Results

In this section, we use the closed-form expression obtained in Section 6.3.2 to evaluate the BER for different particular scenarios.

For the numerical evaluation of the results, we assume the following default configuration: 2x2 MIMO scheme with 16-QAM constellation mapped onto the OFDM subcarriers, and equal power for pilot and data subcarriers ($E_P = E_S$). The same number of taps has been
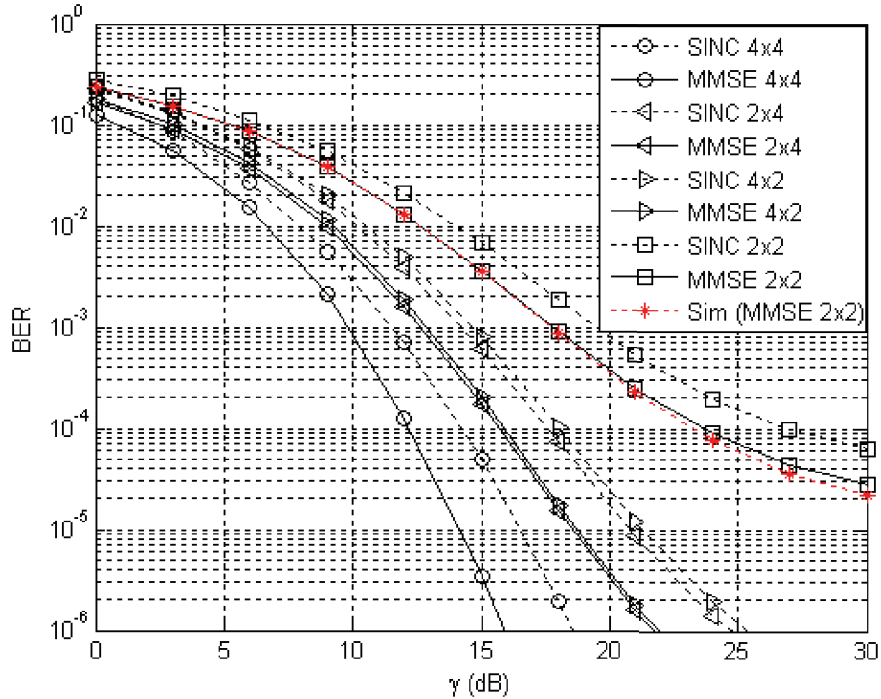
Figure 6.2: BER as a function of the average SNR (γ), for a 16-QAM OFDM system over
Rayleigh fading channel, with sinc and Wiener filters, and a N_TxN_R antenna configuration.

considered both for the prediction and interpolation filters, i.e. $N_P = N_I = 9$. In the case
of sinc-type filters, Hamming windowing is performed. We further consider a feedback delay
$\tau_P = 4$, position of data subcarrier relative to pilot allocation $n_0 = k_0 = 1$, and a frequency-
domain pilot spacing and time-domain pilot spacing $\Delta K = \Delta N = 4$. The normalized mean
delay spread ϵ_T as well as the normalized maximum Doppler shift ϵ_F are both set to 0.02.
BER curves in this section are represented as a function of the average signal to noise ratio
(SNR), namely $\gamma = E_S/N_0$.

In Figure 6.2, the influence of antenna configuration on the BER is studied, for Wiener
and sinc filters. Monte Carlo simulations for the 2x2 case and minimum mean square error
(MMSE) filtering are included, which correctly match with the theoretical results. Due to the
huge number of random variables involved in the analyzed scenario, it is not computationally
feasible to simulate the remainder configurations. The performance loss due to non-optimal
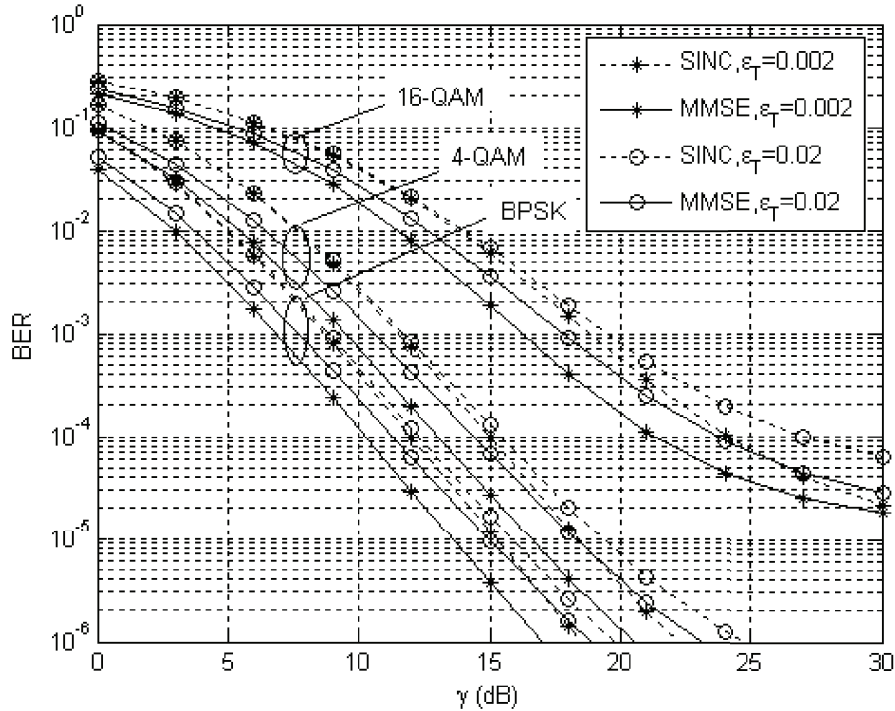
Figure 6.3: BER vs. γ, for BPSK, QPSK and 16-QAM constellations in a 2x2 MIMO-OFDM system over Rayleigh fading channel, with sinc and Wiener filters, for different values of the normalized delay spread ϵ_T

filtering, for a $BER = 10^{-4}$, is in the range of 1.5-2 dB for the studied antenna configurations. It is interesting to highlight that the BER performance for 2x4 MIMO is approximately 3 dB better compared to 4x2 configuration, whereas their performance is coincident when perfect channel estimation is considered [10].

Figures 6.3 to 6.5 represent the BER evolution when different channel parameters are varied, for a 2x2 antenna configuration. In Figure 6.3, it can be appreciated how a longer channel impulse response (i.e. greater values of ϵ_T) produces a more important BER degradation when dense constellations are used.

In Figure 6.4, the effect of the Doppler shift on the BER performance is evaluated. Since larger values of ϵ_F correspond to more rapidly varying channels, the BER performance decreases when ϵ_F is increased. When working at low SNR, the performance of sinc filtering

is barely affected under different Doppler shifts, since this scheme does not take advantage of the knowledge of CSI.
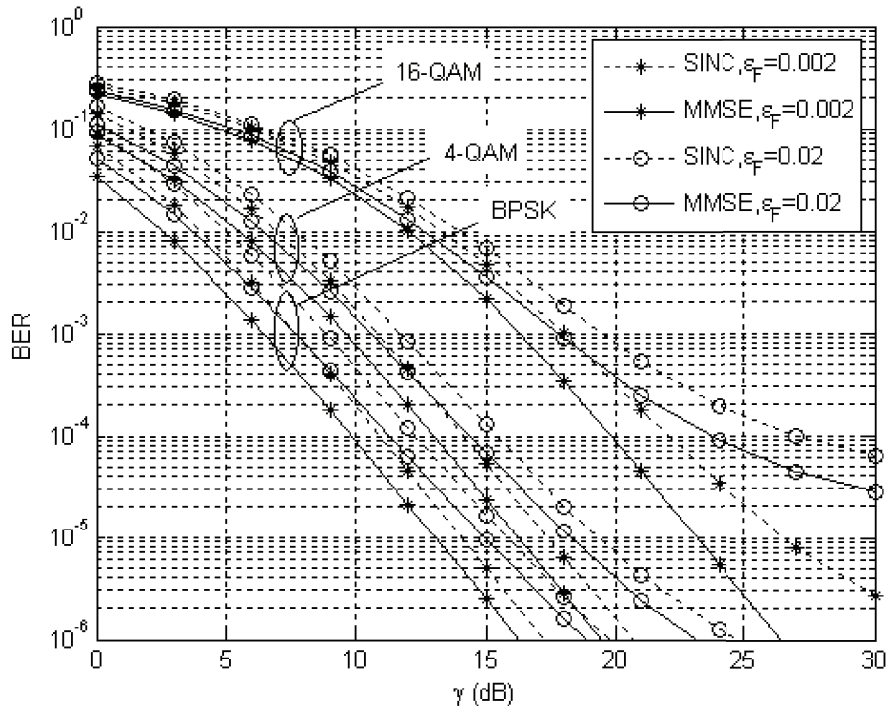
Figure 6.4: BER vs. γ, for BPSK, QPSK and 16-QAM constellations in a 2x2 MIMO-OFDM system over Rayleigh fading channel, with sinc and Wiener filters, for different values of the normalized maximum Doppler shift ϵ_F

Finally, Figure 6.5 shows the effect of the feedback delay on the BER performance. In general terms, when the feedback delay grows, the performance gap between MMSE and sinc filtering is also increased.

6.5 Discussion

An exact BER analysis for MIMO-OFDM systems with transmit beamforming and MRC reception in multipath Rayleigh fading channels, under channel prediction and interpolation errors, was presented. The resulting exact closed-form expression was showed to be composed by a finite sum of elementary functions.
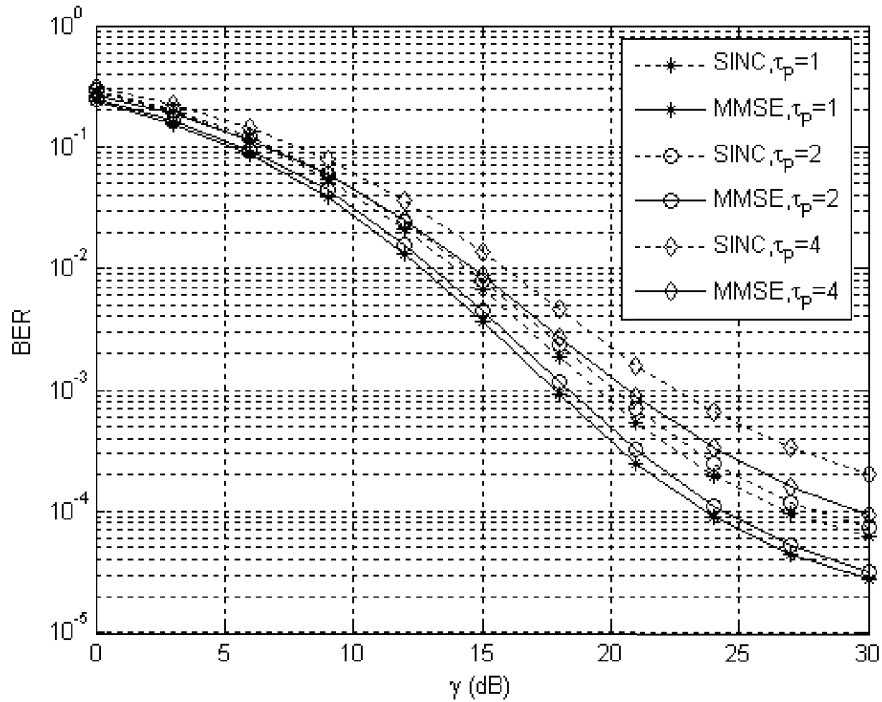
Figure 6.5: BER vs. γ, for a 16-QAM constellation and 2x2 MIMO-OFDM system over Rayleigh fading channel, with sinc and Wiener filters, for different values of the feedback delay τ_P

This expression was used to evaluate the system performance under different channel configurations and number of antennas, with Wiener and sinc filter schemes for both channel prediction and interpolation. Although Wiener filtering outperforms sinc-type filtering, the latter is shown to be a reasonable approach for implementation in a real system, since it offers a good trade-off between performance and complexity.

The main contributions of thus section have been published in [18].

Chapter 7

Conclusion and future work

I N this final chapter, the main conclusions which arise from the contributions of this work are outlined. Besides, some future lines and applications regarding to the work developed in this PhD thesis are suggested.

7.1 Conclusion

In this thesis, the problem of performance analysis in wireless communication systems under non ideal conditions has been addressed. The main contributions of this work in this field can be grouped into two principal points:

Firstly, a *tool for the performance analysis of QAM systems* has been developed. The proposed general framework can be utilized in many scenarios, and includes previous results in the literature as particular cases. By using this analysis method, the computation of the elementary coefficients (which only depends on the constellation mapping) is separated from the probability calculation (which only depends on the statistical distributions of the RVs). Besides, this methodology may be useful to extend previous results in the literature calculated only for particular constellations into general expressions.

On the other hand, the *probability calculation* in systems where the *decision variable* can be expressed in terms of a *general quadratic form D* in complex Gaussian RVs has been tackled, from different perspectives. Previous closed-form results given in [6, 10] for calculating $\Pr\{D < 0\}$ have been used to analyze those scenarios where the involved RVs were circularly symmetric. Additionally, approximate expressions for this probability have

been obtained in terms of the Gaussian Q function. For the general case of non circularly symmetric Gaussian RVs, an exact expression for $\Pr\{D < 0\}$ has been obtained in terms of the Lauricella function $F_D(\cdot)$, as well as two approximate expressions in terms of Appell hypergeometric function $F_1(\cdot)$ and in terms of rational functions.

Thus, the utilization of the proposed general framework for the performance analysis of QAM systems in conjunction with the probability calculation using quadratic forms in complex Gaussian RVs has enabled the analysis of a number of wireless communication systems under a common approach. By means of a proper system modelling, it has been demonstrated that this methodology is a feasible alternative for the analysis of MIMO and OFDM systems affected by different impairments.

Regarding to the analysis of MIMO systems with ICSI in Ricean fading channels, two scenarios which have not been previously analyzed in exact closed-form in the literature been studied:

- A QAM system with MRC reception affected by Ricean-faded interferences. We show that the effect of the LOS component of the interfering signal in the BER varies depending of the value of the Ricean K factor of the interfering signal.

- A MIMO $2 \times N_R$ system employing Alamouti diversity with MRC reception. We show that this scheme can be reduced to an equivalent $1 \times 2N_R$ system where the noise term is enhanced by the appearance of a block code interference due to ICSI.

In these scenarios, approximate expressions for the BER are also provided in terms of the Gaussian Q function which are valid mainly for Ricean channels with a strong LOS component.

Then, the effect of different impairments which affect OFDM systems that make use direct conversion receivers has been analyzed:

- An OFDM system with MRC reception affected by ICSI, CFO and DC-offset. For the particular case of PCSI and single branch reception, a simple expression for the irreducible BER floor due to DC-offset is given. As a rule of thumb, we provide a simple expression for the maximum DC offset allowable in a direct conversion receiver.

- An OFDM system affected by ICSI and IQ imbalances both at the transmitter and receiver sides. We show that the non circular symmetry of the equivalent channel gain must be taken into account for a proper analysis. It is observed that RX IQ imbalance is in general more detrimental that TX IQ imbalance; we also appreciate that the correlation between the channel response at the desired frequency and at the mirror frequency has an important effect in the performance degradation due to IQ imbalance.

Finally, a MIMO-OFDM system that combines transmit beamforming and MRC reception has been considered, in order to determine the effects of ICSI at the transmitter and receiver sides. In this scenario, the BER conditioned to a particular channel state is calculated using the analysis of quadratic forms, and then the BER is obtained by averaging the conditioned BER over all the channel states. It is found that ICSI at the transmitter side has a greater impact in the BER compared to ICSI at the receiver side.

7.2 Future work

After the work developed in this thesis, there exist a number of applications where the proposed methodology may be exploited. They involve either new scenarios, new fading conditions or new impairments. Some examples are indicated below.

Firstly, in this thesis we have identified some scenarios where the classical analysis using quadratic forms in complex Gaussian RVs was not applicable, thus making necessary the calculation of $\Pr\{D < 0\}$ under new assumptions (i.e., non circular symmetry). It may also result interesting the study of new kinds of quadratic forms which enable the analysis of different systems. According to the expression of a general quadratic form given by

$$D \triangleq \sum_{k=1}^{L} A|X_k|^2 + B|Y_k|^2 + CX_kY_k^* + C^*X_k^*Y_k, \tag{7.2.1}$$

one valid example may be the consideration of correlated pairs of random variables X_k and Y_k with arbitrary mean and variance, i.e.,$\mathrm{E}\{X_jX_k^*\} \neq 0$, $\mathrm{E}\{Y_jY_k^*\} \neq 0$ for any $j \neq k$. This will enable the analysis of multi-branch reception over correlated fading channels with quadratic forms.

In OFDM systems, it is usual to consider that synchronization is perfectly accomplished at the receiver side. However, imperfect time and frequency synchronization may lead to the appearance of inter symbol interference (ISI) and inter carrier interference (ICI), respectively. It may result interesting to analyze the effect of these impairments from the perspective exposed in this thesis, i.e., the use of quadratic forms.

Within this thesis, a number of MIMO systems affected by ICSI have been analyzed, which mainly employed MRC reception in the receiver side. The proposed methodology is directly applicable to other reception combining strategies such as equal gain combining or selection combining. As well, it is also feasible the study of MIMO multiplexing systems with the proposed methodology.

Finally, multicarrier systems based on OFDM have been analyzed in this thesis. However, there are other strategies which are being considered for multicarrier transmission. One valid example is Single-Carrier Frequency Division Multiple Access technology (SC-FDMA) [104], which has been selected as transmission scheme for the uplink of 3GPP-LTE radio technology. Since the exact BER calculation of these systems remains as an open problem in some scenarios, it may result interesting to use the proposed methodology in this thesis for the performance analysis.

Appendix A

Resumen en castellano

A.1 Motivaciones de la tesis

La medida de prestaciones en sistemas de comunicaciones ha sido siempre un asunto de extremo interés desde sus orígenes [1–3]. Además de la capacidad del canal, que básicamente proporciona información sobre la máxima tasa de información libre de errores que puede lograrse, estas prestaciones suele cuantificarse en términos de probabilidad de error de símbolo (SER, *Symbol Error Rate*) o de probabilidad de error de bit (BER, *Bit Error Rate*). Dependiendo de las características del canal y del esquema de modulación, el análisis de prestaciones puede llevarse a cabo de diferentes maneras.

Uno de los trabajos de referencia en este área fue publicado por Simon y Alouini [4], en el que se analizan las prestaciones de diversos sistemas de comunicaciones afectados por distintos tipos de desvanecimientos siguiendo una estrategia común. La aparición de nuevos sistemas de comunicaciones digitales que emplean nuevos tipos de modulación o de esquemas de transmisión hace necesaria la evaluación de sus prestaciones, de modo que puedan compararse con las técnicas existentes. Algunos ejemplos son el uso de múltiples antenas (MIMO, *multiple-input multiple-output*) o la técnica de multeplexación por división en frecuencias ortogonales (OFDM, *Orthogonal Frequency Division Multiplexing*). Tanto MIMO como OFDM están integrados en la mayor parte de tecnologías inalámbricas presentes y futuras.

El cálculo analítico de las prestaciones de los sistemas de comunicaciones inalámbricas afectados por distintos tipos de desvanecimientos ya ha sido llevado a cabo, suponiendo que el estado del canal (CSI, *Channel State Information*) es conocido de manera perfecta en

el receptor (e incluso en el transmisor, si es necesario) [5, 6]. Estos resultados son útiles para determinar las prestaciones máximas que pueden alcanzarse en condiciones ideales. Sin embargo, en la prctica existen muchos factores que pueden limitar dichas prestaciones: la aparición de *señales interferentes*, el *conocimiento imperfecto del CSI*, o no idealidades relacionadas con la implementación física de los componentes tales como *offset de frecuencia de portadora*, *desbalanceo de las componentes en fase (I) y cuadratura (Q)* u *offset de continua* son algunos ejemplos.

En estas situaciones, el modelo de sistema es más complicado que el originalmente considerado en [4], debido a la diferente naturaleza de las variables aleatorias (RVs, *Random Variables*) que aparecen. Esto implica no sólo que los cálculos analíticos a realizar sean más complicados, sino que la simulación de estos escenarios puede llegar a ser inviable. Por tanto, la obtención de expresiones cerradas que permitan evaluar de manera exacta las prestaciones de estos sistemas es de vital necesidad, con el fin de poder determinar de manera eficiente cómo estas imperfecciones afectan a las prestaciones del sistema.

Aunque existen distintas alternativas para el cálculo analítico de la BER en estos escenarios, en ocasiones es posible expresar la variable de decisión como una forma cuadrática; así, el cálculo de probabilidades puede realizarse siguiendo una estrategia común.

El cálculo de probabilidades empleando formas cuadráticas fue introducido por Proakis [6, 8] para el caso de RVs Gaussianas circularmente simétricas, posibilitando el análisis de diferentes escenarios [9, 10] en los que la utilización de otras alternativas para el cálculo de la BER era inviable desde un punto de vista práctico. Recientemente, los resultados de Proakis han sido generalizados [11], proporcionando un modo de obtener la función característica de una forma cuadrática general para distintos tipos de desvanecimientos (es decir, RVs de diferente naturaleza). Sin embargo, tanto [6] como [11] asumen que las RVs son circularmente simétricas, es decir, que sus partes reales e imaginarias son independientes y tienen igual varianza. Dado que la condición de circularidad simétrica [12, 13] no siempre se satisface, parece interesante analizar las formas cuadráticas en las que las RVs carecen de esta propiedad.

Otro problema que se presenta a la hora de evaluar las prestaciones de un sistema de comunicaciones está relacionado con el cálculo de la probabilidad para distintas constelaciones. Un gran número de análisis en la bibliografía, aun de incuestionable interés, realizan

de manera individual el análisis para cada constelación, ya sea BPSK (*Binary Phase-Shift Keying*) o del tipo M-QAM (*Quadrature Amplitude Modulation*) [9, 14, 15]. Conforme el tamaño de la constelación aumenta, el cálculo se hace más tedioso, ya que se obtienen de manera explícita las diferentes probabilidades asociadas a que cada bit del símbolo recibido se encuentre dentro de una determinada región de decisión, y luego estas probabilidades individuales se combinan. Por tanto, parece deseable el uso de un método sistemático que permita realizar los cálculos de una manera genérica, independientemente del tamaño de la constelación.

Las motivaciones de esta tesis pueden resumirse en dos objetivos principales:

- Proporcionar un método general para el cálculo de la BER en sistemas basados en QAM para cualquier tamaño de constelación.

- Analizar sistemas MIMO y OFDM afectados por ciertas no idealidades, mediante el uso del cálculo de probabilidades basados en formas cuadráticas Gaussianas.

A.2 Análisis generalizado de la probabilidad de error

En esta sección se presenta una metodología general para el análisis de prestaciones de sistemas QAM. El único requisito es que el mapeo de los bits en las partes en fase y cuadratura se realice de manera independiente, e incluye análisis previos de la bibliografía como casos particulares [16, 17].

La técnica propuesta permite separar el análisis en dos tareas principales, que pueden llevarse a cabo de manera independiente: el cálculo de los *coeficientes elementales*, cuyo valor depende sólo del mapeo elegido para la constelación, y el cálculo de las *componentes de probabilidad de error*, cuyo valor depende únicamente de la distribución de las variables aleatorias en el escenario considerado.

A.2.1 Marco Analítico

Consideremos el problema general del cálculo de la BER cuando la variable de decisión se puede expresar mediante la forma canónica $y = az + \zeta$, donde a (desajuste de ganancia) y ζ (ruido equivalente) son en general RVs complejas. En este modelo, el desajuste de ganancia a incorpora el efecto de la compensación imperfecta de canal en recepción,

mientras que el ruido equivalente ζ incluye los efectos del ruido aditivo, interferencias y otras imperfecciones del receptor. En esta forma canónica z es el símbolo transmitido perteneciente a una constelación QAM rectangular, compuesta de dos constelaciones L_1-PAM y L_2-PAM asociadas con las componentes I y Q. El conjunto de símbolos complejos es $\{s_{u,v} = (2u - L_1 - 1)d + j(2v - L_2 - 1)d\}_{u=1,\ldots,L_1;v=1,\ldots,L_2}$, donde $2d$ es la mínima distancia entre símbolos. Cada símbolo $s_{u,v}$ tiene asociado un conjunto de bits de la componente I $\{b_i^{\mathcal{I}}(u)\}_{i=1,\ldots,\log_2(L_1)}$ y otro de la componente Q $\{b_i^{\mathcal{Q}}(v)\}_{i=1,\ldots,\log_2(L_2)}$. Los límites de las regiones de decisión para las componentes I y Q se denotan como $\{\mathcal{B}_{\mathcal{I}}(k) = (2k - L_1)d\}_{k=1,\ldots,L_1-1}$ y $\{\mathcal{B}_{\mathcal{Q}}(k) = j(2k - L_2)d\}_{k=1,\ldots,L_2-1}$ respectivamente.

La BER puede expresarse como el promedio, sobre todos los bits y símbolos transmitidos, de la probabilidad de error de un bit determinado condicionada a la transmisión de un símbolo determinado:

$$BER_{\text{QAM}} = \frac{1}{L_1 L_2} \sum_{u=1}^{L_1} \sum_{v=1}^{L_2} \frac{1}{\log_2(L_1 L_2)} \left\{ \sum_{i=1}^{\log_2(L_1)} P_{\mathcal{I}}(i,u,v) + \sum_{i=1}^{\log_2(L_2)} P_{\mathcal{Q}}(i,u,v) \right\}, \quad \text{(A.2.1)}$$

donde $P_{\mathcal{I}}(i,u,v) = \Pr\{\text{error en } b_i^{\mathcal{I}}(u)|\, z = s_{u,v}\}$ y $P_{\mathcal{Q}}(i,u,v) = \Pr\{\text{error en } b_i^{\mathcal{Q}}(v)|\, z = s_{u,v}\}$, respectivamente. Cada término $P_{\mathcal{I}}(i,u,v)$ puede expresarse como una combinación lineal de probabilidades de que la parte real de la variable de decisión y esté por encima o por debajo de un número determinado de límites de decisión; igualmente ocurre para la componente Q, considerando la parte imaginaria de y. Esta idea puede formalizarse como

$$BER_{\text{QAM}} = \frac{1}{L_1 L_2} \sum_{u=1}^{L_1} \sum_{v=1}^{L_2} \frac{1}{\log_2(L_1 L_2)} \left[\sum_{i=1}^{\log_2(L_1)} \left\{ \sum_{k=1}^{u-1} \alpha_u^-(i,k) \cdot \mathcal{I}_{u,v}^-(k) + \sum_{k=u}^{L_1-1} \alpha_u^+(i,k) \cdot \mathcal{I}_{u,v}^+(k) \right\} \right.$$
$$\left. + \sum_{i=1}^{\log_2(L_2)} \left\{ \sum_{k=1}^{v-1} \beta_v^-(i,k) \cdot \mathcal{Q}_{u,v}^-(k) + \sum_{k=v}^{L_2-1} \beta_v^+(i,k) \cdot \mathcal{Q}_{u,v}^+(k) \right\} \right],$$
$$\text{(A.2.2)}$$

donde las *componentes de probabilidad de error* (CEP) se definen como

$$\mathcal{I}_{u,v}^-(k) = \Pr\{\Re\{y - \mathcal{B}_{\mathcal{I}}(k)\} < 0|\, z = s_{u,v}\}, \quad \mathcal{I}_{u,v}^+(k) = \Pr\{\Re\{y - \mathcal{B}_{\mathcal{I}}(k)\} > 0|\, z = s_{u,v}\},$$
$$\mathcal{Q}_{u,v}^-(k) = \Pr\{\Im\{y - \mathcal{B}_{\mathcal{Q}}(k)\} < 0|\, z = s_{u,v}\}, \quad \mathcal{Q}_{u,v}^+(k) = \Pr\{\Im\{y - \mathcal{B}_{\mathcal{Q}}(k)\} > 0|\, z = s_{u,v}\}.$$
$$\text{(A.2.3)}$$

Los *coeficientes elementales* $\alpha_u^\pm(i,k)$ y $\beta_v^\pm(i,k)$ toman los valores $\{-1, 0, 1\}$ y representan cambios en el valor correspondiente del bit i a través del k-ésimo límite de decisión para el

símbolo $s_{u,v}$: 0 indica que el valor del bit no cambia, 1 indica que el bit cambia del valor correcto al incorrecto, y -1 indica un cambio de un valor incorrecto a otro correcto. Tanto α como $\mathcal{I}$ están asociados con la compenete I, mientras que β y $\mathcal{Q}$ están asociados con la componente Q. El signo en el superíndice indica que si el k-ésimo límite de decisión está por debajo o por encima (respectivamente - ó +) de la parte real (para α e $\mathcal{I}$) o de la parte imaginaria (para β y $\mathcal{Q}$) del símbolo $s_{u,v}$.

Agrupando los coeficientes $\alpha_u^{\pm}(i,k)$ y $\beta_u^{\pm}(i,k)$ del siguiente modo

$$\alpha_u^{\pm}(k) = \sum_{i=1}^{\log_2(L)} \alpha_u^{\pm}(i,k), \quad \beta_v^{\pm}(k) = \sum_{i=1}^{\log_2(L)} \beta_v^{\pm}(i,k), \tag{A.2.4}$$

se obtiene la expresión final de la probabilidad de error.

$$BER_{\text{QAM}} = \frac{1}{L_1 L_2} \sum_{u=1}^{L_1} \sum_{v=1}^{L_2} \frac{1}{\log_2(L_1 L_2)} \left[\sum_{k=1}^{u-1} \alpha_u^-(k) \cdot \mathcal{I}_{u,v}^-(k) + \sum_{k=u}^{L_1-1} \alpha_u^+(k) \cdot \mathcal{I}_{u,v}^+(k) \right.$$
$$\left. + \sum_{k=1}^{v-1} \beta_v^-(k) \cdot \mathcal{Q}_{u,v}^-(k) + \sum_{k=v}^{L_2-1} \beta_v^+(k) \cdot \mathcal{Q}_{u,v}^+(k) \right]. \tag{A.2.5}$$

Esta expresión (A.2.5) permite calcular la BER en cualquier escenario que pueda reducirse a la forma canónica $y = az + \zeta$, independientemente de la distribución de las RVs a y ζ. De este modo, el cálculo de la BER se reduce a dos operaciones fundamentales: los *coeficientes elementales*, cuyo valor depende únicamente del mapeo de la constelación, y las *componentes de probabilidad de error* cuya expresión vendrá determinada por la distribución de las RVs a y ζ.

Además de esta expresión general, es posible usar expresiones simplificados para ciertos casos de interés, habituales en comunicaciones. Por ejemplo, si se considera por simplicidad una constelación cuadrada $L_1 = L_2 = L$, y el ruido equivalente ζ es circularmente simétrico, es posible aplicar ciertas simetrías para expresar la BER como

$$BER_{\text{QAM}} = \sum_{u=1}^{L} \sum_{v=1}^{L} \sum_{k=u}^{L-1} \omega_u(k) \cdot \mathcal{I}_{u,v}^+(k), \tag{A.2.6}$$

donde

$$\omega_u(k) = \frac{1}{M} \frac{1}{\log_2(M)} \left[\alpha_u^+(k) + \alpha_{L-u+1}^-(L-k) + \beta_u^+(k) + \beta_{L-u+1}^-(L-k) \right]. \tag{A.2.7}$$

Si además se considera que la compensación de canal en recepción es perfecta (es decir $a = 1$), podemos expresar la BER de manera aún más compacta como

$$BER_{\text{QAM}} = \sum_{m=1}^{L-1} \omega(m)\mathcal{I}^{+}(m), \tag{A.2.8}$$

donde

$$\mathcal{I}^{+}(m) = \Pr\left\{\Re\left\{\zeta\right\} > (2m+1)d\right\}. \tag{A.2.9}$$

y

$$\omega(m) = \frac{1}{M\log_2(M)}\left[\sum_{u=1}^{L-m}\alpha_u^{+}(u+m-1) + \alpha_{u+m}^{-}(u) + \beta_u^{+}(u+m-1) + \beta_{u+m}^{-}(u)\right]. \tag{A.2.10}$$

A.2.2 Cálculo de coeficientes

En esta tesis, se propone el cálculo de los coeficientes elementales a partir de la expresión de la secuencia de bits que se mapean en las componentes I/Q como señales discretas. Así, se expresa dicha secuencia como un conjunto de i señales discretas $b_i(m)$ que representan los valores binarios del bit i-ésimo del símbolo m-ésimo. Usando esta definición, la derivada discreta de la secuencia de bits en el límite de decisión k-ésimo viene dada por

$$b_i^{'}(k) = b_i(k+1) - b_i(k), \quad 1 \leq k \leq L-1. \tag{A.2.11}$$

Esta expresión (A.2.11) ofrece información sobre los errores de bit al pasar un límite de decisión. Esta derivada discreta $b_i^{'}(k)$ puede interpretarse del siguiente modo: 0 indica que el valor del bit no cambia, 1 indica que el bit cambia de 0 a 1, y -1 indica que el bit cambia de 1 a 0.

Como los coeficientes $\alpha_u^{\pm}(i,k)$ y $\beta_v^{\pm}(i,k)$ representan cambios en el valor detectado del bit i a través del límite de decisión k-ésimo, pueden expresarse (p.ej. α^{+}) como:

$$\alpha_u^{+}(i,k) = (1 - 2b_i(u))b_i^{'}(k), \tag{A.2.12}$$

donde $(1 - 2b_u(i))$ traduce los valores de $b_i(u)$ del conjunto $\{0,1\}$ a $\{1,-1\}$. El cálculo de $\alpha_u^{-}(i,k)$ y $\beta_v^{\pm}(i,k)$ se realiza de una manera similar

$$\begin{aligned}
\alpha_u^{-}(i,k) &= -(1 - 2b_i(u))b_i^{'}(k), \\
\beta_v^{+}(i,k) &= (1 - 2b_i(v))b_i^{'}(k), \\
\beta_v^{-}(i,k) &= -(1 - 2b_i(v))b_i^{'}(k).
\end{aligned} \tag{A.2.13}$$

Para el caso particular de mapeo tipo Gray es posible encontrar una expresión más compacta:

$$b_i(u) = \frac{1}{2}\left(1 - \Omega\left(i, u\right)\right), \tag{A.2.14}$$

donde $\Omega(i, x)$ se define en (A.2.15) como

$$\Omega\left(i, x\right) \triangleq \operatorname{sign}\left\{\cos\left(\omega_i(x - 1/2)\right)\right\}, \tag{A.2.15}$$

y la frecuencia $\omega_i = \frac{2\pi}{2^{i+1}}$ incluye la periodicidad de la señal discreta $b_i(u)$. En este caso, la derivada de la secuencia de bits es

$$b_i'(k) = b_i(k+1) - b_i(k) = \frac{1}{2}\left(\Omega\left(i, k\right) - \Omega\left(i, k+1\right)\right) = \frac{1}{2}\left(\Omega\left(i, k\right) - \Omega\left(i, -k\right)\right), \quad \text{(A.2.16)}$$

donde $k = 1 \ldots L - 1$. Combinando (A.2.14) y (A.2.16) se obtiene

$$\alpha_u^+(i, k) = (1 - 2b_i(u))b_i'(k) = \frac{1}{2}\Omega\left(i, m\right)\left[\Omega\left(i, k\right) - \Omega\left(i, -k\right)\right]. \tag{A.2.17}$$

A.3   Cálculo de probabilidades con formas cuadráticas

En muchos sistemas de comunicaciones, es habitual que la variable de decisión pueda expresarse como un caso especial de una forma cuadrática general D, definida como

$$D \triangleq \sum_{k=1}^{L} A|X_k|^2 + B|Y_k|^2 + CX_kY_k^* + C^*X_k^*Y_k, \tag{A.3.1}$$

donde $A, B \in \mathbb{R}$ y $C \in \mathbb{C}$ son constantes, y X_k e Y_k son pares de RVs complejas arbitrariamente distribuidas. Esta tesis se centra en las formas cuadráticas con RVs Gaussianas complejas, que aparecen de manera natural en diferentes escenarios a la hora de evaluar la BER.

A.3.1   Circularidad simétrica

Caso general

En [6] se presenta una expresión cerrada para el cálculo de $\Pr\{D < 0\}$, sujeta a dos condiciones: (1) que los L pares $\{X_k, Y_k\}$ sean mutuamente independientes e idénticamente distribuidos, y (2) que las RVs $\{X_k - \mathrm{E}\{X_k\}\}$ e $\{Y_k - \mathrm{E}\{Y_k\}\}$ sean circularmente simétricas, es decir, que sus partes real e imaginaria sean independientes y de igual varianza [13].

En este escenario, la probabilidad $\Pr\{D < 0\}$ se calcula como

$$P_b \triangleq \Pr\{D < 0\} = \frac{1}{2\pi} \int_{-\infty}^{0} dD \int_{-\infty}^{\infty} \Phi(\omega) e^{-j\omega D} d\omega, \tag{A.3.2}$$

donde $\Phi(\omega)$ es la función característica de D.

Usando los resultados de [28], la función característica de la forma cuadrática puede expresarse como

$$\Phi(\omega) = \frac{1}{(1 - j\omega\lambda_1)(1 - j\omega\lambda_2)} \exp\left(\frac{j\omega \mathbf{m}_k^{\mathcal{H}} \mathbf{Q} \mathbf{m}_k + \omega^2 \lambda_1 \lambda_2 \mathbf{m}_k^{\mathcal{H}} \mathbf{R}^{-1} \mathbf{m}_k}{(1 - j\omega\lambda_1)(1 - j\omega\lambda_2)}\right), \tag{A.3.3}$$

donde λ_i son los autovalores de la matriz $\mathbf{RQ}$.

Así, la expresión final (exacta y cerrada) de esta probabilidad [10] es

$$P_b = Q_1(a, b) + \sum_{m=0}^{L-1} C_m(a, b, \eta) I_m(ab) \times \exp\left\{-\frac{(a^2 + b^2)}{2}\right\}, \tag{A.3.4}$$

donde $Q_1(a, b)$ es la función Q de Marcum, $I_m(x)$ es la función de Bessel de primera especie y orden m, y los parámetros a, b, η y $C_m(\cdot)$ se calculan de acuerdo a las expresiones de la Tabla A.1.

Caso asintótico

Usando algunas de las relaciones asintóticas en [5]

$$Q_1(a, b) \sim \sqrt{\frac{b}{a}} Q(b - a), \qquad \text{si } b \to \infty, \tag{A.3.5}$$

$$I_m(ab) \sim \frac{\exp(ab)}{\sqrt{2\pi ab}}, \qquad \text{si } a \cdot b \to \infty, \tag{A.3.6}$$

$$Q(x) \sim \frac{\exp(-\frac{x^2}{2})}{\sqrt{2\pi}x}, \qquad \text{si } (b - a) \to \infty, \tag{A.3.7}$$

se puede obtener una expresión aproximada para la probabilidad buscada

$$\Pr\{D < 0\} \approx T \cdot Q(b - a), \tag{A.3.8}$$

donde el parámetro T se calcula como

$$T \triangleq \sqrt{\frac{b}{a}} + \frac{b - a}{\sqrt{ab}} \sum_{m=0}^{N_R - 1} C_m(a, b, \eta). \tag{A.3.9}$$

Table A.1: Cálculo de Probabilidad usando formas cuadráticas Gaussianas

FUNCTIONS AND PARAMETERS	DEFINITIONS
$\{\lambda_i\}_{i=1,2}$	$\frac{1}{2}\operatorname{tr}(\mathbf{R}\mathbf{Q}) + (-1)^{i-1}\sqrt{\left(\frac{1}{2}\operatorname{tr}(\mathbf{R}\mathbf{Q})\right)^2 - \det(\mathbf{R}\mathbf{Q})}$
η	$\left\|\dfrac{\lambda_1}{\lambda_2}\right\|$
a	$\sqrt{\dfrac{2\lambda_2\left(\Sigma_{k=1}^L \mathbf{m}_k^{\mathcal{H}}\left[\mathbf{Q} - \lambda_1\mathbf{R}^{-1}\right]\mathbf{m}_k\right)}{(\lambda_1 - \lambda_2)^2}}$
b	$\sqrt{\dfrac{2\lambda_1\left(\Sigma_{k=1}^L \mathbf{m}_k^{\mathcal{H}}\left[\mathbf{Q} - \lambda_2\mathbf{R}^{-1}\right]\mathbf{m}_k\right)}{(\lambda_1 - \lambda_2)^2}}$
$C_m(a,b,\eta)$	$\begin{cases} -1 + \dfrac{1}{(1+\eta)^{2L-1}}\sum\limits_{n=0}^{L-1}\binom{2L-1}{n}\eta^n, & m = 0 \\ \dfrac{1}{(1+\eta)^{2L-1}}\sum\limits_{n=0}^{L-1-m}\binom{2L-1}{n}\left[\left(\dfrac{b}{a}\right)^m\eta^n - \left(\dfrac{a}{b}\right)^m\eta^{2L-1-n}\right], & m \neq 0 \end{cases}$

A.3.2 No circularidad simétrica

En la sección A.3.1 se ha introducido el análisis de formas cuadráticas cuando las RVs Gaussianas son circularmente simétricas. Aquí, se introduce el análisis para formas cuadráticas en las que las RVs no son circularmente simétricas, para el caso particular de media nula.

Caso General

En este caso, se emplearán los mapeos y la notación s $\mathbf{x} \to \check{\mathbf{x}}$ y $\mathbf{A} \to \check{\mathbf{A}}$, definidos en [29]

$$\check{\mathbf{x}} \triangleq \begin{bmatrix} \Re(\mathbf{x}) \\ \Im(\mathbf{x}) \end{bmatrix} = \begin{bmatrix} \mathbf{x_r} \\ \mathbf{x_i} \end{bmatrix} \in \mathbb{R}^{2n}, \qquad \check{\mathbf{A}} \triangleq \begin{bmatrix} \Re(\mathbf{A}) & -\Im(\mathbf{A}) \\ \Im(\mathbf{A}) & \Re(\mathbf{A}) \end{bmatrix} \in \mathbb{R}^{2m\times 2p}. \tag{A.3.10}$$

Así, se puede expresar la forma cuadrática como

$$D = \check{\mathbf{x}}_k^T \check{\mathbf{Q}} \check{\mathbf{x}}_k. \tag{A.3.11}$$

La función característica de D viene dada por

$$\Phi(\omega) = \frac{1}{\displaystyle\prod_{i=1}^{4} \sqrt{1 - 2j\lambda_i \omega}}, \tag{A.3.12}$$

donde λ_i son los autovalores de la matriz $\mathbf{R\breve{Q}}$ [30].

Es posible calcular analíticamente $\Pr\{D < 0\}$, obteniéndose

$$\Pr\{D < 0\} = \sqrt{\frac{\omega_1 \omega_2 \omega_4}{d_{1,3} d_{2,3} \omega_3}} F_D\left(\frac{1}{2}, 1, \frac{1}{2}, \frac{1}{2}; 1; \frac{d_{3,4}}{\omega_3}, -\frac{d_{3,4}}{d_{1,3}}, -\frac{d_{3,4}}{d_{2,3}}\right), \tag{A.3.13}$$

donde $\omega_{i=1\ldots4}^{\mathcal{I}^-} = \frac{-1}{2\lambda_i}$, $d_{i,j} = \omega_i - \omega_j$, y F_D es la función de Lauricella.

Análisis asintótico 1

Cuando el grado de circularidad simétrica en las RVs no es fuerte, puede demostrarse que $d_{1,3} \approx d_{2,3}$. Por tanto, se puede usar la siguiente relación entre $F_D(\cdot)$ y la función hipergeométrica de Appell $F_1(\cdot)$

$$F_D(\frac{1}{2}, 1, \frac{1}{2}, \frac{1}{2}; 1; x_1, x, x) \equiv F_1(\frac{1}{2}, 1, 1; 1; x_1, x), \tag{A.3.14}$$

para expresar de modo aproximado $\Pr\{D < 0\}$ como

$$\Pr\{D < 0\} \approx \sqrt{\frac{\omega_1 \omega_2 \omega_4}{d_{1,3} d_{2,3} \omega_3}} F_1\left(\frac{1}{2}, 1, 1; 1; \frac{d_{3,4}}{\omega_3}, \frac{d_{3,4}}{\bar{d}}\right), \tag{A.3.15}$$

donde $\bar{d} \triangleq \frac{d_{1,3} + d_{2,3}}{2}$.

Análisis asintótico 2

Si la no circularidad simétrica se reduce aún más, puede asumirse que $|\omega_3| << |d_{1,3}|$ y $|d_{3,4}| <<< |d_{1,3}|$, respectivamente. Por tanto, puede esperarse que $x \to 0$ en (A.3.15). Usando algunas equivalencias [33, eq. 9.121], se obtiene

$$F_1(\frac{1}{2}, 1, 1; 1; x_1, x \to 0) \approx \frac{1}{\sqrt{1 - x_1}}. \tag{A.3.16}$$

Finalmente, se puede obtener una segunda expresión aproximada para la probabilidad buscada

$$\Pr\{D < 0\} \approx \frac{\sqrt{\omega_1 \omega_2}}{\omega_3 - \frac{\omega_1 + \omega_2}{2}}. \tag{A.3.17}$$

A.4 Aplicaciones

A.4.1 BER en sistemas MIMO con desvanecimientos Rice

Caso 1: Interferencia tipo Rice

Se considera un sistema $1 \times N_R$ en el que la señal recibida en la antena k viene dada por

$$r_k = g_k z + h_k \rho_i + w_k, \tag{A.4.1}$$

donde z es el símbolo M-QAM transmitido, g_k y h_k son RVs Gaussianas de medias m_{g_k}, m_{h_k} y varianzas σ_g^2, σ_h^2 respectivamente, ρ_i es el símbolo interferente y w_k es el ruido AWGN de media cero y varianza σ_w^2.

La probabilidad de error puede calcularse mediante el análisis de formas cuadráticas presentado en (A.3.1), obteniendo una expresión exacta y cerrada de la BER, así como una expresión asintótica para el caso simplificado de interferencia Rayleigh y estimación de canal perfecta. La Fig. A.1 muestra la BER en función de la relación señal a interferencia γ_I, para distintos valores del factor K_I de la señal interferente.
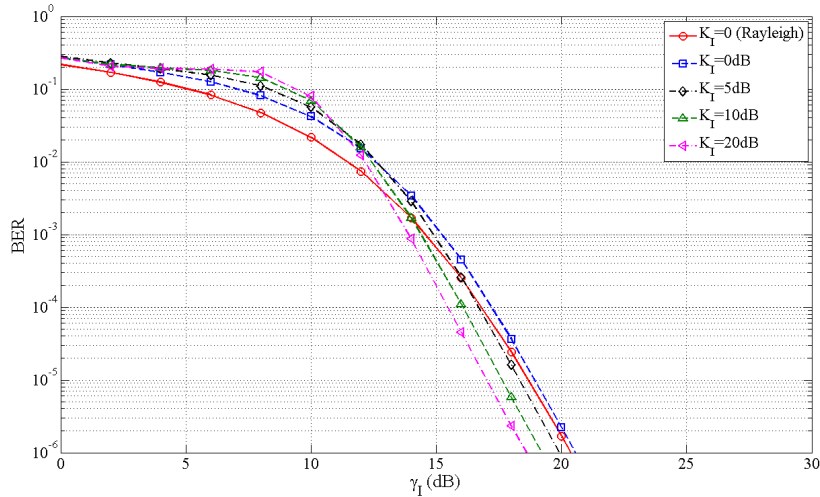

Figure A.1: BER vs γ_I, para diferentes K_I, N_R=2, 16-QAM, K_g=10 dB.

Cuando γ_I es baja, la componente LOS de la interferencia desplaza el símbolo recibido fuera de las regiones de decisión. Como la magnitud de este desplazamiento crece con K_I, la

BER también aumenta con K_I. Por el contrario, si γ_I es aún más baja, el símbolo recibido puede llegar a desplazarse más allá de varias regiones de decisión, provocando más de un bit erróneo por símbolo. Para valores elevados de γ_I, la BER aumenta cuando K_I disminuye.

Caso 2: Alamouti-MRC

En este caso, se considera un sistema MIMO $2 \times N_R$, en el que se emplea el esquema de transmisión de Alamouti [41] junto con recepción MRC. Durante dos intervalos de símbolo consecutivos, se transmiten z_1 y z_2 de acuerdo al esquema de codificación descrito en [41]. Se ha demostrado que en este escenario, la variable de decisión para los símbolos z_i es equivalente a la de un escenario $1 \times 2N_R$, en el que los términos equivalentes de ruido en la antena receptora j se ven aumentados por efecto del error de estimación de canal $\Psi_{i,j}$:

Nuevamente, en este escenario la probabilidad de error puede expresarse de manera exacta y cerrada en términos de las funciones Q de Marcum e I_ν de Bessel. También es posible hallar una expresión asintótica usando la función Q de Gauss, cuando la componente LOS es dominante. En la Fig. A.2, se comparan las prestaciones de un sistema $2 \times N_R$ Alamouti-MRC con las de un sistema $1 \times 2N_R$ MRC convencional [9], en presencia de error de estimación de canal.
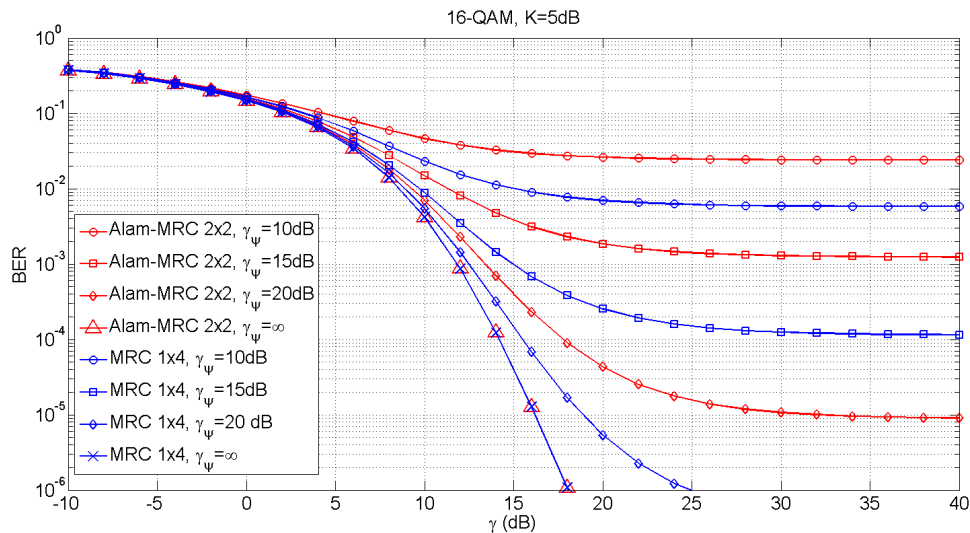

Figure A.2: Alamouti-MRC $2 \times N_R$ vs. $1 \times 2N_R$ MRC. BER vs SNR para distintos valores de ICSI.

Puede verse que ambos esquemas se comportan de manera idéntica cuando la estimación de canal es perfecta. Sin embargo, Alamouti-MRC sufre de una mayor degradación de la BER debido al efecto del ICSI, ya éste que causa un aumento del ruido equivalente.

A.4.2 BER en OFDM con recepción directa

En esta sección, el análisis se centra en dos de las principales imperfecciones asociadas con los receptores OFDM por conversión directa (DCRs), que son muy utilizados en la actualidad para el desarrollo de cabezales de radio integrados en sistemas inalámbricos de bajo coste: el offset de continua (DC) y el desbalanceo de las componentes en fase y cuadratura (IQ). Además, el efecto del ICSI se incluye en ambos escenarios.

Caso 1: Offset de DC

En el modelo de sistema considerado, la señal recibida en banda base en la antena receptora v-ésima puede expresarse como

$$y_v[n] = \frac{1}{\sqrt{N}} \sum_{m=-N/2}^{N/2-1} H_{v,m} X_m e^{\frac{j2\pi n(m+\varepsilon)}{N}} + \eta_v + w_v[n], \qquad (A.4.2)$$

donde N es el número de subportadoras, $n = 0 \ldots N-1$ es el índice de tiempo discreto del símbolo OFDM, X_m es el símbolo BPSK transmitido en la m-ésima subportadora, η_v es el offset de DC, ϵ es el offset de frecuencia de portadora (CFO) normalizado, $w_v[n]$ es el ruido AWGN y $H_{v,m}$ es la respuesta en frecuencia del canal.

Tras la compensación del CFO, el offset de DC se desplaza a la frecuencia discreta ϵ, produciendo una interferencia $\zeta_k(\varepsilon)$ que será más acusada en las portadoras adyacentes. Es este escenario, la BER se ha calculado de manera exacta y cerrada empleando únicamente funciones de Bessel. Así mismo, se ha obtenido una expresión muy simple de la BER irreducible en la portadora k debida al CFO y al offset de DC

$$P_k \approx \frac{|\eta_v \zeta_k(\varepsilon)|^2}{4E_s}. \qquad (A.4.3)$$

También se ha derivado una expresión que determina el máximo offset de DC admisible en un receptor para un valor objetivo de SNR en recepción $\bar{\gamma}_{th}$,

$$|\eta_v(max)|^2 = \frac{E_s}{8|\zeta_k(\varepsilon)|^2} \left(1 - \sqrt{\frac{\bar{\gamma}_{th}}{1+\bar{\gamma}_{th}}} \right). \qquad (A.4.4)$$

En la Fig. 5.2 se muestra la BER promedio en función de la SNR. Cuando existe PCSI, el suelo de BER debido al offset de DC se estima eficientemente usando (A.4.3).
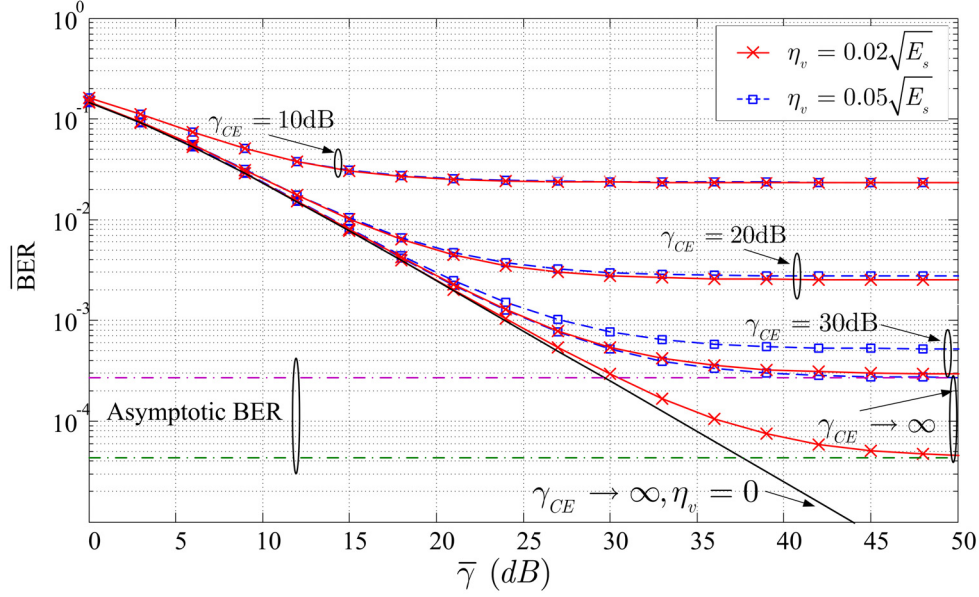

Figure A.3: BER vs SNR, N_R=1, BPSK, para distintos valores de DC offset e ICSI.

Caso 1: Desbalanceo IQ

En el modelo de sistema considerado, la señal recibida en la portadora k puede expresarse como

$$r_k = g_k z_k + h_{-k} z_{-k} + w_k, \tag{A.4.5}$$

donde $k \in \{-N/2, \ldots, N/2 - 1\}$, N es el número de subportadores del símbolo OFDM, z_k y z_{-k} son los símbolos QAM transmitidos en las subportadoras k y $-k$, respectivamente. El término $h_{-k} z_{-k}$ se conoce como interferencia espejo (MCI).

Los términos restantes en (A.4.5) se expresan como

$$g_k = K_1 G_1 H_k + K_2 G_2 H_{-k}^*, \tag{A.4.6}$$

$$h_{-k} = K_2 G_1^* H_{-k}^* + K_1 G_2^* H_k, \tag{A.4.7}$$

$$w_k = K_1 n_k + K_2 n_{-k}^*, \tag{A.4.8}$$

donde H_k y H_{-k} representan la respuesta en frecuencia del canal en las subportadoras k y $-k$, y los términos n_k y n_{-k} representan el ruido AWGN. Finalmente, G_i y K_i ($i = 1, 2$) modelan el efecto del desbalanceo IQ en transmisor y receptor, respectivamente:

$$G_1 = \frac{1 + \alpha_t e^{j\varphi_t}}{2}, \qquad\qquad G_2 = \frac{1 - \alpha_t e^{-j\varphi_t}}{2}, \qquad (A.4.9)$$

$$K_1 = \frac{1 + \alpha_r e^{-j\varphi_r}}{2}, \qquad\qquad K_2 = \frac{1 - \alpha_r e^{j\varphi_r}}{2}. \qquad (A.4.10)$$

En este escenario, puede demostrarse que g_k es una RV Gaussiana no circularmente simétrica. Por tanto, el análisis de BER se lleva a cabo empleando las expresiones derivadas en (A.3.2). Así, la BER se expresa de manera exacta en términos de la función F_D de Lauricella. También se han obtenido dos expresiones aproximadas, válidas para distintas magnitudes del desbalanceo IQ.

En la Fig. A.4 es posible apreciar el efecto de la correlación entre H_k y H_{-k}. Se observa cómo el efecto del desbalanceo IQ depende fuertemente del valor de dicha correlación. Por tanto, la asunción de independencia estadística [81, 83] lleva a una estimación pesimista de la BER.
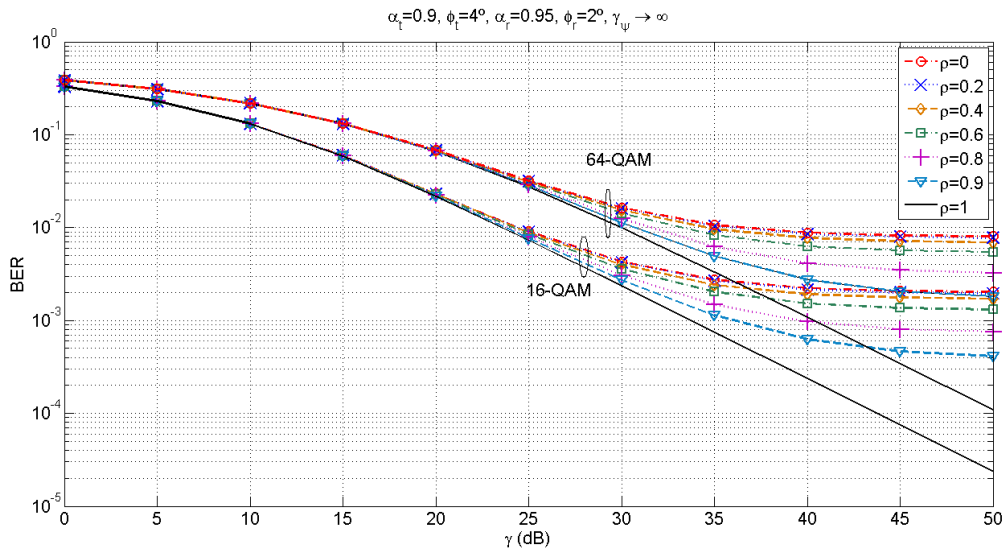

Figure A.4: BER vs SNR, en función de la correlación ρ, PCSI.

A.4.3 BER en sistemas MIMO-OFDM *Beamforming* con errores de estimación de canal

El modelo de sistema MIMO-OFDM con *beamforming* en transmisión y recepción MRC se muestra en Fig. A.5. En este sistema, el símbolo z se transmite por el conjunto de N_T antenas transmisoras mediante un vector de pesos $\hat{\mathbf{v}}$, que se envía desde el receptor a través de un canal de retorno con retardo τ_P.
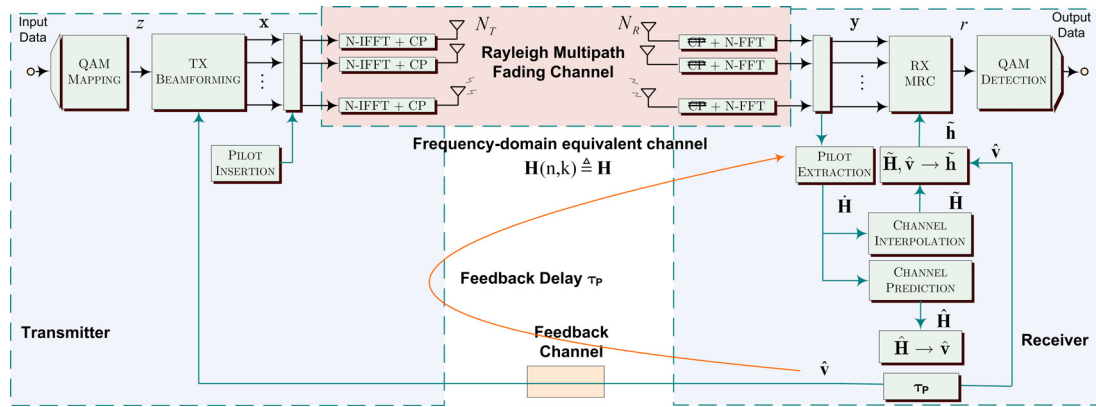

Figure A.5: Modelo de sistema MIMO-OFDM Beamforming-MRC e ICSI

En este escenario, se calcula la BER condicionada a un estado del canal usando el análisis de formas cuadráticas para RVs circularmente simétricas. La CEP se define como

$$\mathcal{I}_{u,v}(m; \hat{\mathbf{H}}) = \Pr\left\{ \Re\{r\} - \mathcal{B}(m) > 0 \mid \hat{\mathbf{H}}, z = s_{u,v} \right\}. \tag{A.4.11}$$

De este modo, la probabilidad de error final se obtiene promediando la BER condicionada con todos los posibles estados del canal. En la Fig. A.6 se evalúan las prestaciones para distintas configuraciones de antena, cuando la estimación de canal usa filtros de Wiener y de tipo sinc. Es interesante destacar que la BER en la configuración 2×4 es unos 3 dB mejor que en la 4×2, mientras que en el caso de PCSI sus prestaciones coinciden [10].

A.5 Conclusiones

En esta tesis, se ha considerado el problema del análisis de prestaciones en sistemas de comunicaciones inalámbricas no ideales. Las principales contribuciones de esta tesis en dicho campo pueden agruparse en dos puntos:
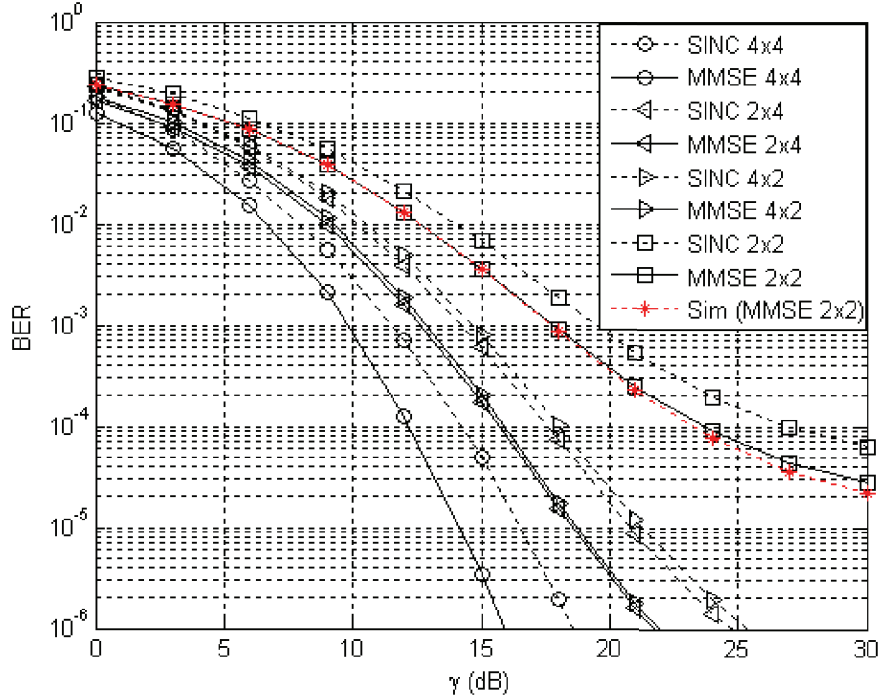
Figure A.6: BER vs SNR, 16-QAM, canal Rayleigh, interpoladores tipo sinc y de Wiener, configuración $N_T \times N_R$.

En primer lugar, se ha desarrollado una *herramienta para el cálculo de probabilidad en sistemas QAM*. El marco analítico que se propone puede ser utilizado en multitud de escenarios, e incluye análisis previos de la bibliografía como casos particulares. Usando esta metodología, el cálculo de los coeficientes elementales (que sólo depende del mapeo de la constelación) se separa del cálculo de probabilidades (que sólo depende de la distribución estadística de las RVs).

Por otra parte, se ha abordado el *cálculo de probabilidades* en sistemas donde la *variable de decisión* puede expresarse como una *forma cuadrática con RVs Gaussianas*, desde diferentes perspectivas. Se han usado y extendido los resultados de [6, 10] para analizar escenarios en los que las RVs son circularmente simétricas. Para el caso general de RVs no circularmente simétricas, se ha encontrado una expresión exacta y cerrada para $\Pr\{D < 0\}$, en términos de la función $F_D(\cdot)$ de Lauricella, así como dos expresiones aproximadas en términos de la función hipergeométrica de Appell $F_1(\cdot)$ y de funciones racionales.

De este modo, el uso conjunto del marco analítico para el análisis de prestaciones de sistemas QAM y del cálculo de probabilidades usando formas cuadráticas ha permitido llevar a cabo el análisis de varios sistemas de comunicaciones inalámbricas siguiendo una metodología común. Mediante la definición adecuada de modelos de sistema, se ha demostrado que esta técnica es una alternativa viable para el cálculo de la BER en sistemas MIMO-OFDM no ideales.

En lo relativo a sistemas MIMO con estimación de canal imperfecta en canales Rice, dos escenarios que no habían sido analizados en la bibliografía han sido estudiados:

- Un sistema QAM con recepción MRC afectado por interferencias de tipo Rice. Se ha demostrado que el efecto de la componente LOS de la señal interferente en la BER varía dependiendo de la magnitud de la dicha componente (es decir, del parámetro K de Rice).

- Un sistema MIMO $2 \times N_R$ que usa la técnica de Alamouti junto con recepción MRC. Se ha demostrado que este esquema puede reducirse a un sistema $1 \times 2N_R$ equivalente en el que el ruido equivalente aumenta debido al efecto de la interferencia en el código de Alamouti debido al error de estimación de canal.

En estos escenarios, también se han propuesto expresiones aproximadas para la BER usando la función Q de Gauss, válidas para canales Rice con una fuerte componente LOS.

También, se ha analizado el efecto de diferentes imperfecciones que afectan a sistemas OFDM que emplean recepción por conversión directa:

- Un sistema OFDM con recepción MRC y estimación de canal imperfecta, CFO y offset de DC. Para el caso particular de estimación de canal perfecta y recepción con una sola antena, se proporciona una expresión muy simple para el suelo de error irreducible en la BER debido al offset de DC. También se establece una regla de diseño para el máximo offset de DC admisible en un receptor, para una SNR determinada.

- Un sistema OFDM con desbalanceo I/Q en transmisor y receptor y estimación imperfecta de canal. Se ha demostrado que la ganancia equivalente del canal es una RV sin circularidad simétrica. En los resultados se aprecia que la correlación entre la respuesta en frecuencia en la portadora deseada y en la interferente espejo tiene un importante efecto en la BER.

Finalmente, se ha analizado un sistema MIMO-OFDM que combina *beamforming* en transmisión y MRC en recepción, con el fin de establecer el efecto del conocimiento imperfecto del estado del canal (ICSI) en ambos extremos de la comunicacin. En este escenario, se calcula la BER condicionada a un estado del canal mediante formas cuadráticas, y esta BER se promedia sobre todos sus posibles estados para obtener la expresión final. Se ha comprobado que el efecto del ICSI en la BER es mayor en el transmisor que en el receptor.

Bibliography

[1] H. Nyquist, "Certain factors affecting telegraph speed," *American Institute of Electrical Engineers, Transactions of the*, vol. XLIII, pp. 412 –422, jan. 1924.

[2] R. V. L. Hartley, "Transmission of information," *Bell Syst. Tech. Journal*, vol. 7, pp. 535–563, 1928.

[3] C. E. Shannon, "A mathematical theory of communication," *Bell Systems Technical Journal*, vol. 27, pp. 379–423,623–656, 1948.

[4] M. Simon and M. Alouini, "A unified approach to the performance analysis of digital communication over generalized fading channels," *Proceedings of the IEEE*, vol. 86, pp. 1860 –1877, sep 1998.

[5] M. K. Simon and M.-S. Alouini, *Digital Communication over Fading Channels (Wiley Series in Telecommunications and Signal Processing)*. Wiley-IEEE Press, December 2004.

[6] J. G. Proakis, *Digital Communications*. New York: Mc Graw-Hill, 5th ed., 2004.

[7] M.-S. Alouini and A. Goldsmith, "A unified approach for calculating error rates of linearly modulated signals over generalized fading channels," *Communications, IEEE Transactions on*, vol. 47, pp. 1324 –1334, sep. 1999.

[8] J. Proakis, "On the Probability of Error for Multichannel Reception of Binary Signals," *Communication Technology, IEEE Transactions on*, vol. 16, pp. 68 –71, feb. 1968.

[9] L. Cao and N. C. Beaulieu, "Closed-form BER results for MRC diversity with channel estimation errors in Ricean fading channels," *IEEE Trans. Wireless Commun.*, vol. 4, pp. 1440–1447, July 2005.

[10] E. Martos-Naya, J. F. Paris, U. Fernandez-Plazaola, and A. J. Goldsmith, "Exact BER analysis for M-QAM modulation with transmit beamforming under channel prediction errors," *IEEE Trans. Wireless Commun.*, vol. 7, pp. 3674–3678, Oct. 2008.

[11] M. Di Renzo, F. Graziosi, and F. Santucci, "On the cumulative distribution function of quadratic-form receivers over generalized fading channels with tone interference," *Communications, IEEE Transactions on*, vol. 57, pp. 2122 –2137, jul. 2009.

[12] B. Picinbono, "On circularity," *IEEE Transactions on Signal Processing*, vol. 42, pp. 3473 –3482, dec 1994.

[13] E. Ollila, "On the Circularity of a Complex Random Variable," *IEEE Signal Proc. Letters*, vol. 15, pp. 841 –844, 2008.

[14] X. Tang, M. S. Alouini, and A. J. Goldsmith, "Effect of channel estimation error on M-QAM BER performance in Rayleigh fading," *IEEE Trans. Commun.*, vol. 47, pp. 1856–1864, Dec. 1999.

[15] P. Tan and N. Beaulieu, "Effect of Channel Estimation Error on Bit Error Probability in OFDM Systems over Rayleigh and Ricean Fading Channels," *IEEE Trans. Commun.*, vol. 56, no. 4, pp. 675–685, 2008.

[16] K. Cho and D. Yoon, "On the general BER expression of one- and two-dimensional amplitude modulations," *IEEE Trans. Commun.*, vol. 50, pp. 1074–1080, July 2002.

[17] L. Najafizadeh and C. Tellambura, "BER analysis of arbitrary QAM for MRC diversity with imperfect channel estimation in generalized Ricean fading channels," *IEEE Trans. Veh. Technol.*, vol. 55, pp. 1239–1248, July 2006.

[18] F. J. Lopez-Martinez, E. Martos-Naya, J. F. Paris, and A. J. Goldsmith, "BER Analysis for MIMO-OFDM Beamforming with MRC under Channel Prediction and Interpolation Errors," in *Proc. IEEE Global Telecommunications Conf. GLOBECOM 2009*, pp. 1–7, 2009.

[19] F. J. Lopez-Martinez, E. Martos-Naya, J. F. Paris, and U. Fernandez-Plazaola, "Generalized BER Analysis of QAM and its Application to MRC under Imperfect CSI and Interference in Ricean Fading Channels," *IEEE Transactions on Vehicular Technology*, vol. 59, pp. 2598–2604, June 2010.

[20] F. J. Lopez-Martinez, E. Martos-Naya, J. F. Paris, and J. T. Entrambasaguas, "BER analysis of direct conversion OFDM systems with MRC under channel estimation errors," *IEEE Communications Letters*, vol. 14, pp. 423–425, May 2010.

[21] F. J. Lopez-Martinez, E. Martos-Naya, K. K. Wong, and J. Entrambasaguas, "Closed-Form BER Analysis of Alamouti-MRC Systems with ICSI in Ricean Fading Channels," *IEEE Communications Letters*, vol. 1, no. Accepted for publication, pp. 1–3, 2011.

[22] F. J. Lopez-Martinez, E. Martos-Naya, J. F. Paris, and J. Entrambasaguas, "Exact Closed-Form BER Analysis of OFDM Systems in the presence of IQ imbalances and ICSI," *IEEE Transactions on Wireless Communications*, vol. 1, no. 2nd round of reviews, pp. 1–7, 2011.

[23] L. Hanzo, W. Webb, and T. Keller, *Quadrature Amplitude Modulation: From Basics to Adaptive Trellis-Coded, Turbo-Equalised and Space-Time Coded OFDM, CDMA and MC-CDMA Systems*. J. Wiley & Sons, 2th ed., November 2004.

[24] J. F. Paris, M. C. Aguayo-Torres, and J. T. Entrambasaguas, "Impact of channel estimation error on adaptive modulation performance in flat fading," *IEEE Trans. Commun.*, vol. 52, pp. 716–720, May 2004.

[25] L. Szczecinski, C. Gonzalez, and S. Aissa, "Exact expression for the BER of rectangular

QAM with arbitrary constellation mapping," *IEEE Trans. Commun.*, vol. 54, pp. 389–392, Mar. 2006.

[26] A. Maaref and S. Aissa, "Exact closed-form expression for the bit error rate of orthogonal STBC in Nakagami fading channels," in *Vehicular Technology Conference, 2004. VTC2004-Fall. 2004 IEEE 60th*, vol. 4, pp. 2493–2497, Sept. 2004.

[27] E. K. S. Au, S. Jin, M. R. McKay, W. H. Mow, X. Gao, and I. B. Collings, "Analytical Performance of MIMO-SVD Systems in Ricean Fading Channels with Channel Estimation Error and Feedback Delay," *IEEE Trans. Wireless Commun.*, vol. 7, pp. 1315–1325, Apr. 2008.

[28] G. L. TURIN, "The characteristic function of Hermitian quadratic forms in complex normal variables," *Biometrika*, vol. 47, no. 1-2, pp. 199–201, 1960.

[29] E. Telatar, "Capacity of multi-antenna Gaussian channels," *European Transactions on Telecommunications*, vol. 10, no. 6, pp. 585–596, 1999.

[30] A. Mathai, S. Prvost, and T. Hayakawa, *Bilinear Forms and Zonal Polynomials*. No. 102, Ney York: Springer-Verlag, 1995.

[31] J. Sylvester, "A demonstration of the theorem that every homogeneous quadratic polynomial is reducible by real orthogonal substitutions to the form of a sum of positive and negative squares," *Philosophical Magazine IV*, pp. 138–142, 1852.

[32] T. Q. Duong, H. Shin, and E.-K. Hong, "Error probability of binary and M-ary signals with spatial diversity in Nakagami-q (Hoyt) fading channels," *EURASIP J. Wirel. Commun. Netw.*, vol. 2007, pp. 1–8, 2007.

[33] I. S. Gradshteyn and I. M. Ryzhik, *Table of Integrals, Series and Products*. Academic Press Inc, 7th edition ed., 2007.

[34] J. Romero-Jerez and A. Goldsmith, "Receive Antenna Array Strategies in Fading and Interference: An Outage Probability Comparison," *IEEE Trans. Wireless Commun.*, vol. 7, no. 3, pp. 920–932, 2008.

[35] X. Zhang and N. C. Beaulieu, "A Closed-Form BER Expression for BPSK Using MRC in Correlated CCI and Rayleigh Fading," *IEEE Trans. Commun.*, vol. 55, pp. 2249–2252, Dec. 2007.

[36] X. Zhang and N. C. Beaulieu, "Explicit Analytical Expressions for Outage and Error Rate of Diversity Cellular Systems in the Presence of Multiple Interferers and Correlated Rayleigh Fading," *IEEE Trans. Commun.*, vol. 55, pp. 2303–2315, Dec. 2007.

[37] Z. Du, J. Cheng, and N. C. Beaulieu, "BER Analysis of BPSK Signals in Ricean-Faded Cochannel Interference," *IEEE Trans. Commun.*, vol. 55, pp. 1994–2001, Oct. 2007.

[38] S. Zhou and G. Giannakis, "How accurate channel prediction needs to be for transmit-beamforming with adaptive modulation over Rayleigh MIMO channels?," *IEEE Transactions on Wireless Communications*, vol. 3, pp. 1285 – 1294, July 2004.

[39] C. Yuen and B. Hochwald, "Achieving near-capacity at low SNR on a multiple-antenna multiple-user channel," *IEEE Transactions on Communications*, vol. 57, pp. 69 –74, January 2009.

[40] X. Liu and L. Hanzo, "Exact BER of rectangular-constellation QAM subjected to asynchronous co-channel interference and Nakagami-m fading," *Electronics Letters*, vol. 42, no. 15, pp. 868–869, 2006.

[41] S. Alamouti, "A simple transmit diversity technique for wireless communications," *IEEE Journal on Selected Areas in Communications*, vol. 16, pp. 1451 –1458, Oct 1998.

[42] M. Ju, H.-K. Song, and I.-M. Kim, "Exact BER analysis of distributed Alamouti's code for cooperative diversity networks," *IEEE Transactions on Communications*, vol. 57, pp. 2380 –2390, Aug. 2009.

[43] Z. Yi and I.-M. Kim, "Approximate BER expressions of distributed alamouti's code in dissimilar cooperative networks with blind relays," *IEEE Transactions on Communications*, vol. 57, pp. 3571 –3578, December 2009.

[44] R. Schober, W. Gerstacker, and L.-J. Lampe, "Performance analysis and design of STBCs for frequency-selective fading channels," *IEEE Trans. Wireless Communications*, vol. 3, pp. 734 – 744, May 2004.

[45] A. Vielmon, Y. Li, and J. Barry, "Performance of Alamouti transmit diversity over time-varying Rayleigh-fading channels," *IEEE Transactions on Wireless Communications*, vol. 3, pp. 1369 – 1373, Sept. 2004.

[46] D.-B. Lin, P.-H. Chiang, and H.-J. Li, "Performance analysis of two-branch transmit diversity block-coded ofdm systems in time-varying multipath rayleigh-fading channels," *IEEE Transactions on Vehicular Technology*, vol. 54, pp. 136 – 148, Jan. 2005.

[47] I.-M. Kim, "Exact BER analysis of OSTBCs in spatially correlated MIMO channels," *IEEE Transactions on Communications*, vol. 54, pp. 1365 –1373, Aug. 2006.

[48] D. Gu and C. Leung, "Performance analysis of transmit diversity scheme with imperfect channel estimation," *Electronics Letters*, vol. 39, pp. 402 – 403, Feb 2003.

[49] P. Garg, R. Mallik, and H. Gupta, "Exact error performance of square orthogonal space- time block coding with channel estimation," *IEEE Transactions on Communications*, vol. 54, pp. 430 – 437, March 2006.

[50] L. Jacobs and M. Moeneclaey, "Comments on "exact error performance of square orthogonal space-time block coding with channel estimation"," *IEEE Trans. Communications*, vol. 57, pp. 3249 –3251, Nov. 2009.

[51] W. Li and N. Beaulieu, "Effects of channel-estimation errors on receiver selection-combining schemes for Alamouti MIMO systems with BPSK," *IEEE Trans. Communications*, vol. 54, pp. 169 – 178, Jan. 2006.

[52] W. Li, N. Beaulieu, and Y. Chen, "Generalized receiver selection combining schemes for alamouti MIMO systems with MPSK," *IEEE Transactions on Communications*, vol. 57, pp. 1599 –1602, June 2009.

[53] A. Loke and F. Ali, "Direct conversion radio for digital mobile phones-design issues, status, and trends," *IEEE Trans. Microw. Theory Tech.*, vol. 50, no. 11, pp. 2422–2435, 2002.

[54] R. Svitek and S. Raman, "DC offsets in direct-conversion receivers: characterization and implications," *IEEE Microw. Mag.*, vol. 6, no. 3, pp. 76–86, 2005.

[55] A. Goldsmith, *Wireless Communications.* Cambridge University Press, 2005.

[56] S. Marsili, "DC offset estimation in OFDM based WLAN application," in *Proc. IEEE Global Telecommunications Conference GLOBECOM '04*, vol. 6, pp. 3531–3535, 29 Nov.–3 Dec. 2004.

[57] J. van de Beek, M. Sandell, and P. Borjesson, "ML estimation of time and frequency offset in OFDM systems," *IEEE Trans. Signal Process.*, vol. 45, pp. 1800–1805, July 1997.

[58] C. K. Ho, S. Sun, and P. He, "Low complexity frequency offset estimation in the presence of DC offset," in *Proc. IEEE International Conference on Communications ICC '03*, vol. 3, pp. 2051–2055 vol.3, 2003.

[59] H. Lin, X. Wang, and K. Yamashita, "A low-complexity carrier frequency offset estimator independent of DC offset," *IEEE Commun. Lett.*, vol. 12, no. 7, pp. 520–522, 2008.

[60] IEEE, "Standard for local and metropolitan area networks part 16: Air interface for broadband wireless access systems," May 2009.

[61] 3GPP, "TS 36.211 V8.7.0. Physical Channels and Modulation (Release 8)," June 2009.

[62] K. N. Le, "Insights on ICI and its effects on performance of OFDM systems," *Digit. Signal Process.*, vol. 18, no. 6, pp. 876–884, 2008.

[63] L. Rugini and P. Banelli, "BER of OFDM systems impaired by carrier frequency offset in multipath fading channels," *IEEE Trans. Wireless Commun.*, vol. 4, no. 5, pp. 2279–2288, 2005.

[64] P. Dharmawansa, N. Rajatheva, and H. Minn, "An exact error probability analysis of OFDM systems with frequency offset," *IEEE Trans. Commun.*, vol. 57, no. 1, pp. 26–31, 2009.

[65] C.-H. Yih, "Effects of channel estimation error in the presence of CFO on OFDM BER in frequency-selective Rayleigh fading channels," *Journal of Communications*, vol. 3, no. 3, 2008.

[66] C.-H. Yih, "BER analysis of OFDM systems impaired by DC offset and carrier frequency offset in multipath fading channels," *IEEE Commun. Lett.*, vol. 11, no. 11, pp. 842–844, 2007.

[67] C.-H. Yih, "Analysis and compensation of DC offset in OFDM systems over frequency-selective Rayleigh fading channels," *IEEE Trans. Veh. Technol.*, vol. 58, no. 7, pp. 3436–3446, 2009.

[68] A. Orozco-Lugo, M. Lara, and D. McLernon, "Channel estimation using implicit training," *IEEE Trans. Signal Process.*, vol. 52, no. 1, pp. 240–254, 2004.

[69] H. Cheon and D. Hong, "Effect of channel estimation error in OFDM-based WLAN," *IEEE Commun. Lett.*, vol. 6, no. 5, pp. 190–192, 2002.

[70] M. Valkama, M. Renfors, and V. Koivunen, "Advanced methods for I/Q imbalance compensation in communication receivers," *Signal Processing, IEEE Transactions on*, vol. 49, pp. 2335 –2344, oct 2001.

[71] J. Tubbax, B. Come, L. Van der Perre, S. Donnay, M. Engels, H. D. Man, and M. Moonen, "Compensation of IQ imbalance and phase noise in OFDM systems," *IEEE Transactions on Wireless Communications*, vol. 4, pp. 872 – 877, may 2005.

[72] A. Tarighat, R. Bagheri, and A. Sayed, "Compensation schemes and performance analysis of IQ imbalances in OFDM receivers," *IEEE Transactions on Signal Processing*, vol. 53, pp. 3257 – 3268, aug. 2005.

[73] D. Tandur and M. Moonen, "Joint Adaptive Compensation of Transmitter and Receiver IQ Imbalance Under Carrier Frequency Offset in OFDM-Based Systems," *IEEE Trans. on Signal Processing*, vol. 55, pp. 5246 –5252, nov. 2007.

[74] M. Inamori, A. Bostamam, Y. Sanada, and H. Minami, "IQ imbalance compensation scheme in the presence of frequency offset and dynamic DC offset for a direct conversion receiver," *IEEE Transactions on Wireless Communications*, vol. 8, pp. 2214 –2220, may 2009.

[75] Y. Yoshida, K. Hayashi, H. Sakai, and W. Bocquet, "Analysis and Compensation of Transmitter IQ Imbalances in OFDMA and SC-FDMA Systems," *IEEE Transactions on Signal Processing*, vol. 57, pp. 3119 –3129, aug. 2009.

[76] Q. Zou, A. Tarighat, and A. Sayed, "Joint compensation of IQ imbalance and phase noise in OFDM wireless systems," *IEEE Transactions on Communications*, vol. 57, pp. 404 –414, february 2009.

[77] J. Gao, X. Zhu, H. Lin, and A. Nandi, "Independent component analysis based semi-blind I/Q imbalance compensation for MIMO OFDM systems," *IEEE Transactions on Wireless Communications*, vol. 9, pp. 914 –920, march 2010.

[78] H. Minn and D. Munoz, "Pilot Designs for Channel Estimation of OFDM Systems with Frequency-Dependent I/Q Imbalances," in *IEEE Wireless Communications and Networking Conference, 2009. WCNC 2009.*, pp. 1 –6, april 2009.

[79] V. V. Gottumukkala and H. Minn, "Optimal Pilot Power Allocation for OFDM Systems with Transmitter and Receiver IQ Imbalances," in *IEEE Global Telecommunications Conference, 2009. GLOBECOM 2009.*, pp. 1 –5, 30 2009-dec. 4 2009.

[80] D. Munoz and H. Minn, "Pilot Designs with Guard Bands for Channel Estimation of MIMO OFDM Systems with Frequency-Dependent I/Q Imbalances," in *IEEE 70th Vehicular Technology Conference Fall (VTC 2009-Fall), 2009.*, pp. 1 –5, sept. 2009.

[81] M. Windisch and G. Fettweis, "Performance Degradation due to I/Q Imbalance in Multi-Carrier Direct Conversion Receivers: A Theoretical Analysis," in *IEEE International Conference on Communications, 2006. ICC '06.*, vol. 1, pp. 257 –262, june 2006.

[82] M. Krondorf and G. Fettweis, "OFDM link performance analysis under various receiver impairments," *EURASIP J. Wirel. Commun. Netw.*, vol. 2008, pp. 1–14, 2008.

[83] T. Schenk, E. Fledderus, and P. Smulders, "Performance Analysis of Zero-IF MIMO OFDM Transceivers with IQ Imbalance," *Journal of Communications*, vol. 2, no. 7, pp. 9–19, 2007.

[84] V. Aalo and G. Efthymoglou, "On the MGF and BER of Linear Diversity Schemes in Nakagami Fading Channels with Arbitrary Parameters," pp. 1 –5, apr. 2009.

[85] R. Radaydeh, "Average Error Performance of M-ary Modulation Schemes in Nakagami-q (Hoyt) Fading Channels," *Communications Letters, IEEE*, vol. 11, pp. 255 –257, mar. 2007.

[86] R. Radaydeh, "Mrc in the presence of asynchronous cochannel interference over frequency-selective rayleigh fading channels," *Vehicular Technology, IEEE Transactions on*, vol. 58, pp. 4329 –4341, oct. 2009.

[87] K. Peppas, F. Lazarakis, A. Alexandridis, and K. Dangakis, "Error performance of digital modulation schemes with MRC diversity reception over eta-mu fading channels," *Wireless Communications, IEEE Transactions on*, vol. 8, pp. 4974 –4980, oct. 2009.

[88] K. Peppas, F. Lazarakis, T. Zervos, A. Alexandridis, and K. Dangakis, "Sum of Non-Identical Independent Squared eta-mu Variates and Applications in the Performance

Analysis of DS-CDMA Systems," *Wireless Communications, IEEE Transactions on*, vol. 9, pp. 2718 –2723, sep. 2010.

[89] J. Cavers, "An analysis of pilot symbol assisted modulation for Rayleigh fading channels," *IEEE Trans. Veh. Technol.*, vol. 40, no. 4, pp. 686–693, 1991.

[90] B. Xia and J. Wang, "Effect of channel-estimation error on QAM systems with antenna diversit," *IEEE Trans. Commun.*, vol. 53, pp. 481–488, Mar. 2005.

[91] M. Ozdemir and H. Arslan, "Channel estimation for wireless OFDM systems," *IEEE Communications Surveys & Tutorials*, vol. 9, no. 2, pp. 18–48, 2007.

[92] S. Coleri, M. Ergen, A. Puri, and A. Bahai, "Channel estimation techniques based on pilot arrangement in OFDM systems," *IEEE Trans. Broadcast.*, vol. 48, no. 3, pp. 223–229, 2002.

[93] J. Paris, E. Martos-Naya, U. Fernandez-Plazaola, and J. Lopez-Fernandez, "Analysis of Adaptive MIMO Transmit-Beamforming under Channel Prediction Errors Based on Incomplete Lipschitz-Hankel Integrals," *IEEE Trans. Veh. Technol.*, vol. 58, pp. 2815–2824, July 2009.

[94] M. Larsen, A. Swindlehurst, and T. Svantesson, "Performance Bounds for MIMO-OFDM Channel Estimation," *Signal Processing, IEEE Transactions on*, vol. 57, pp. 1901 –1916, May 2009.

[95] P. Loskot and N. C. Beaulieu, "Performance Analysis of Coded MIMO-OFDM Systems Over Generalized Ricean Fading Channels," in *Proc. Canadian Conference on Electrical and Computer Engineering CCECE '06*, pp. 1634–1639, 2006.

[96] M. Torabi, S. A'issa, and M. Soleymani, "On the BER Performance of Space-Frequency Block Coded OFDM Systems in Fading MIMO Channels," *IEEE Trans. Wireless Commun.*, vol. 6, no. 4, pp. 1366–1373, 2007.

[97] W. C. Jakes, *Microwave mobile communications / edited by William C. Jakes, Jr.* Wiley, New York :, 1974.

[98] S. Bulumulla, S. Kassam, and S. Venkatesh, "A systematic approach to detecting OFDM signals in a fading channel," *IEEE Trans Commun*, vol. 48, no. 5, pp. 725–728, 2000.

[99] S. Zhou and G. Giannakis, "Optimal transmitter eigen-beamforming and space-time block coding based on channel mean feedback," *IEEE Trans. Signal Process.*, vol. 50, no. 10, pp. 2599–2613, 2002.

[100] A. Papoulis and S. U. Pillai, *Probability, Random Variables, and Stochastic Processes.* New York: Mc-Graw Hill, 4th ed., 2002.

[101] A. Zanella, M. Chiani, and M. Win, "On the marginal distribution of the eigenvalues of wishart matrices," *Communications, IEEE Transactions on*, vol. 57, pp. 1050 –1060, apr. 2009.

[102] A. Maaref and S. Aissa, "Closed-form expressions for the outage and ergodic Shannon capacity of MIMO MRC systems," *IEEE Trans. Commun.*, vol. 53, no. 7, pp. 1092–1095, 2005.

[103] M. Simon and M.-S. Alouini, "Some new results for integrals involving the generalized Marcum Q function and their application to performance evaluation over fading channels," *IEEE Trans. Wireless Commun.*, vol. 2, no. 4, pp. 611–615, 2003.

[104] H. G. Myung, J. Lim, and D. J. Goodman, "Single carrier FDMA for uplink wireless transmission," *Vehicular Technology Magazine, IEEE*, vol. 1, no. 3, pp. 30 –38, 2006.